INVESTIGATION OF THE RNA-PROTEIN INTERACTIONS IN BACTERIAL RIBONUCLEASE P (RNASE P)

by

Jean Kristin Smith-Koutmos

A dissertation submitted in partial fulfillment
of the requirements for the degree of
Doctor of Philosophy
(Chemistry)
in The University of Michigan
2009

Doctoral Committee:
Professor Carol A. Fierke, Chair
Professor David R. Engelke
Associate Professor Melanie S. Sanford
Associate Professor Nils G. Walter
Assistant Professor Katrin Karbstein

I dedicate my thesis to Markos Koutmos.

Marko, your belief that I can do anything has given me confidence to accomplish things I would have never believed possible. You bring out the best in me. Thank you for your love, support, and endless patience.

ACKNOWLEDGEMENTS

This work would have been impossible without the support and help of others. I want to begin by thanking my many friends who have supported me throughout my time in graduate school. In particular, Dr. Markos Koutmos, Dr. John Hoerter, Dr. Susanne Wisen, Dr. David Rueda, and Dr. Stephanie Gantt have been not only good friends, but also friends with whom I have shared my scientific curiosity. Most significantly, I would like to thank my husband, Markos Koutmos, for all of his support. He has taught me how to live my life to the fullest and treasure every day. I also want to thank my family, especially my four siblings (Keith, Kimberly, Paul and Jonathan) for always believing in me and in each other.

I would like to thank all of my lab members, past and current, for their helpful discussions. My advisor, Professor Carol Fierke, has been a wonderful mentor, and her example is a source of inspiration to me. Furthermore, I want to acknowledge the members of the RNase P subgroup (Dr. Andrew J. Andrews, Dr. John Hsieh, Wan Lim, Dr. Nathan Zahler, and Dr. Jeremy Day-Storms). I have also learned an immense amount from the collaborations that I have been involved in, and I would like to thank Anette Casiano, Dr. Sam Paczini, Mark Ditzler and Hai Pham for all that they have taught me. Additionally, the monthly Fierke - Engelke RNase P group meeting have provided me with a wealth of useful feedback, and fostered many interesting discussions.

Each of my thesis chapters corresponds to a manuscript that will hopefully be published. As such, the work presented was conducted not only by me, but by my co-authors as well. A list of authors and their contributions are given below.

Chapter I contains sections from two separate manuscripts. The first has been published in Biopolymers Vol. 87 (5-6); 329-338. The authors on this paper are J. Kristin Smith, John Hsieh, and Carol A. Fierke. I wrote the manuscript, and John contributed Figure I-III. The second manuscript is a book chapter that has been submitted for a book entitled "Ribonuclease P," edited by Fenyong Liu and to be published by Springer. The book chapter is entitled "Bacterial RNase P Kinetic Mechanism" and the authors are Kristin S. Koutmou, John Hsieh, and Carol A. Fierke.

Chapter II was adapted from two separate manuscripts. The authors on the first manuscript are Nathan H. Zahler, Kristin S. Koutmou, Jeffrey C. Kurz, Jungsan Sohn, Frank E. Campbell, Somashekarappa Niranjanakumari, Michael E. Harris and Carol A. Fierke. Nathan wrote the paper, performed the genomic analyses presented in the introduction, and he and Kristin contributed data to Tables II-2, Figures II-2 and II-3; Jeff and Jungsan contributed data to Tables II-1 and II-2; Frank E. Campbell Somashekarappa Niranjanakumari made protein. The authors for the second manuscript are Kristin S. Koutmou, Nathan H. Zahler, and Carol A. Fierke. Nathan contributed the preliminary data to Figure II-3. Chapter III was based entirely on this second manuscript, and Kristin S. Koutmou performed all of the experiments described in the third chapter.

Chapter IV will be submitted as a manuscript with the authors listed as follows: Kristin S. Koutmou, Jeremy Day Storms, and Carol A. Fierke. Kristin performed all of the experiments except for those related to the data presented in Table IV-1. These data were collected by Dr. Jeremy Day-Storms.

Chapter V will be submitted as a manuscript. The authors on this paper are Melissa Getz, Kristin S. Koutmou, Samuel Paczini, Anette Negroni-Casiano, James E. Penner-Hahn, Hashim Al-Hashimi, and Carol A. Fierke. Kristin designed experiments, expressed and purified RNA, prepared EXAFS samples, and wrote the manuscript; Melissa performed NMR experiments drafted the NMR results; Sam performed XAS experiments and wrote a draft of the XAS results. Figure B-1 in Appendix B came from Anette Casiano. Kristin S. Koutmou prepared and labeled the sample.

TABLE OF CONTENTS

Dedication……ii

Acknowledgements……iii

List of Figures……..viii

List of Tables……..…….xiii

List of Schemes…….……xiv

List of Equations……....xv

List of Appendices……..…….xvi

CHAPTER I.....1

IMPORTANCE OF RNA-PROTEIN-METAL INTERACTIONS IN BACTERIAL RIBONUCLEASE P STRUCTURE AND CATALYSIS.....1

Introduction.....1

Bacterial RNase P.....4

Structural Perspectives on RNA-Protein Interactions in the RNase P Holoenzyme.....10

Pre-tRNA Substrate Recognition.....14

RNA-Protein Interactions and Metal Dependent Catalysis.....17

Conclusions.....19

References for Chapter I.....20

CHAPTER II.....29

SEQUENCE PREFERENCE IN THE INTERACTION OF BACTERIAL RIBONUCLEASE P WITH PRE-TRNA 5' LEADERS 29

Background *29*

Results *34*

Discussion *43*

Materials and Methods *47*

References for Chapter II *52*

CHAPTER III 56

SPECIFIC CONTACTS BETWEEN THE P PROTEIN SUBUNIT OF *BACILLUS SUBTILIS* RNASE P AND THE 5' LEADER OF PRE-TRNA CONTRIBUTE TO MOLECULAR RECOGNITION 56

Background *56*

Results *60*

Discussion *68*

Materials and Methods *74*

References for Chapter III *77*

CHAPTER IV 81

THE RNR MOTIF OF THE *B. SUBTILIS* RNASE P PROTEIN PLAYS A ROLE IN STRUCTURING THE P RNA ACTIVE SITE AND PRE-TRNA SUBSTRATE FOR INTERACTION 81

Background *81*

Results *87*

Discussion *99*

Materials and Methods *105*

References for Chapter IV *112*

CHAPTER V 116

IDENTIFICATION AND CHARACTERIZATION OF A TIGHTLY BOUND METAL IN A MODEL OF THE P4 HELIX OF THE METALLO-RIBOZYME RIBONUCLEASE P 116

Introduction *116*

Results *121*

Materials and Methods *135*

References for Chapter IV *140*

CHAPTER VI **146**

CONCLUSIONS AND FUTURE DIRECTIONS 146

Overview *146*

Conclusions *146*

Future Directions *149*

References for Chapter VI *157*

LIST OF FIGURES

Figure I-1. RNase P catalyzes the metal dependent cleavage of the 5' end of precursor tRNAs to form a mature tRNA (blue) and 5' leader (red). 2

Figure I-2. Crystal structures of bacterial RNase P RNAs. (B) and (D) show two different views of the *B. stearothermophilus* P RNA structure [56]. (A) and (C) illustrate two views of the *T. maritima* P RNA structure [55]. 5

Figure I-3. Interaction between B. subtilis RNase P RNA and P protein. (Left) Secondary structure of the catalytic domain of *B. subtilis* P RNA, based on topology from the X-ray structure of the *B. stearothermophilus* P RNA indicating sites that are cleaved by copper-o-phenanthroline-labeled P proteins in the following regions: green diamonds, N terminus; red arrows, RNR motif; and stars, the metal binding loop (MBL). Additionally, highlighted nucleotides indicate sites where P protein binding reduces (red), enhances (blue) or has a variable effect (green) on cleavage during in-gel Fe(II)-EDTA cleavage assays. (Right) Structure of *B. subtilis* P protein. Labels indicate the location of the N-terminus (green), the RNR motif (red), metal binding loop (blue), and central cleft (gray). 7

Figure I-4. Structural models of RNase P holoenzyme with substrate bound from (A*) B. stearothermophilus* (B) B. subtilis P RNA is shown in blue, P protein shown in red, and yeast $tRNA^{Phe}$ (A) and *B. subtilis* pre-$tRNA^{Asp}$ (B) in brown. The P protein is positioned to interact with both P RNA and the 50 end of substrates in both models. A closer look at the position of the most highly conserved region of the P protein, the RNR motif, is shown for the *B. stearothermophilus* (C) and the *B. subtilis* (D) RNase P models. Both models place this region of the protein at the interface of the tRNA, P protein, and P RNA. Helix P4 is colored green and J19/4 is highlighted in yellow in the P RNAs of (C) and (D). 11

Figure II-1. A) Proposed structure of the interface between pre-tRNA and P protein based on affinity cleavage [20] data showing the mature tRNA section of pre-tRNA (red), P protein (blue) and the pre-tRNA 5' leader backbone (yellow). The position of the RNase P cleavage site is shown by a red sphere, and the position of leader nucleotide N(-4) is shown in yellow. B) Structure of substrates based on *B. subtilis* pre-tRNA^{Asp}. The RNase P cleavage site (arrow) and recognition elements near the cleavage site (bold) are indicated on the pre-tRNA secondary structure [14,16,17]. 5' leaders and nomenclature for substrates used in this study are shown..... 31

Figure II-2. Dependence of A(-4) and G(-4) Substrate Affinity on Calcium Concentration. $K_{D,obs}$ values for A(-4) (open circles) and G(-4) (filled circles) substrates as a function of $[Ca(II)]_f$. Reaction conditions are 50 mM MES, 50 mM Tris, pH 6.0, 37˚C with indicated $[Ca(II)]_f$ concentrations. KCl concentrations were adjusted to maintain constant ionic strength (See Materials and Methods). Error bars represent the 40

Figure II-3. Adenosine analogs at N(-4) alter the affinity of pre-tRNA for RNase P. (A) Precursor tRNA^{Asp} substrate possessing a four nucleotide long 5' leader. The N(-4) position is underlined. (B) Structure of the nucleotide bases incorporated at N(-4) of pre-tRNA^{Asp}, including: adenosine (A(-4)), guanosine (G(-4)), purine (P(-4)), 2-aminopurine 44

Figure III-1. (A) Structural model of *B. subtilis* RNase P with pre-tRNA^{asp} bound derived from affinity cleavage and cross-linking data [26]. P RNA is shown in blue, P protein in red, and tRNA^{Asp} in brown. The 5' leader of the substrate is highlighted in green. The most highly conserved protein region, the RNR motif, is in yellow. (B) View of *B. subtilis* RNase P protein (red) and pre-tRNA 5' leader (black) from the *B. subtilis* holoenzyme model (P RNA in blue) [35]. The N(-4) position is highlighted in green. 59

Figure III-2. (A) Map of sites where single cysteine mutations in the *B. subtilis* P protein alter the value of $K_{D, obs}$ for pre-tRNA^{Asp}. The side chain color reflects the magnitude of the effect of the mutation on the value of $K_{D, obs}$: yellow, ≤ 3-fold increase; blue 3 to 25-fold increase; green > 25-fold increase. (B) *B. subtilis* P protein crystal structure with the effect of alanine mutations on the binding selectivity for A at N(-4) compared to G at this position. The residues that did not alter

the binding specificity ratio when mutated to alanine are highlighted in yellow, and those that abolished the sequence preference at N(-4) are colored in green. 63

Figure IV-IV-1. Structural view of *B. subtilis* RNase P (A) Crystal structure of *B. subtilis* RNase P protein [16]. The 14 amino acids with >67% sequence conservation are highlighted in blue [15]. The most conserved region of the protein is termed the RNR motif, as denoted with text. (B) View of the location of the RNR motif in the *B. subtilis* RNase P holoenzyme model with bound pre-tRNA [22]. The protein is in red, the P RNA in blue, and the pre-tRNA in brown. Helix P4 in P RNA is highlighted in green. This figure is oriented looking down the center of the RNR motif α-helix. The first three residues (R60, N61, and R62) are shown, and sit at the interface of the P RNA and pre-tRNA^{Asp}. 84

Figure IV-2. (A) Binding curves for measuring $K_{D,obs}$ of ○ wild type, □ R60A, and ◇ R65A RNase P for pre-tRNA^{Asp} determined by centrifugational gel filtration in 50 mM MES, 50 mM Tris, 400 mM KCl, 10 mM $CaCl_2$, at 37°C. (B) Fluorescence titration data for measuring K_1 in 50 mM MES, 50 mM Tris, 180 mM KCl, 2 mM $[Co(NH_3)_6]•Cl_3$, at 37°C (○ WT, □ R60A, ◇ R62A). Data shown in Table IV-3. (C) Calcium dependence of pre-tRNA binding to RNase P ($K_{D,obs,Ca}$). RNase P (2μM R60A, 300 nM WT and R62A) was mixed with pre-tRNA^{Asp} (20 nM) to form E•S in 2 mM $[Co(NH_3)_6]•Cl_3$ $CaCl_2$ is titrated into the solution to stabilize the ES* complex. A single isotherm (equation 5) are fit to the data and the $K_{D,obs,Ca}$ values are listed in Table IV-4 (○ WT, □ R60A, ◇ R62A). 91

Figure IV-3. Stopped flow traces of Fl-pre-tRNA^{3nt} with a three-nucleotide long leader binding to (A) WT RNase P and (B) R60A RNase . The directionality of the first phase is different for the wild type and R60A mutant, demonstrating that the fluoroscein at the 5' end of Fl-pre-tRNA^{3nt} is in a different environment. 93

Figure IV-4. (A) pH dependence of wild type, R60A, and R62A cleavage rates in 50 mM MES, 50 mM Tris, 180 mM KCl, 10 mM $CaCl_2$, 37°C, pH 5-8, (B) pH dependence of wild type cleavage rates cleavage rates in 50 mM MES, 50 mM Tris, 180 mM KCl, 10 mM $MgCl_2$, 37°C, pH 5-8, (C) Single-turnover time course for R60A in 50 mM MES, 50 mM Tris, 180 M KCl, 10 mM $MgCl_2$, 37°C, pH 6.0. 96

Figure V-1. RNase P structure, reaction, and conservation (A) Structural model of the *B. subtilis* RNase P holoenzyme (ref). P RNA is shown in blue, RNase P protein is red, and pre-tRNA substrate is shown in brown. The P4 helix in PRNA is highlighted in green, and the pre-tRNA cleavage site is denoted in black. (B) Schematic of the RNase P reaction. (C) A close-up view of the P4 helix (green) in P RNA (blue). This figure demonstrates that P4 is located near the pre-tRNA cleavage site (black) and the RNase P protein (red) in the holoenzyme model. (D) Secondary structure of bacterial P RNAs. All nucleotide that have conserved sequences are de-noted with letters..... 120

Figure V-2. Metal localization and detection of inner sphere binding sites in P4 detected by Mn^{2+} and a combination of $Co(NH_3)_6^{3+}/Zn^{2+}$. (A) Chemical shift changes upon addition of 16 mM Zn^{2+}, 0.2mM $Co(NH_3)_6^{3+}$/ 1mM Zn^{2+} and normalized intensities (=1-I_M/I_F) upon addition of 3 μM Mn^{2+} are shown as a function of residue number for the following vectors: C8H8 (black), C6H6 (green), C1'H1' (red), C5H5 (blue) and C2H2 (pink), N1H1/N3H3 (yellow). (B) Sites in P4 with unique chemical shift environments measured in 15 mM Mg^{2+} (red), 0.5 mM $Co(NH_3)_6^{3+}$ (green), 0.2 mM $Co(NH_3)_6^{3+}$/1 mM Zn^{2+} (blue), and 16 mM Zn^{2+} (purple). (C) The aromatic region of a 2D HSQC experiment on the P4 construct both in the absence (black) and in the presence of 60 M Mn^{2+} (red). Highlighted by a black box is the main site for metal binding. (D) Secondary structure of P4..... 125

Figure V-3. (A) Normalized XANES spectra of zinc-RNA samples: 1 mM Zn^{2+} + 4 mM P4 (black, solid), 2 mM Zn^{2+} + 2 mM $Co(NH_3)_6^{3+}$ + 4 mM P4 (black, dashed), and 2 mM Zn^{2+} (red, solid). All samples were 10 mM in MES, 10 mM in $NaNO_3$, 30% glycerol, pH ~ 6. (B) Fourier transform (k = 2.55-10.8 $Å^{-1}$) of the k^3-weighted EXAFS data showing (in black) the first and second shell scattering peaks for Zn^{2+} in the presence of RNA and $Co(NH_3)_6^{3+}$ and (in red) the first shell scattering peak for Zn^{2+} in a buffer control sample. Dashed lines represent the best fits to these data: (black) 6 N/O scatterers and 6 C scatterers, and (red) 6 N/O scatterers. (inset) k^3-weighted EXAFS spectra of Zn^{2+} with (black, also contains $Co(NH_3)_6^{3+}$) and without (red) P4 construct. 128

Figure V-4. Inner sphere binding observed in SRP crystal structure and proposed in P4. Crystal structure of Human SRP at 2.0 Å resolution (PDB ID#1D4R) showing tandem guanine residues binding Mg^{2+} with inner and outer sphere coordination[41]. Proposed model of inner sphere binding with the bases of P4, an inner sphere contact in G22 and an outer sphere contact in G23. 131

Figure A-1. Stopped flow traces of wild-type RNase P with Fl-pre-$tRNA^{5nt}$ in magnesium, showing the pH dependent appearance of a second phase…….....…….161

Figure B-1. C-domain overlay with P4 (blue), P4-A bulge included (green) and C-domain (red)……. 167

LIST OF TABLES

Table II-1. Effects of block mutation of leader sequences..... 35

Table II-2. Effects of mutation at N(-4) and N(-5) on RNase P substrate affinity. 38

Table III-1. Affinities of RNase P containing either a wild type or mutant P protein subunit for the G(-4) pre-tRNA. 61

Table III-2. Affinities of RNase P containing either wild type or alanine mutant P protein for the A(-4) and G(-4) pre-tRNA substrates. 64

Table III-3. Affinities of wild type, F20A, Y34A, and Y34F P protein mutants for A(-4), P(-4), DAP(-4) and G(-4) substrates. 67

Table IV-1. Binding of P RNA to P protein with RNR motif mutants, and number of ionic interactions.... 88

Table IV-2. RNR motif mutants affinities for pre-tRNA^{Asp} with a 5 nucleotide long 5' leader under conditions of 10 mM $CaCl_2$ 89

Table IV-3. K_1 values measured by fluorescence titrations 90

Table IV-4. Values for the apparent calcium affinity ($K_{D,obs,Ca}$) measured by fluorescence titrations..... 94

Table IV-5. Single turnover rate constants under varying pH and divalent metal conditions..... 97

Table A-1. Summary of the effect of RNR motif mutants on the metal concentration necessary to activate RNase P catalysis……..161

Table A-2. Affinities of RNR motif mutants for pre-tRNAs at 25^{o}C……..…….162

Table A-3. Preliminary trFRET distance measurements……..……..…..…..….163

Table A-4. Single turnover rate constants for mutants that impact N(-4) sequence selectivity……..…163

Table A-5. Affinity of wild-type and a C52G/G379C, C53G/G378C *B. subtilis* RNase P for pre-tRNA^{Asp} with a 5 nucleotide long 5' leader under various conditions……164

Table B-1. Optimized transcription conditions for synthesis of C-domain P RNA. …….....166

LIST OF SCHEMES

Scheme I-1 Minimal kinetic mechanism of bacterial RNase P. 6

Scheme IV-1. (A) The minimal kinetic mechanism for bacterial RNase P, where E is RNase P holoenzyme, S is pre-tRNA, P is mature tRNA, L is the 5' leader, E•S is the substrate bound complex, E•P•L is the enzyme•tRNA•5' leader complex [12], (B) Definitions of all kinetic and thermodynamic constants discussed in the text. 85

Scheme IV-2 (A) The expanded minimal kinetic mechanism. Where E is RNase P holoenzyme, S is pre-tRNA substrate, M^{2+} is divalent metal (B) Equilibrium constant expressions to define the terms in (A). 95

LIST OF EQUATIONS

Equation III-1 76

Equation IV-1 107

Equation IV-2 107

Equation IV-3 108

Equation IV-4 109

Equation IV-5 110

Equation IV-6 111

LIST OF APPENDICES

Appendix A……………………………………………………………...…………………………………160

Appendix B……………………………………………………………………………..…………………165

CHAPTER II [i]

IMPORTANCE OF RNA-PROTEIN-METAL INTERACTIONS IN BACTERIAL RIBONUCLEASE P STRUCTURE AND CATALYSIS

Introduction

Ribonucleoprotein complexes (RNPs) are involved in a plethora of essential processes in nature, including protein translation [1,2], mRNA splicing [3,4], telomere maintenance [5], rRNA maturation [6] and tRNA maturation [7,8]. A subset of these essential RNA-protein complexes are ribozymes, molecules wherein an RNA catalyzes the chemistry of the reaction. The ribosome and ribonuclease P (RNase P) are among the most extensively studied and conserved ribozymes, and they are also the only naturally occurring catalytic RNAs that so far have been shown to catalyze multiple turnover reactions *in vivo*.

RNase P is a ribonucleoprotein complex that catalyzes the maturation of the 5' end of precursor tRNAs (pre-tRNAs) by cleaving a specific phosphodiester bond to yield a mature tRNA with a 5' phosphate (Figure I-1). Until this year RNase P was thought to be ubiquitous, however, the archeaon *Nanoarchaeum equitans* was discovered to synthesize leaderless tRNAs, rendering the maturation of the 5' by RNase P unnecessary

[i] Chapter I is reprinted from with permission from Wiley and Sons. Biopolymers 2007 87(5-6); 329-338

[9]. Given that this is the only known example of an organism that does not require RNase P, it is still a near-universally conserved enzyme. Bacterial RNase P recognizes and cleaves a variety of RNAs, not just pre-tRNAs, that possess a motif in which a short 5' single stranded RNA flanks a short duplex RNA stem [10]. Examples of putative *in vivo* substrates for RNase P include pre-4.5S RNA, pre-tmRNA, C/D intron-encoded snoRNAs, and riboswitches [11-16]. In addition to tRNA maturation, RNase P might also be involved in degrading mRNA and regulating gene expression *in vivo* [11]. Therefore, there is active research aimed at using RNase P for gene-therapy or as an antimicrobial target [17,18].

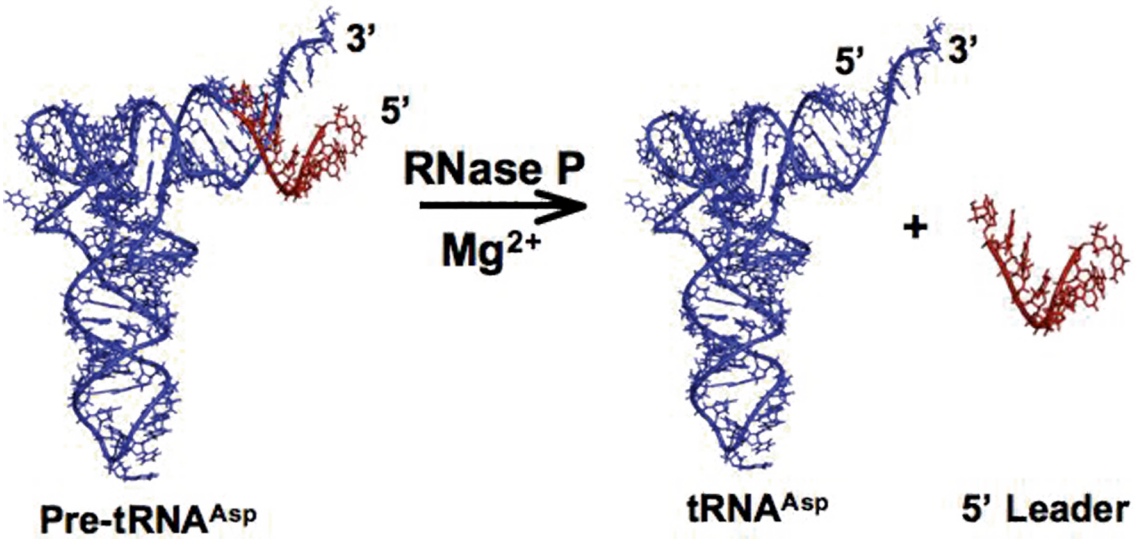

Figure II-1. RNase P catalyzes the metal dependent cleavage of the 5' end of precursor tRNAs to form a mature tRNA (blue) and 5' leader (red).

Bacterial and nuclear RNase Ps are comprised of a catalytic RNA and associated protein(s), with both modules being required for the *in vivo* function of this essential enzyme [19]. Although RNase P has been studied for over 20 years, only lately have the vital roles of the protein components been thoroughly investigated. Recent experiments on bacterial RNase P have revealed roles for the protein and protein-RNA interactions as

varied as stabilization of the holoenzyme complex, alteration of the conformation of P RNA, enhancement of pre-tRNA substrate recognition and affinity, and alteration of metal affinity and location [20-24]. Therefore, a synopsis of the published data is warranted to shed some light on the intriguing role of the P protein in RNA-protein interactions within bacterial RNase P. These interactions will be the focus of this introduction.

The large RNA (P RNA) components of the RNase P holoenzyme complexes from *E. coli* and *B. subtilis* were two of the first ribozymes discovered [25]. Subsequently, the catalytic activities of the P RNA subunit alone from Archea and Eukaryotes were demonstrated *in vitro*, furthering the idea that RNase P is an ancient and conserved RNA enzyme found in all kingdoms of life [26,27]. P RNA is the component of the holoenzyme that directly catalyzes substrate cleavage in all three domains of life; however, the P protein modestly enhances the single turnover cleavage rate constant in bacteria at saturating metal ion concentrations [20,21]. The protein component has a larger effect on the observed RNase P-catalyzed cleavage rate constant at sub-saturating substrate and metal. Like many ribozymes, RNase P catalysis is both metal and pH dependent [20,28,29]. However, unlike catalysis by small ribozymes that produce a 2',3'-cyclic phosphate and a 5' hydroxyl group [30-32], RNase P catalyzes the cleavage of a specific phosphodiester bond that produces 5' phosphate and 3' hydroxyl end groups [33,34]. These observations suggest that different chemical mechanisms are used by small ribozymes compared to RNase P.

The number of proteins associated with the catalytic P RNA varies greatly between Bacteria, Archea and Eukaryotes. RNase P from chloroplast and mitochondria

from higher eukaryotes has been proposed to be composed solely of protein; this was verified recently when an all-protein RNase P was successfully identified and recombinantly purified from human mitochondria [35,36]. *In vitro* reconstitution of RNase P holoenzyme from Archea requires at least four proteins, while nine essential proteins are associated with the yeast nuclear enzyme [27,33,37-39]. In contrast, bacterial RNase P has the simplest holoenzyme configuration, consisting of one protein and a single P RNA, thereby providing a tractable system in which to investigate P RNA-protein interactions in this conserved RNP [40]. Bacterial RNase P protein (P protein) is essential *in vivo*, indicating that RNA-protein interactions play a central role in the function of this enzyme [19]. These differences in structure between bacterial and eukaryotic RNase P coupled with its indispensability for cell viability make the bacterial enzyme an attractive drug target [41,42]. The functional requirement for structurally similar P proteins *in vivo* for RNase P from all three domains highlights the importance of understanding the role of RNA-protein interactions, and how they contribute to the overall RNase P-catalyzed reaction.

Bacterial RNase P

Prior to discussing RNA-protein interactions in RNase P, a brief introduction into the structure and mechanism of the bacterial enzyme will be given. The composition of bacterial RNase P, a single P protein associated with the P RNA, makes it the most straightforward, and therefore comprehensively studied RNase P to date. Bacterial RNase P enzymes are classified into two groups based on their P RNA secondary structures, typified by the organisms *Escherichia coli* and *Bacillus subtilis,* referred to as A-type (Ancestral type) and B-type (*Bacillus* type) RNase Ps [43]. Interestingly, the P

RNAs from these organisms are similar enough that the *B. subtilis* P protein can promote *E. coli* P RNA activity and vice versa *in vitro* [23,24,44]. Recently, type A and B RNase Ps were also shown to be interchangeable with each other *in vivo*, hinting that the P protein recognizes a region of structure that is conserved between the two classes of bacterial RNase Ps [45]. Additionally, *B. subtilis* P protein can modestly enhance the activity of some archael P RNAs as well, suggesting both that the binding site for P protein is conserved and that one or more of the functions of the P protein is also conserved throughout all three domains of life [46].

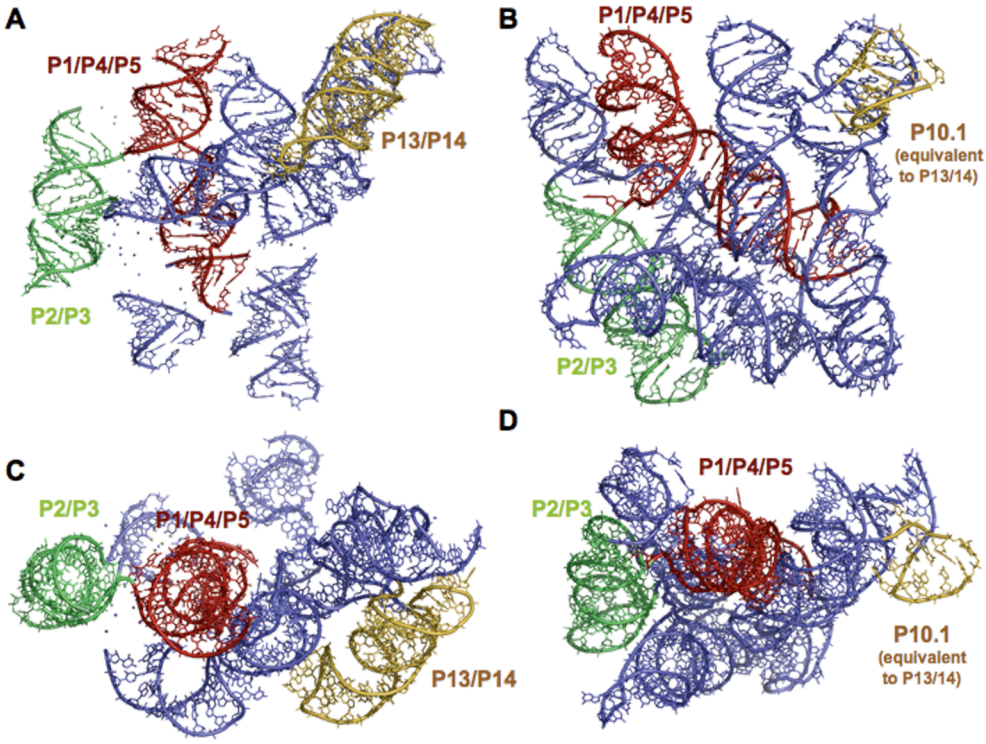

Figure II-2. Crystal structures of bacterial RNase P RNAs. (B) and (D) show two different views of the *B. stearothermophilus* P RNA structure [56]. (A) and (C) illustrate two views of the *T. maritima* P RNA structure [55].

The structure of P RNA is central to its ability to catalyze pre-tRNA cleavage. RNase P RNAs consist of two domains, the substrate binding domain (S-domain) and the catalytic domain (C-domain) [43,47]. These domains can fold independently and the

catalytic domain retains RNase P activity [48-50]. The S-domain has been shown to interact with the T stem-loop regions of pre-tRNA and increase substrate affinity and specificity [49,51,52]. High resolution x-ray crystal structures of the S-domain from both type A and B P RNAs have been solved [53,54]. Although the S-domains of two types of P RNA differ in both secondary structure and overall fold, the cores of the substrate domains are remarkably similar and likely preserved for the recognition of pre-tRNA [54]. The crystal structures of full-length type A (from *T. maritima*) and type B (from *B. stearothermophilus*) P RNAs have been solved [7,55,56]. Although only about two-thirds of the P RNAs are resolved in the structures, the data reveal similar features in the catalytic cores of both P RNAs, including the coaxial stacks in P1/P4/P5, P2/P3, and P8/P9 (Figure I-2).

A conformational change in the P RNA has been proposed to occur upon both P protein and substrate binding (Figure I-3) [23,57]. The substrate-induced conformational change in the holoenzyme is suggested in the kinetic mechanism of the enzyme (Scheme I-1) [21,58,59]. Given that the x-ray crystal structures of RNase P RNA or holoenzyme complexed with either pre-tRNA or tRNA are not yet available, the conformation observed in the published P RNA crystal structures might not reflect the catalytically active form. As a result, multiple models of the holoenzyme complex have been proposed [60-62] and will be discussed in detail later.

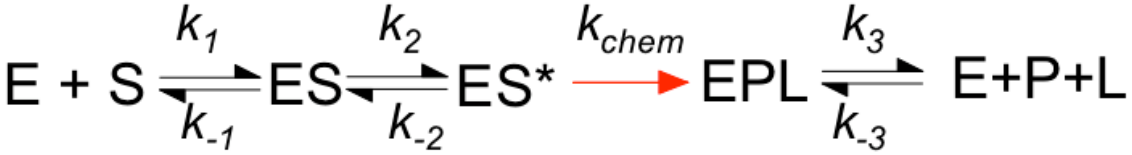

Scheme II-1 Minimal kinetic mechanism of bacterial RNase P.

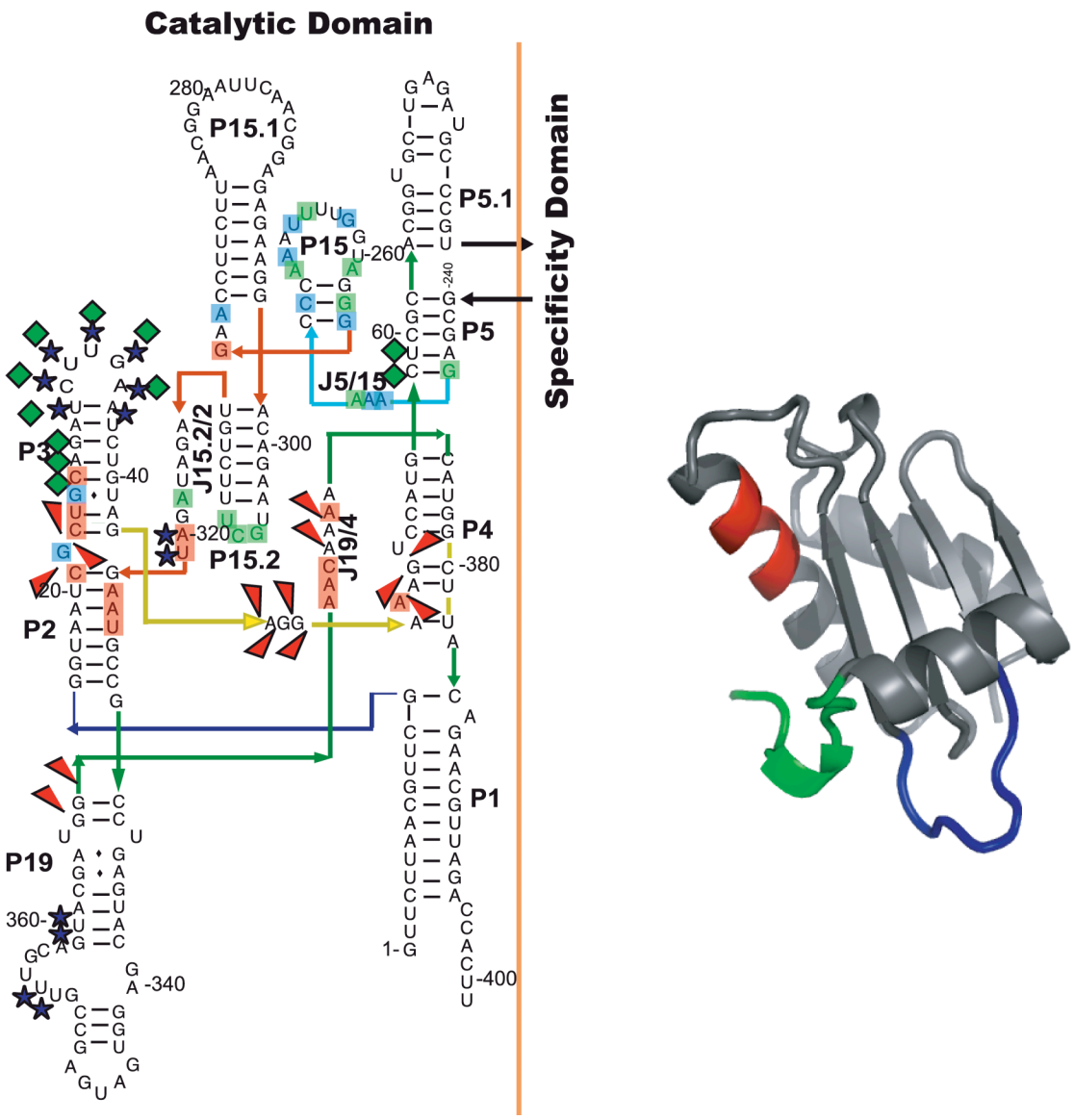

Figure II-3. Interaction between *B. subtilis* RNase P RNA and P protein. (Left) Secondary structure of the catalytic domain of *B. subtilis* P RNA, based on topology from the X-ray structure of the *B. stearothermophilus* P RNA indicating sites that are cleaved by copper-*o*-phenanthroline-labeled P proteins in the following regions: green diamonds, N terminus; red arrows, RNR motif; and stars, the metal binding loop (MBL). Additionally, highlighted nucleotides indicate sites where P protein binding reduces (red), enhances (blue) or has a variable effect (green) on cleavage during in-gel Fe(II)-EDTA cleavage assays. (Right) Structure of *B. subtilis* P protein. Labels indicate the location of the N-terminus (green), the RNR motif (red), metal binding loop (blue), and central cleft (gray).

Although RNase P RNA can cleave substrate in the absence of P protein *in vitro* under high salt concentrations, the P protein is necessary for RNase P cleavage *in vivo*, presumably enhancing the catalytic activity at low metal ion concentrations [19,22,63,64]. P protein enhances k_{cat}/K_M values of catalysis by the *B. subtilis* holoenzyme for cleavage of pre-tRNA^{Asp} by 2000-fold over that of P RNA alone under steady-state conditions and moderate concentrations of magnesium [20]. However, under single turnover conditions with saturating concentrations of *B. subtilis* RNase P and metal ions, the cleavage rate constant for pre-tRNA^{Asp} is enhanced by < 10-fold, suggesting that the P protein does not directly stabilize the cleavage transition state relative to the bound ground state [20,51,65,66].

While the P protein modestly effects the global folding of P RNA, it also provides a number of other contributions in addition to assisting folding [59,67]. For instance, *B. subtilis* P protein contacts the 5' leader sequence of pre-tRNA in the RNase P•pre-tRNA complex to enhance the affinity of the holoenzyme for pre-tRNA^{Asp} substrate by 10^4 fold [20]. Although the presence of the protein does not always have the exact same magnitude of effect for all pre-tRNA substrates, as demonstrated for *E. coli* RNase P, it does consistently increase both the affinity of the enzyme for substrate and enhance cleavage rate constants [21]. The fact that the impact of the protein can be different for distinct substrates indicates that the role of the protein may be more complicated than originally anticipated [21]. Accordingly, the P protein is proposed to play a direct role in substrate recruitment [68-70]. Additionally, the concentration of magnesium ions required to activate catalysis is also significantly reduced in the RNase P holoenzyme compared to P RNA alone [22,64]. Given the known and proposed functions of the

bacterial P protein, including assisting in P RNA folding, and recruitment of substrates and metal ions, understanding RNA-protein interactions is key to gaining a comprehensive understanding of RNase P.

The structure of the *B. subtilis* RNase P protein was first solved by x-ray crystallography to 2.8 Å resolution [71]. This protein adopts an α-β sandwich fold and is structurally homologous to other RNA binding proteins, including the C-terminal domain of ribosomal protein S5 and domain VI of elongation factor G [71]. The crystal structure of the *B. subtilis* P protein reveals three distinct regions that might be able to interact with RNA: an unusual left-handed βαβ connection that contains the highly conserved RNR motif, a central cleft formed by four anti-parallel β-strands and flanked by an α-helix, and the "metal binding loop" which contains a cluster of polar residues that bind two zinc ions in the crystal structure (Figure I-3) [71-73]. Despite the low sequence similarity among the RNase P proteins, the three dimensional structure of the *B. subtilis* P protein is similar to that of the *S. aureus* and *T. maritima* P proteins [74,75]. Additionally, the structure of a protein subunit from archeal RNase P, a homolog of the eukaryotic RNase P protein Pop5p [76], is also similar to that of the bacterial P protein, suggesting a similar functional role across all three kingdoms of life [77].

The RNR motif is the most conserved feature of bacterial P proteins, and is proposed to stabilize binding interactions between the P protein and P RNA in the holoenzyme [71,73]. In Chapter IV we examine the role of the RNR motif in the RNase P kinetic mechanism. The metal binding loop in the *B. subtilis* protein is not a well-conserved feature of P proteins, but these residues may increase the affinity of the holoenzyme for metal ions [71]. Cross-linking and affinity cleavage studies indicate that

the central cleft of the P protein is vital to the recognition of pre-tRNA substrates by the RNase P complex [60]. Specifically, the central cleft is proposed to interact with the 5' leader of the pre-tRNA substrates [69,70]. RNase P protein forms multiple interactions with both of the RNAs in the RNase P system, the pre-tRNA substrate and the P RNA enzyme. These interactions as well as their implications on RNase P activity and catalysis will be analyzed further.

Structural Perspectives on RNA-Protein Interactions in the RNase P Holoenzyme

Although crystal structures of each of the three components of the bacterial RNase P system (P RNA, P protein, and tRNA) have been solved independently of one another, no high-resolution structure of the RNase P holoenzyme, or the holoenzyme•pre-tRNA complex have been solved thus far. Therefore, our best understanding of the holoenzyme and substrate-bound complexes are structural models of *E. coli* (A type) [51,61], *B. stearothermophilus* (B type) [23], and *B. subtilis* (B type) RNase P [60,61]. Although these holoenzyme models differ in detail from the recently published P RNA structures, the overall topology of P RNA in each of these models and the x-ray structures is similar [60]. Therefore, we will focus on the recent *B. subtilis* and *B. stearothermophilus* RNase P holoenzyme•pre-tRNA and holoenzyme•tRNA complex models respectively (Figure I-4).

For the development of the *B. subtilis* holoenzyme•pre-tRNA model presented in Niranjanakumari, *et al.* structural calculations were performed starting from the x-ray crystal structure of the P protein, and a model of the P RNA•pre-tRNA complex (Figure I-4B and D) [60,71,78]. Structural constraints were obtained from hydroxyl radical cleavage catalyzed by copper-*o*-phenanthroline probes positioned at a number of sites in

the P protein via site-specific modification of single cysteines [60]. This probe requires direct contact with the RNA for cleavage, therefore providing more constrained distances between the cleavage site and P protein than other cleavage reagents [60]. In the resultant model, key regions of the P protein are in close proximity (< 15 Å) to functionally important regions of P RNA and pre-tRNA (Figure I-4B and D).

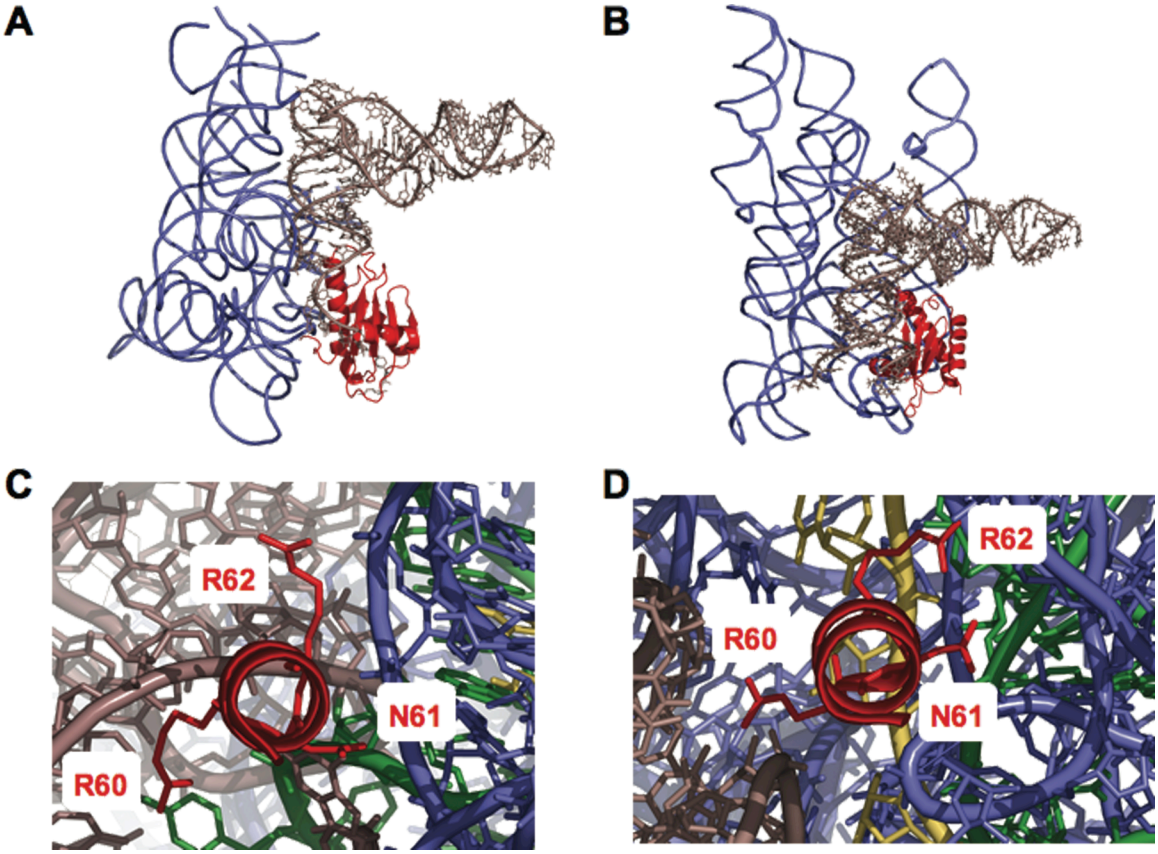

Figure II-4. Structural models of RNase P holoenzyme with substrate bound from (A*) B. stearothermophilus* and (B) *B. subtilis* P RNA is shown in blue, P protein shown in red, and yeast $tRNA^{Phe}$ (A) and *B. subtilis* pre-$tRNA^{Asp}$ (B) in brown. The P protein is positioned to interact with both P RNA and the 50 end of substrates in both models. A closer look at the position of the most highly conserved region of the P protein, the RNR motif, is shown for the *B. stearothermophilus* (C) and the *B. subtilis* (D) RNase P models. Both models place this region of the protein at the interface of the tRNA, P protein, and P RNA. Helix P4 is colored green and J19/4 is highlighted in yellow in the P RNAs of (C) and (D).

For example, the central cleft of the P protein is proximal to the 5' leader sequence of pre-tRNA, and the metal binding loop and N-terminus of the P protein are near the P3 stem-loop of P RNA. Additionally, the model places the conserved RNR motif close to the P RNA helix P4 (Figure I-4D). Further evidence for the P protein contacting the catalytic portion of the P RNA is provided by the demonstration that the affinities of the P protein for the catalytic domain of P RNA and full-length P RNA are nearly identical [44]. The proximity of the RNR motif in the P protein to the P RNA helix P4 may be noteworthy because this is the most highly conserved region of the P RNA, possessing 11 of the 21 unchanging nucleotides in P RNA [79-82]. Moreover, P4 is necessary for positioning divalent metal ions required for catalysis, and forms part of the putative active site of the holoenzyme [79-82].

A model of the *B. stearothermophilus* RNase P holoenzyme•tRNA complex has been developed from in-gel probing of iodine-induced cleavage of thiophosphate-labeled *B. stearothermophilus* and *E. coli* P RNAs [23]. This model places the P protein binding site in the same general location of P RNA as the *B. subtilis* model. However, the two models differ in the orientation of the P protein relative to P RNA and in the specific contacts between the P protein and P RNA, with the *B. stearothermophilus* model predicting more extensive interactions between tRNA and the RNR motif of P protein than the *B. subtilis* model. Figures I-4C and D highlight the position of the conserved RNR motif in the two B type holoenzyme models [23,60]. The structural resolution of both models is only about 10 Å, and therefore specific contacts proposed by these models will need further evaluation. In fact, given that the models are based on two entirely

different sets of biochemical data and are still similar to each other within their 10 Å resolution lends validity to both models.

A number of biochemical and biophysical studies have been undertaken to probe the effect of interactions between the P RNA and the P protein on the structural fold and stability of the holoenzyme. These studies support the idea that P protein binds a conserved area of the P RNA, stabilizing the local P RNA structure, as well as stabilizing the P RNA contacts with the pre-tRNA substrates [23,24,83]. The proposed structural roles of the P protein in *E. coli* (A type), and *B. subtilis* (B type) RNase P holoenzymes have recently been investigated further with melting studies that provide evidence that there is a link between protein binding and the conformation of the P RNA structure [24].

Moreover, binding to P RNA also stabilizes the bacterial P protein structure. Folding studies have demonstrated that the *B. subtilis* P protein is predominately in an unfolded state in solution or is "natively unfolded" in the absence of anions; the folded state of P protein observed in the crystal structure is stabilized by bound anions [84,85]. Consistent with this, Harris and co-workers employed thermal melting studies, intrinsic fluorescence, and CD spectral experiments to confirm that both the P RNA and P protein from *E. coli* undergo conformational changes upon holoenzyme formation, and that P RNA stabilizes the folding of the *E. coli* P protein [83]. These data therefore indicate that there is a link between the folding of P protein and P RNA and the holoenzyme formation. By determining the salt-dependence of P RNA-P protein affinity, Day-Storms *et al.* established that there are three to four ions that dissociate upon formation of *B. subtilis* RNase P holoenzyme, consistent with the formation of RNA-protein ionic contacts [44].

The RNase P holoenzyme from both *E. coli* and *B. subtilis* can dimerize or aggregate under a variety of conditions as demonstrated by small angle x-ray scattering (SAXS), native gel, and light scattering analyses [24,86,87]. This dimerization is inhibited by the presence of substrate and requires the P protein subunit. Therefore dimerization is proposed to be due primarily to contacts between the P RNA and P protein subunits [23,24,86,87]. The *in vivo* relevance of the dimer is still unclear.

Overall, RNA-protein interactions in the RNase P holoenzyme contribute significantly to the function of this molecule. P RNA and P protein stabilize each other's structures, and the proximity of P protein to pre-tRNA and the P RNA active site in the holoenzyme models suggests that RNA-protein interactions may be key for forming the proper active site conformation in low salt and metal conditions. Additionally, RNA-protein interactions may contribute to other less well-characterized structural aspects of the holoenzyme, including dimerization [87].

Pre-tRNA Substrate Recognition

The contact between pre-tRNA and P protein during RNase P substrate recognition is the best-studied aspect of RNA-protein interactions in this RNP. RNase P cleaves the 5' leader of all pre-tRNAs, and therefore must be able to recognize a wide variety of substrates [10,12,88]. In addition, the protein component significantly enhances the ability of the *E. coli* RNase P to catalyze pre-4.5S rRNA cleavage *in vitro,* likely by enhancing the affinity of the holoenzyme for this substrate [12,25,66]. Biochemical data suggest that there are extensive interactions between the P RNA and the pre-tRNA substrate near the cleavage site, D-loop, T-stem loop and acceptor stem, as well as an extensively characterized base pairing interaction with the 3' CCA

[49,50,84,89-94]. The 3' CCA contact has been shown to be necessary *in vivo* for efficient pre-tRNA processing [45]. The P RNA C-domain is proposed to recognize the pre-tRNA acceptor stem, cleavage site, and the conserved CCA sequence on the 3' end of the pre-tRNA [58,90,91,94-96]. In contrast, Pan and coworkers demonstrated that the S-domain of P RNA interacts with the T-stem loop of pre-tRNA [49,97,98]. Notably, there may be differences in how A type and B type RNase P enzymes discriminate between their substrates; the *B. subtilis* P protein causes a much larger enhancement of the affinity of the holoenzyme for pre-tRNA compared to mature tRNA than the *E. coli* P protein [24]. This is possibly inherent to the P RNAs, because the loss of substrate/product discrimination is still seen in chimera RNase P holoenzymes formed with *E. coli* P protein and *B. subtilis* P RNA and visa versa [24]. However, even given the differences, the P protein enhances substrate discrimination in both classes of RNase P. Furthermore, the importance of the P protein•pre-tRNA leader interaction may vary with the structure of the pre-tRNA and the concentrations of metals and salts [21]. Thus far, no sequence specific substrate contacts between the substrate and the P protein have been identified in the literature. However, here in Chapters II and III we report and characterize the sequence specific recognition of 5' leaders by RNase P protein.

RNase P recognizes a variety of atypical substrates, including pre-tRNAs that lack some of the canonical recognition elements. To better understand these interactions, Fierke and colleagues analyzed the effect of the P protein on the kinetic scheme for cleavage of a pre-tRNA that contains all of the canonical recognition elements (pre-$tRNA^{Asp}$ from *B. subtilis)*. They demonstrated that P RNA binds mature tRNA with an affinity slightly higher than pre-tRNA, while the *B. subtilis* holoenzyme has a

significantly higher affinity for pre-tRNA than for tRNA [20,68]. The holoenzyme preference for binding pre-tRNA over mature tRNA by *B. subtilis* RNase P holoenzyme suggests the formation of a direct contact between the pre-tRNA 5' leader and P protein in the holoenzyme. This interaction is confirmed by photo-crosslinking and affinity cleavage studies demonstrating that the 5' leader of pre-tRNA is in close proximity to the central cleft, but not to the RNR motif or metal binding loop of the P protein [60,69]. Furthermore, time-resolved fluorescence resonance energy transfer (trFRET) studies further show that the 4^{th} to 7^{th} nucleotides of the 5' leader contact the P protein in *B. subtilis* RNase P [70]. Harris and coworkers recently demonstrated that *E. coli* RNase P holoenzyme has similar affinity for all of the *E. coli* pre-tRNAs, regardless of sequence variation, while the affinity of P RNA for this same group of pre-tRNA substrates had significant variation [21]. Therefore, interactions between the P protein and pre-tRNAs contribute to the uniformity of the binding affinity for RNase P for pre-tRNAs. Specifically, uniform binding is the result of variations in the energetic contributions between the 5' leader and P protein, which serves to compensate for weaker interactions between P RNA and pre-tRNA. Similarly, the observed uniformity in cleavage rates can also be attributed to P protein contributions for some pre-tRNAs that lack conserved sequence elements, such as the 3' CCA [21]. This is consistent with a mechanism in which the effects of the P protein on the affinity of RNase P for pre-tRNA are related to a conformational change that accompanies substrate binding [21,58,90,98]. This is very similar to what has also been seen for the recognition of amino-acylated tRNAs by EF-Tu; here variations in the tRNA sequences lead to alterations in the affinity for EF-Tu compensating for the different thermodynamic contributions of the esterified amino acid

to yield uniform affinity for the amino-acylated tRNAs [99,100]. These data clearly demonstrate that the P protein plays an important role in substrate recognition in RNase P, allowing the enzyme to bind and cleave a wide array of substrates with comparable efficiency.

RNA-Protein Interactions and Metal Dependent Catalysis

Many RNAs require magnesium ions for their catalytic action, including RNase P [101,102]. RNase P needs divalent metal ions for a number of functions including folding, substrate binding and catalysis [22,29,103,104]. Phosphodiester bond hydrolysis can be catalyzed by hydroxide ions acting alternatively as a nucleophile or a general base. Distinguishing between these two mechanisms is important because they represent two possible strategies for enzymatic activation of a water nucleophile. ^{18}O solvent isotope effect studies suggest that RNase P bond cleavage catalyzed by *E. coli* RNase P has a concerted or S_N2-like mechanism, where nucleophilic attack is activated by metal ion coordination [105]. This is consistent with models proposed for other metal dependent ribozymes, which propose a concerted S_N2 like mechanism for phosphodiester cleavage [79,106,107]. The binding sites of magnesium ions essential for catalysis in RNase P have not yet been clearly delineated, although several sites, including positions in helix P4, have been implicated in metal binding [108,109]. Investigating metal binding sites in helix P4 is the focus of Chapter V. RNase P holoenzyme reaches optimal catalytic activity at lower magnesium ion concentrations than the P RNA ribozyme alone [22,110,111]. Since current holoenzyme models place the P protein in close proximity to the P RNA P4 helix (see above), the P protein is ideally positioned to influence these

critical metal binding sites, either by interacting with P RNA to indirectly alter metal binding, or by directly interacting with essential magnesium ions.

However, the precise mechanism through which the P protein enhances metal affinity of the holoenzyme is not yet entirely understood. Thus far, it has been impossible to distinguish metal ions that stabilize P RNA structure important for catalysis from metal ions that directly stabilize the reaction transition state. To further complicate analysis of the effects of metal ions in the RNase P holoenzyme, a large number of magnesium ions interact non-specifically with the backbones of P RNA and pre-tRNA, through Coulombic interactions to neutralize the net negative charge of the polyanion and thereby stabilize a folded structure [112]. Nonspecifically bound magnesium ions may also stabilize the formation of negative charge in a cleavage reaction [113].

Several lines of observation suggest that one or more magnesium ion(s) specifically bind to a site in helix P4, the same area of the P RNA that cross-links to the P protein, and where the putative catalytic site of the enzyme is located. First, deletion of the P4 helix dramatically reduces RNase P activity [80,114]. Second, sulfur substitution at the non-bridging oxygens at the phosphodiester bonds on nucleotides A49 and A50 in *B. subtilis* (A67 and A68 in *E. coli*) in helix P4 decreases the cleavage rate constant enormously without affecting the affinity of pre-tRNA, and some of these reductions in activity can be recovered by adding manganese ions [80,82,108]. Harris and co-workers provide evidence that the formation of the P1-P4 multi-helix junction is dependent on a cluster of metal ions and that this structure contributes to catalysis [115]. Further corroboration for metal binding in P4 comes from NMR studies that demonstrate specific magnesium binding sites in a stem-loop that serves as a model for the P4 helix [109,116].

Furthermore the P protein is proposed to stabilize the local P RNA structure near P4 [24,60]. These data, together with structural holoenzyme models placing the P protein near P RNA helix P4, suggest that the P protein could stabilize the P RNA structure to enhance the affinity of one or more metal ions bound to helix P4 and to facilitate catalysis [80].

Conclusions

RNA-protein interactions play a variety of crucial roles in the essential ribonucleoprotein RNase P. The preponderance of evidence indicates that P RNA-protein interactions do not play a direct role in stabilizing the transition state of the reaction catalyzed by RNase P. However, protein-RNA interactions make several significant and essential contributions to catalysis by (a) stabilizing the structure of P RNA, (b) interacting with the pre-tRNA substrate to enhance affinity, and (c) reducing the dependence on magnesium ions. Despite the fact that RNase P has generally been regarded as noteworthy in the literature because it is a large catalytic RNA, it is imperative to not underestimate the importance of the synergy between the RNA and protein components in this enzyme. Although several roles for the RNA-protein interactions have been clearly delineated, there are still more proposed functions that need further investigation. The goal of the work presented in this thesis is to advance our understanding of how the synergy between the RNA, protein, and metal components of RNase P contributes to this essential biological reaction.

References for Chapter I

1. Noller HF: RNA structure: reading the ribosome. *Science* 2005, 309:1508-1514.

2. Wilson KS, Noller HF: Molecular movement inside the translational engine. *Cell* 1998, 92:337-349.

3. Patel AA, Steitz JA: Splicing double: insights from the second spliceosome. *Nat Rev Mol Cell Biol* 2003, 4:960-970.

4. Staley JP, Guthrie C: Mechanical devices of the spliceosome: motors, clocks, springs, and things. *Cell* 1998, 92:315-326.

5. Autexier C, Lue NF: The structure and function of telomerase reverse transcriptase. *Annu Rev Biochem* 2006, 75:493-517.

6. Meier UT: The many facets of H/ACA ribonucleoproteins. *Chromosoma* 2005, 114:1-14.

7. Torres-Larios A, Swinger KK, Pan T, Mondragon A: Structure of ribonuclease P--a universal ribozyme. *Curr Opin Struct Biol* 2006, 16:327-335.

8. Evans D, Marquez SM, Pace NR: RNase P: interface of the RNA and protein worlds. *Trends Biochem Sci* 2006, 31:333-341.

9. Randau L, Schroder I, Soll D: Life without RNase P. *Nature* 2008, 453:120-123.

10. Gopalan V, Vioque A, Altman S: RNase P: variations and uses. *J Biol Chem* 2002, 277:6759-6762.

11. Li Y, Altman S: A specific endoribonuclease, RNase P, affects gene expression of polycistronic operon mRNAs. *Proc Natl Acad Sci U S A* 2003, 100:13213-13218.

12. Peck-Miller KA, Altman S: Kinetics of the processing of the precursor to 4.5 S RNA, a naturally occurring substrate for RNase P from Escherichia coli. *J Mol Biol* 1991, 221:1-5.

13. Komine Y, Kitabatake M, Yokogawa T, Nishikawa K, Inokuchi H: A tRNA-like structure is present in 10Sa RNA, a small stable RNA from Escherichia coli. *Proc Natl Acad Sci U S A* 1994, 91:9223-9227.

14. Haebel PW, Gutmann S, Ban N: Dial tm for rescue: tmRNA engages ribosomes stalled on defective mRNAs. *Curr Opin Struct Biol* 2004, 14:58-65.

15. Altman S, Wesolowski D, Guerrier-Takada C, Li Y: RNase P cleaves transient structures in some riboswitches. *Proc Natl Acad Sci U S A* 2005, 102:11284-11289.

16. Coughlin DJ, Pleiss JA, Walker SC, Whitworth GB, Engelke DR: Genome-wide search for yeast RNase P substrates reveals role in maturation of intron-encoded box C/D small nucleolar RNAs. *Proc Natl Acad Sci U S A* 2008, 105:12218-12223.

17. Trang P, Kim K, Liu F: Developing RNase P ribozymes for gene-targeting and antiviral therapy. *Cell Microbiol* 2004, 6:499-508.

18. Willkomm DK, Gruegelsiepe H, Goudinakis O, Kretschmer-Kazemi Far R, Bald R, Erdmann VA, Hartmann RK: Evaluation of bacterial RNase P RNA as a drug target. *Chembiochem* 2003, 4:1041-1048.

19. Gossringer M, Kretschmer-Kazemi Far R, Hartmann RK: Analysis of RNase P protein (rnpA) expression in Bacillus subtilis utilizing strains with suppressible rnpA expression. *J Bacteriol* 2006, 188:6816-6823.

20. Kurz JC, Niranjanakumari S, Fierke CA: Protein component of Bacillus subtilis RNase P specifically enhances the affinity for precursor-tRNAAsp. *Biochemistry* 1998, 37:2393-2400.

21. Sun L, Campbell FE, Zahler NH, Harris ME: Evidence that substrate-specific effects of C5 protein lead to uniformity in binding and catalysis by RNase P. *Embo J* 2006, 25:3998-4007.

22. Kurz JC, Fierke CA: The affinity of magnesium binding sites in the Bacillus subtilis RNase P x pre-tRNA complex is enhanced by the protein subunit. *Biochemistry* 2002, 41:9545-9558.

23. Buck AH, Kazantsev AV, Dalby AB, Pace NR: Structural perspective on the activation of RNase P RNA by protein. *Nat Struct Mol Biol* 2005.

24. Buck AH, Dalby AB, Poole AW, Kazantsev AV, Pace NR: Protein activation of a ribozyme: the role of bacterial RNase P protein. *Embo J* 2005, 24:3360-3368.

25. Guerrier-Takada C, Gardiner K, Marsh T, Pace N, Altman S: The RNA moiety of ribonuclease P is the catalytic subunit of the enzyme. *Cell* 1983, 35:849-857.

26. Kikovska E, Svard SG, Kirsebom LA: Eukaryotic RNase P RNA mediates cleavage in the absence of protein. *Proc Natl Acad Sci U S A* 2007, 104:2062-2067.

27. Hall TA, Brown JW: Archaeal RNase P has multiple protein subunits homologous to eukaryotic nuclear RNase P proteins. *Rna* 2002, 8:296-306.

28. Beebe JA, Fierke CA: A kinetic mechanism for cleavage of precursor tRNA(Asp) catalyzed by the RNA component of Bacillus subtilis ribonuclease P. *Biochemistry* 1994, 33:10294-10304.

29. Beebe JA, Kurz JC, Fierke CA: Magnesium ions are required by Bacillus subtilis ribonuclease P RNA for both binding and cleaving precursor tRNAAsp. *Biochemistry* 1996, 35:10493-10505.

30. Doudna JA, Cech TR: The chemical repertoire of natural ribozymes. *Nature* 2002, 418:222-228.

31. DeRose VJ: Two decades of RNA catalysis. *Chem Biol* 2002, 9:961-969.

32. Hanna R, Doudna JA: Metal ions in ribozyme folding and catalysis. *Curr Opin Chem Biol* 2000, 4:166-170.

33. Hsieh J, Andrews AJ, Fierke CA: Roles of protein subunits in RNA-protein complexes: lessons from ribonuclease P. *Biopolymers* 2004, 73:79-89.

34. Harris ME, Christian EL: Recent insights into the structure and function of the ribonucleoprotein enzyme ribonuclease P. *Curr Opin Struct Biol* 2003, 13:325-333.

35. Holzmann J, Frank P, Loffler E, Bennett KL, Gerner C, Rossmanith W: RNase P without RNA: identification and functional reconstitution of the human mitochondrial tRNA processing enzyme. *Cell* 2008, 135:462-474.

36. Thomas BC, Gao L, Stomp D, Li X, Gegenheimer PA: Spinach chloroplast RNase P: a putative protein enzyme. *Nucleic Acids Symp Ser* 1995:95-98.

37. Terada A, Honda T, Fukuhara H, Hada K, Kimura M: Characterization of the archaeal ribonuclease P proteins from Pyrococcus horikoshii OT3. *J Biochem (Tokyo)* 2006, 140:293-298.

38. Tsai HY, Pulukkunat DK, Woznick WK, Gopalan V: Functional reconstitution and characterization of Pyrococcus furiosus RNase P. *Proc Natl Acad Sci U S A* 2006, 103:16147-16152.

39. Chamberlain JR, Lee Y, Lane WS, Engelke DR: Purification and characterization of the nuclear RNase P holoenzyme complex reveals extensive subunit overlap with RNase MRP. *Genes Dev* 1998, 12:1678-1690.

40. Frank DN, Adamidi C, Ehringer MA, Pitulle C, Pace NR: Phylogenetic-comparative analysis of the eukaryal ribonuclease P RNA. *Rna* 2000, 6:1895-1904.

41. Stathopoulos C, Tsagla A, Tekos A, Drainas D: Effect of peptidyltransferase inhibitors on ribonuclease P activity from Dictyostelium discoideum. Effect of antibiotics on RNase P. *Mol Biol Rep* 2000, 27:107-111.

42. Tekos A, Stathopoulos C, Tsambaos D, Drainas D: RNase P: a promising molecular target for the development of new drugs. *Curr Med Chem* 2004, 11:2979-2989.

43. Brown JW, Haas ES, James BD, Hunt DA, Liu JS, Pace NR: Phylogenetic analysis and evolution of RNase P RNA in proteobacteria. *J Bacteriol* 1991, 173:3855-3863.

44. Day-Storms JJ, Niranjanakumari S, Fierke CA: Ionic interactions between PRNA and P protein in Bacillus subtilis RNase P characterized using a magnetocapture-based assay. *Rna* 2004, 10:1595-1608.

45. Wegscheid B, Condon C, Hartmann RK: Type A and B RNase P RNAs are interchangeable in vivo despite substantial biophysical differences. *EMBO Rep* 2006, 7:411-417.

46. Pannucci JA, Haas ES, Hall TA, Harris JK, Brown JW: RNase P RNAs from some Archaea are catalytically active. *Proc Natl Acad Sci U S A* 1999, 96:7803-7808.

47. Brown JW, Pace NR: Structure and evolution of ribonuclease P RNA. *Biochimie* 1991, 73:689-697.

48. Loria A, Pan T: Domain structure of the ribozyme from eubacterial ribonuclease P. *Rna* 1996, 2:551-563.

49. Pan T, Loria A, Zhong K: Probing of tertiary interactions in RNA: 2'-hydroxyl-base contacts between the RNase P RNA and pre-tRNA. *Proc Natl Acad Sci U S A* 1995, 92:12510-12514.

50. Loria A, Pan T: Modular construction for function of a ribonucleoprotein enzyme: the catalytic domain of Bacillus subtilis RNase P complexed with B. subtilis RNase P protein. *Nucleic Acids Res* 2001, 29:1892-1897.

51. Westhof E, Altman S: Three-dimensional working model of M1 RNA, the catalytic RNA subunit of ribonuclease P from Escherichia coli. *Proc Natl Acad Sci U S A* 1994, 91:5133-5137.

52. Harris ME, Nolan JM, Malhotra A, Brown JW, Harvey SC, Pace NR: Use of photoaffinity crosslinking and molecular modeling to analyze the global architecture of ribonuclease P RNA. *Embo J* 1994, 13:3953-3963.

53. Krasilnikov AS, Yang X, Pan T, Mondragon A: Crystal structure of the specificity domain of ribonuclease P. *Nature* 2003, 421:760-764.

54. Krasilnikov AS, Xiao Y, Pan T, Mondragon A: Basis for structural diversity in homologous RNAs. *Science* 2004, 306:104-107.

55. Kazantsev AV, Krivenko AA, Harrington DJ, Holbrook SR, Adams PD, Pace NR: Crystal structure of a bacterial ribonuclease P RNA. *Proc Natl Acad Sci U S A* 2005, 102:13392-13397.

56. Torres-Larios A, Swinger KK, Krasilnikov AS, Pan T, Mondragon A: Crystal structure of the RNA component of bacterial ribonuclease P. *Nature* 2005, 437:584-587.

57. Pomeranz Krummel DA, Altman S: Multiple binding modes of substrate to the catalytic RNA subunit of RNase P from Escherichia coli. *Rna* 1999, 5:1021-1033.

58. Zahler NH, Sun L, Christian EL, Harris ME: The pre-tRNA nucleotide base and 2'-hydroxyl at N(-1) contribute to fidelity in tRNA processing by RNase P. *J Mol Biol* 2005, 345:969-985.

59. Loria A, Niranjanakumari S, Fierke CA, Pan T: Recognition of a pre-tRNA substrate by the Bacillus subtilis RNase P holoenzyme. *Biochemistry* 1998, 37:15466-15473.

60. Niranjanakumari S, Day-Storms JJ, Ahmed M, Hsieh J, Zahler NH, Venters RA, Fierke CA: Probing the architecture of the B. subtilis RNase P Holoenzyme active site by crosslinking and affinity cleavage. *Rna* 2007, 13:512-535.

61. Tsai HY, Masquida B, Biswas R, Westhof E, Gopalan V: Molecular modeling of the three-dimensional structure of the bacterial RNase P holoenzyme. *J Mol Biol* 2003, 325:661-675.

62. Rox C, Feltens R, Pfeiffer T, Hartmann RK: Potential contact sites between the protein and RNA subunit in the Bacillus subtilis RNase P holoenzyme. *J Mol Biol* 2002, 315:551-560.

63. Kole R, Baer MF, Stark BC, Altman S: E. coli RNAase P has a required RNA component. *Cell* 1980, 19:881-887.

64. Sun L, Harris ME: Evidence that binding of C5 protein to P RNA enhances ribozyme catalysis by influencing active site metal ion affinity. *Rna* 2007.

65. Talbot SJ, Altman S: Kinetic and thermodynamic analysis of RNA-protein interactions in the RNase P holoenzyme from Escherichia coli. *Biochemistry* 1994, 33:1406-1411.

66. Tallsjo A, Kirsebom LA: Product release is a rate-limiting step during cleavage by the catalytic RNA subunit of Escherichia coli RNase P. *Nucleic Acids Res* 1993, 21:51-57.

67. Westhof E, Wesolowski D, Altman S: Mapping in three dimensions of regions in a catalytic RNA protected from attack by an Fe(II)-EDTA reagent. *J Mol Biol* 1996, 258:600-613.

68. Crary SM, Niranjanakumari S, Fierke CA: The protein component of Bacillus subtilis ribonuclease P increases catalytic efficiency by enhancing interactions with the 5' leader sequence of pre-tRNAAsp. *Biochemistry* 1998, 37:9409-9416.

69. Niranjanakumari S, Stams T, Crary SM, Christianson DW, Fierke CA: Protein component of the ribozyme ribonuclease P alters substrate recognition by directly contacting precursor tRNA. *Proc Natl Acad Sci U S A* 1998, 95:15212-15217.

70. Rueda D, Hsieh J, Day-Storms JJ, Fierke CA, Walter NG: The 5' Leader of Precursor tRNA(Asp) Bound to the Bacillus subtilis RNase P Holoenzyme Has an Extended Conformation. *Biochemistry* 2005, 44:16130-16139.

71. Stams T, Niranjanakumari S, Fierke CA, Christianson DW: Ribonuclease P protein structure: evolutionary origins in the translational apparatus. *Science* 1998, 280:752-755.

72. Jovanovic M, Sanchez R, Altman S, Gopalan V: Elucidation of structure-function relationships in the protein subunit of bacterial RNase P using a genetic complementation approach. *Nucleic Acids Res* 2002, 30:5065-5073.

73. Gopalan V, Baxevanis AD, Landsman D, Altman S: Analysis of the functional role of conserved residues in the protein subunit of ribonuclease P from Escherichia coli. *J Mol Biol* 1997, 267:818-829.

74. Spitzfaden C, Nicholson N, Jones JJ, Guth S, Lehr R, Prescott CD, Hegg LA, Eggleston DS: The structure of ribonuclease P protein from Staphylococcus aureus reveals a unique binding site for single-stranded RNA. *J Mol Biol* 2000, 295:105-115.

75. Kazantsev AV, Krivenko AA, Harrington DJ, Carter RJ, Holbrook SR, Adams PD, Pace NR: High-resolution structure of RNase P protein from Thermotoga maritima. *Proc Natl Acad Sci U S A* 2003, 100:7497-7502.

76. Walker SC, Engelke DR: Ribonuclease P: the evolution of an ancient RNA enzyme. *Crit Rev Biochem Mol Biol* 2006, 41:77-102.

77. Wilson RC, Bohlen CJ, Foster MP, Bell CE: Structure of Pfu Pop5, an archaeal RNase P protein. *Proc Natl Acad Sci U S A* 2006, 103:873-878.

78. Massire C, Jaeger L, Westhof E: Derivation of the three-dimensional architecture of bacterial ribonuclease P RNAs from comparative sequence analysis. *J Mol Biol* 1998, 279:773-793.

79. Frank DN, Pace NR: Ribonuclease P: unity and diversity in a tRNA processing ribozyme. *Annu Rev Biochem* 1998, 67:153-180.

80. Crary SM, Kurz JC, Fierke CA: Specific phosphorothioate substitutions probe the active site of Bacillus subtilis ribonuclease P. *Rna* 2002, 8:933-947.

81. Christian EL, Zahler NH, Kaye NM, Harris ME: Analysis of substrate recognition by the ribonucleoprotein endonuclease RNase P. *Methods* 2002, 28:307-322.

82. Christian EL, Kaye NM, Harris ME: Helix P4 is a divalent metal ion binding site in the conserved core of the ribonuclease P ribozyme. *Rna* 2000, 6:511-519.

83. Guo X, Campbell FE, Sun L, Christian EL, Anderson VE, Harris ME: RNA-dependent folding and stabilization of C5 protein during assembly of the E. coli RNase P holoenzyme. *J Mol Biol* 2006, 360:190-203.

84. Oh BK, Frank DN, Pace NR: Participation of the 3'-CCA of tRNA in the binding of catalytic Mg2+ ions by ribonuclease P. *Biochemistry* 1998, 37:7277-7283.

85. Henkels CH, Kurz JC, Fierke CA, Oas TG: Linked folding and anion binding of the Bacillus subtilis ribonuclease P protein. *Biochemistry* 2001, 40:2777-2789.

86. Fang XW, Yang XJ, Littrell K, Niranjanakumari S, Thiyagarajan P, Fierke CA, Sosnick TR, Pan T: The Bacillus subtilis RNase P holoenzyme contains two RNase P RNA and two RNase P protein subunits. *Rna* 2001, 7:233-241.

87. Barrera A, Fang X, Jacob J, Casey E, Thiyagarajan P, Pan T: Dimeric and monomeric Bacillus subtilis RNase P holoenzyme in the absence and presence of pre-tRNA substrates. *Biochemistry* 2002, 41:12986-12994.

88. Hartmann RK, Heinrich J, Schlegl J, Schuster H: Precursor of C4 antisense RNA of bacteriophages P1 and P7 is a substrate for RNase P of Escherichia coli. *Proc Natl Acad Sci U S A* 1995, 92:5822-5826.

89. Hardt WD, Schlegl J, Erdmann VA, Hartmann RK: Role of the D arm and the anticodon arm in tRNA recognition by eubacterial and eukaryotic RNase P enzymes. *Biochemistry* 1993, 32:13046-13053.

90. Zahler NH, Christian EL, Harris ME: Recognition of the 5' leader of pre-tRNA substrates by the active site of ribonuclease P. *Rna* 2003, 9:734-745.

91. Oh BK, Pace NR: Interaction of the 3'-end of tRNA with ribonuclease P RNA. *Nucleic Acids Res* 1994, 22:4087-4094.

92. Hardt WD, Schlegl J, Erdmann VA, Hartmann RK: Kinetics and thermodynamics of the RNase P RNA cleavage reaction: analysis of tRNA 3'-end variants. *J Mol Biol* 1995, 247:161-172.

93. Brannvall M, Pettersson BM, Kirsebom LA: Importance of the +73/294 interaction in Escherichia coli RNase P RNA substrate complexes for cleavage and metal ion coordination. *J Mol Biol* 2003, 325:697-709.

94. Kirsebom LA, Svard SG: Base pairing between Escherichia coli RNase P RNA and its substrate. *Embo J* 1994, 13:4870-4876.

95. Brannvall M, Fredrik Pettersson BM, Kirsebom LA: The residue immediately upstream of the RNase P cleavage site is a positive determinant. *Biochimie* 2002, 84:693-703.

96. Busch S, Kirsebom LA, Notbohm H, Hartmann RK: Differential role of the intermolecular base-pairs G292-C(75) and G293-C(74) in the reaction catalyzed by Escherichia coli RNase P RNA. *J Mol Biol* 2000, 299:941-951.

97. Loria A, Pan T: Recognition of the T stem-loop of a pre-tRNA substrate by the ribozyme from Bacillus subtilis ribonuclease P. *Biochemistry* 1997, 36:6317-6325.

98. Loria A, Pan T: The cleavage step of ribonuclease P catalysis is determined by ribozyme-substrate interactions both distal and proximal to the cleavage site. *Biochemistry* 1999, 38:8612-8620.

99. Fahlman RP, Dale T, Uhlenbeck OC: Uniform binding of aminoacylated transfer RNAs to the ribosomal A and P sites. *Mol Cell* 2004, 16:799-805.

100. LaRiviere FJ, Wolfson AD, Uhlenbeck OC: Uniform binding of aminoacyl-tRNAs to elongation factor Tu by thermodynamic compensation. *Science* 2001, 294:165-168.

101. Lott WB, Pontius BW, von Hippel PH: A two-metal ion mechanism operates in the hammerhead ribozyme-mediated cleavage of an RNA substrate. *Proc Natl Acad Sci U S A* 1998, 95:542-547.

102. Gondert ME, Tinsley RA, Rueda D, Walter NG: Catalytic core structure of the trans-acting HDV ribozyme is subtly influenced by sequence variation outside the core. *Biochemistry* 2006, 45:7563-7573.

103. Smith D, Pace NR: Multiple magnesium ions in the ribonuclease P reaction mechanism. *Biochemistry* 1993, 32:5273-5281.

104. Pan T: Higher order folding and domain analysis of the ribozyme from Bacillus subtilis ribonuclease P. *Biochemistry* 1995, 34:902-909.

105. Cassano AG, Anderson VE, Harris ME: Analysis of solvent nucleophile isotope effects: evidence for concerted mechanisms and nucleophilic activation by metal coordination in nonenzymatic and ribozyme-catalyzed phosphodiester hydrolysis. *Biochemistry* 2004, 43:10547-10559.

106. Kurz JC, Fierke CA: Ribonuclease P: a ribonucleoprotein enzyme. *Curr Opin Chem Biol* 2000, 4:553-558.

107. Shan S, Kravchuk AV, Piccirilli JA, Herschlag D: Defining the catalytic metal ion interactions in the Tetrahymena ribozyme reaction. *Biochemistry* 2001, 40:5161-5171.

108. Christian EL, Smith KM, Perera N, Harris ME: The P4 metal binding site in RNase P RNA affects active site metal affinity through substrate positioning. *Rna* 2006, 12:1463-1467.

109. Getz MM, Andrews AJ, Fierke CA, Al-Hashimi HM: Structural plasticity and Mg2+ binding properties of RNase P P4 from combined analysis of NMR residual dipolar couplings and motionally decoupled spin relaxation. *Rna* 2007, 13:251-266.

110. Gardiner KJ, Marsh TL, Pace NR: Ion dependence of the Bacillus subtilis RNase P reaction. *J Biol Chem* 1985, 260:5415-5419.

111. Reich C, Olsen GJ, Pace B, Pace NR: Role of the protein moiety of ribonuclease P, a ribonucleoprotein enzyme. *Science* 1988, 239:178-181.

112. Record MT, Jr., Anderson CF, Lohman TM: Thermodynamic analysis of ion effects on the binding and conformational equilibria of proteins and nucleic acids: the roles of ion association or release, screening, and ion effects on water activity. *Q Rev Biophys* 1978, 11:103-178.

113. Gluick TC, Gerstner RB, Draper DE: Effects of Mg2+, K+, and H+ on an equilibrium between alternative conformations of an RNA pseudoknot. *J Mol Biol* 1997, 270:451-463.

114. Waugh DS, Pace NR: Gap-scan deletion analysis of Bacillus subtilis RNase P RNA. *Faseb J* 1993, 7:188-195.

115. Kaye NM, Christian EL, Harris ME: NAIM and site-specific functional group modification analysis of RNase P RNA: magnesium dependent structure within the conserved P1-P4 multihelix junction contributes to catalysis. *Biochemistry* 2002, 41:4533-4545.

116. Schmitz M, Tinoco I, Jr.: Solution structure and metal-ion binding of the P4 element from bacterial RNase P RNA. *Rna* 2000, 6:1212-1225.

CHAPTER III

SEQUENCE PREFERENCE IN THE INTERACTION OF BACTERIAL RIBONUCLEASE P WITH PRE-TRNA 5' LEADERS[ii]

Background

5’ leader sequences are removed from precursor tRNA (pre-tRNA) molecules by the ribonucleoprotein enzyme ribonuclease P (RNase P) (for review, see [1-3]). In Bacteria, RNase P is comprised of a single ~400 nucleotide RNA subunit (P RNA) that is catalytic *in vitro*, and a single small (~120 amino acid) protein subunit (P protein) required for activity *in vivo* [4]. Together, these subunits function synergistically in both substrate recognition and catalysis [5-10]. In species such as *Bacillus subtilis* and *Escherichia coli*, RNase P has a broad substrate specificity and correctly processes the products of more than 80 pre-tRNA genes [11,12]. Intriguingly, while several substrate features recognized by RNase P are known, the substrate pools in both of these species

[ii] Chapter II was adapted from the manuscript in preparation entitled “Sequence preference in the interaction of bacterial ribonuclease P with pre-tRNA 5’ leaders” by N.H. Zahler, K.S. Koutmou, J.C. Kurz, J. Sohn, F.E. Campbell, S. Niranjanakumari, M. E. Harris and C.A. Fierke. Nathan H. Zahler wrote the paper, and Kristin S. Koutmou contributed drafts of Figure II-1B, and portions of results and materials and methods sections. Kristin S. Koutmou also participated in editing the manuscript. Results section “Identification of functional groups involved in *B. subtilis* specificity at N(-4)” reported here will appear in a manuscript in preparation entitled “Specific contacts between P protein subunit of *B. subtilis* RNase P and the 5’ leader of pre-tRNA contribute to molecular recognition” by K.S. Koutmou, N.H. Zahler, and C.A. Fierke.

include examples that lack multiple known recognition elements, suggesting the possibility that additional recognition elements remain to be identified [6,11-13].

Previous studies have established that both the RNA and protein subunits of bacterial RNase P contribute to molecular recognition of pre-tRNA substrates. P RNA contacts substrates through both base pairing and backbone interactions. Backbone contacts include interactions with 2' hydroxyls in the acceptor stem and D stem-loop [14]. Proximal to the cleavage site, P RNA base pairs with the substrate nucleotide on the 5' side of the cleavage site (N(-1)); [13,15] and the 3' RCCA substrate motif [16,17]. Together, these interactions contribute to cleavage site specificity and increase substrate binding affinity and catalysis. In addition to RNA-RNA contacts, multiple lines of evidence suggest that P protein contacts the 5' leader of pre-tRNA substrates [6,18-21]. In *B. subtilis* RNase P, the P protein subunit increases binding affinity for substrates with increasing leader length [18]. Numerous biochemical investigations indicate that a large cleft formed by the central β-sheet and α-helix a of P protein is the likely site of P protein•5' leader interactions (Figure II-1A) [20-23]. Specifically, time resolved fluorescence resonance energy transfer (trFRET) experiments indicate that P protein central cleft may contact nucleotides N(-4) through N(-7) (numbering as in Figure II-1) [22]; however, affinity-cleavage assays and molecular modeling suggest that other P protein regions could also interact with nucleotides closer to the pre-tRNA cleavage site [20]. Unlike P RNA, no specific interactions between P protein and pre-tRNA have been identified or characterized, leaving the exact positioning of the 5' leader an open question.

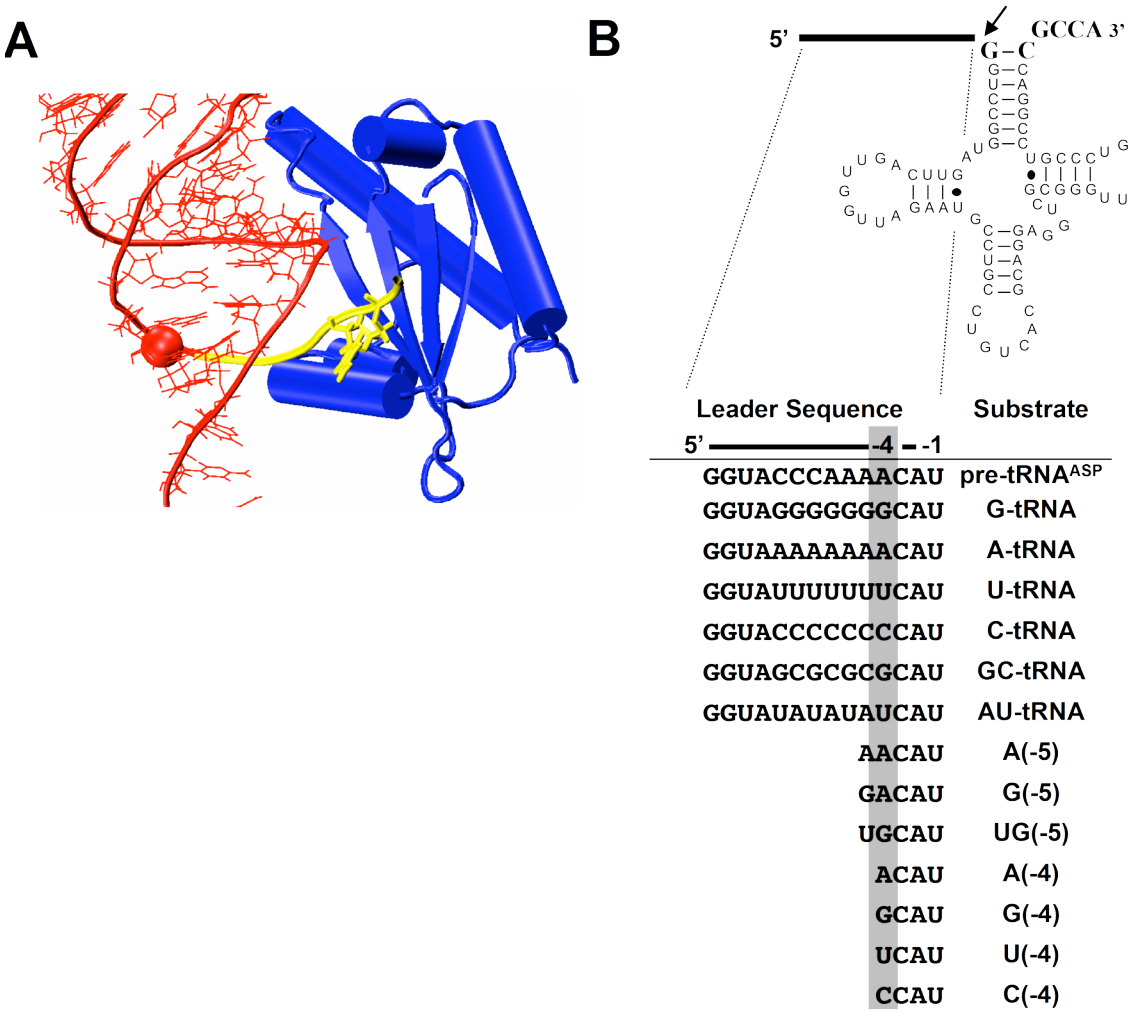

Figure III-1. A) Proposed structure of the interface between pre-tRNA and P protein based on affinity cleavage [20] data showing the mature tRNA section of pre-tRNA (red), P protein (blue) and the pre-tRNA 5' leader backbone (yellow). The position of the RNase P cleavage site is shown by a red sphere, and the position of leader nucleotide N(-4) is shown in yellow. **B)** Structure of substrates based on *B. subtilis* pre-tRNA^{Asp}. The RNase P cleavage site (arrow) and recognition elements near the cleavage site (bold) are indicated on the pre-tRNA secondary structure [14,16,17]. 5' leaders and nomenclature for substrates used in this study are shown.

Through contacts to both pre-tRNA and P RNA, P protein plays an important functional role, modulating several aspects of RNase P catalysis, including binding of divalent metal ions. P protein enhances the affinity of the RNase P holoenzyme for magnesium ions that contribute to substrate binding and catalysis and reduces the monovalent salt requirement for catalysis [24,25]. Notably, P protein also alters the Mn(II) rescue of phosphorothioate substitutions in P RNA helix P4, a region that is a catalytically important divalent metal binding site [3,26-29]. These effects may arise in part from direct interactions between P protein and functionally important metal ions; however biochemical analyses have suggested that P protein also functions as a structural linchpin in the RNase P holoenzyme•pre-tRNA complex, helping to organize the enzyme's active site and enhancing reactivity under physiological conditions [20,30,31].

The importance of P protein for RNase P function *in vivo* was also highlighted by an investigation of naturally occurring and non-canonical pre-tRNA substrates in *E. coli* [6]. Importantly, this study found that the influence of interactions between *E. coli* RNase P and pre-tRNA leaders on the RNase P reaction is both sequence specific and modular. The ability of P protein to enhance substrate affinity and single turnover catalytic rate varies between substrate and is dependent upon the 5' leader sequence. Furthermore, the binding and catalytic enhancements specific to a 5' leader sequence are transferable between substrates independent of the tRNA sequence. Overall, the results suggest the possibility of thermodynamic compensation between mature tRNA and leader sequence elements of pre-tRNA substrates, similar to that previously observed for the aminoacyl tRNA binding protein EF-Tu [32]. This observation also raises the intriguing possibility that the interaction between P protein and substrate leaders may contribute to

substrate specificity; however the complete molecular basis for this discrimination remains to be determined.

Recent analyses of the nucleotide frequency at positions N(-1) through N(-7) in the 5' leader of 161 Bacteria species revealed that more than 91% of species have at least one sequence preference between N(-1) and N(-4) [33]. As already discussed, the reasons for N(-1) conservation are immediately evident, as it base pairs with PRNA to facilitate cleavage site recognition [15]. However, the reasons for sequence preferences at N(-2) through N(-4) have not been clarified. In *B. subtilis* and *E. coli* 30% of pre-tRNAs have a sequence preference at N(-4). At this 5' leader position, *E. coli* has an A / C over G / U preference at this position, while *B. subtilis* exhibits an A / U over G / C preference. Interestingly, the sequence preferences reported in *B. subtilis* genomic analyses were stronger than those observed in *E. coli*.

Here, we investigate the sequence specificity of interactions between Bacterial RNase P and the 5' leaders of pre-tRNA substrates using a biochemical approach. We find that *in vitro B. subtilis* RNase P displays a substrate binding preference for adenosine and discrimination against guanosine at N(-4). The contribution of this interaction to binding affinity is highly dependent upon divalent ion concentrations with a Hill coefficient > 4.5, leading to enhanced A / G discrimination at low (2 to 3.5 mM) divalent ion concentrations. *E. coli* RNase P also exhibits a sequence preference at N(-4) for substrate binding affinity. However, unlike *B. subtilis*, *E. coli* RNase P has a weak preference favoring A and C at N(-4). We altered the structure of the base at N(-4) of pre-tRNA to further characterize the origins of this observed sequence specific recognition at N(-4). These studies reveal that sequence preferences at N(-4) for *B.*

subtilis RNase P can be attributed to a combination of hydrogen bonding and steric interactions between the N(-4) nucleotide and RNase P. Importantly, the specific preferences observed for *B. subtilis* and *E. coli* RNase P *in vitro* are also reflected in the pre-tRNA gene sequences of these species. This correlation suggests that specificity at N(-4) is likely to influence recognition and processing of substrates *in vivo*. Moreover, these results suggest that analyzing the 5' leader sequences of tRNA genes can provide broad insight into RNase P substrate recognition in Bacteria.

Results

Adenosine preference at N(-4) in *B. subtilis* RNase P

Leader sequences rich in A and U have previously been reported to increase substrate binding affinity for *B. subtilis* RNase P [34]; however, the origin of these effects with respect to specific positions within the leader sequence is unclear. The sequence preference can be partially explained by the conserved preference of Bacterial RNase P for a U at position N(-1) [13]. To better assess the ability of *B. subtilis* RNase P to discriminate between substrates based upon leader nucleotides distal to the RNase P cleavage site, we initially examined the influence of block mutations between positions N(-4) and N(-10) of pre-tRNA substrates (Figure II-1B). The region between N(-4) and N(-10) encompasses nucleotides previously hypothesized to interact with P protein, and mutating this region avoids complications due to altering N(-1) [21]. To assess the impact of these mutations on catalysis, single turnover rate constants were determined at saturating enzyme concentrations in the presence of 10 mM Mg(II). Effects on binding affinity were measured using centrifuge gel-filtration chromatography, as previously

described [6,19] (see Materials and Methods). Substrate binding measurements were performed in the presence of Ca(II), which supports RNase P substrate binding but decreases the rate at which substrate is converted to product by several orders of magnitude [35]. Finally, to facilitate interpretation of results, experiments were carried out using *B. subtilis* pre-tRNA^{Asp}, a widely used substrate that is canonical with respect to all known sequence-specific RNase P recognition elements (Figure II-1B).

Table III-1.[iii] Effects of block mutation of leader sequences.

	B. subtilis		*E. coli*
Substrate	$K_{D,\,obs}$ (nM)[a]	k_{obs} (s^{-1})[b]	$K_{D,\,obs}$ (nM)[c]
WT pre-tRNA^{Asp}	0.4 ± 0.2	0.27 ± 0.03	0.4 ± 0.2
G-tRNA	1.7 ± 0.3	0.23 ± 0.06	0.4 ± 0.2
A-tRNA	0.28 ± 0.08	0.26 ± 0.04	0.4 ± 0.2
U-tRNA	0.14 ± 0.02	0.26 ± 0.04	n.d.[d]
C-tRNA	0.5 ± 0.1	0.31 ± 0.04	0.3 ± 0.1
GC-tRNA	0.8 ± 0.2	0.11 ± 0.01	n.d.
AU-tRNA	0.3 ± 0.1	0.35 ± 0.04	n.d.

[a] Reaction Conditions: 10 mM $CaCl_2$, 400 mM KCl, 50 mM MES, 50 mM Tris, pH 6.0, 37˚C.
[b] Reaction Conditions: 10 mM $MgCl_2$, 400 mM KCl, 50 mM MES, 50 mM Tris, pH 6.0, 37˚C.
[c] Reaction Conditions: 10 mM $CaCl_2$, 200 mM KCl, 50 mM MES, 50 mM Tris, pH 6.0, 37˚C.
[d] Values not determined.

As shown in Table II-1, block mutations in 5' leaders decrease substrate binding affinity ($K_{D,obs}$) by up to 10-fold, with little effect (< 2-fold) on single turnover rate constants. A block mutation introducing an all-U (U-tRNA) sequence from N(-4) to N(-10) leads to a small increase in binding affinity. C-tRNA and A-tRNA do not

[iii]Data in Table II-1 collected by J.C. Kurz and J. Sohn

significantly alter binding affinity. However, mutation of the wild type sequence to a sequence composed entirely of G (G-tRNA) leads to a significant, 4-fold increase in $K_{D,obs}$. This result indicates that *B. subtilis* RNase P discriminates against G at one or more positions in the leader sequence. To further investigate this possibility, we examined the effects of 5' leaders with alternating GC or AU sequences (Table II-1 and Figure II-1B, substrates GC-tRNA and AU-tRNA). Consistent with previous results, we observe that a G/C rich leader modestly decreases affinity, while an A/U rich leader results in affinity similar to the already A/U rich wild-type leader sequence. Moreover, the decreased affinity noted for the G/C leader sequence relative to the wild type and all-C sequences suggests that one or more of the nucleotides at N(-4), N(-6) and N(-8) are involved in this sequence selectivity.

Previously, we showed that a functional interaction between pre-tRNA and P protein takes place at or near position N(-5) [18]. Specifically, increasing the leader length of pre-tRNA^{Asp} from four (5'-GCAU-tRNA^{Asp}) to five nucleotides (5'-GACAU-tRNA^{Asp}) increases binding affinity with *B. subtilis* RNase P by 2.2 kcal/mol; no further increase is observed for longer leaders up to 33 nucleotides in length [18]. Accordingly, we investigated the possibility that the sequence preference observed in block mutations arises from positions N(-5) and N(-4) using pre-tRNA^{Asp} substrates bearing 5- and 4-nucleotide leaders, respectively. At 10 mM Ca(II), both A(-5) and G(-5) substrates bind with comparable affinity and $K_{D,obs}$ values < 0.5 nM (data not shown). In contrast, the binding affinity of pre-tRNA^{Asp} with a 4 nucleotide leader shows a minor dependence on the identity of the nucleotide at N(-4) under these conditions. Substrates with an

adenosine at N(-4) bind with a $K_{D,obs}$ of 2.3 ± 0.5 nM, while $K_{D,obs}$ for G(-4) substrates is 5 ± 1 nM, suggesting the possibility of an interaction with this nucleotide.

Folding, substrate binding and the catalytic activity of RNase P are all highly dependent upon divalent metal ion concentrations [24,31,36]. To better assess the ability of the observed sequence preference at N(-4) to influence RNase P molecular recognition *in vivo*, we measured binding affinities for substrates at 2 mM $[Ca(II)]_f$, a concentration that better approximates *in vivo* conditions [37,38]. Correct folding of P RNA also requires the binding of numerous divalent ions [24,39-41]. To correctly fold and equilibrate RNase P at the desired $[Ca(II)]_f$, we implemented a buffer-exchange protocol. PRNA was initially folded according to our standard protocol, diluted into a large volume of buffer containing the desired $[Ca(II)]_f$ and re-concentrated prior to addition of P protein (see Materials and Methods). RNase P prepared in this manner behaved as expected at high $[Ca(II)]_f$. Furthermore, reducing $[Ca(II)]_f$ to 2 mM had little or no impact on the binding of some substrates, indicating that a significant fraction of RNase P prepared is correctly folded under these conditions (See below).

At 2 mM $[Ca(II)]_f$, we observed no significant difference in $K_{D,obs}$ values for substrates that vary the identity of the nucleotide base at N(-5). Substrates with a terminal A, G or U at N(-5) differ by less than 2-fold, indicating that sequence specificity does not involve this position (Table II-2). In contrast, changing the nucleotide base identity at N(-4) for substrates with 4-nucleotide leaders significantly impacts $K_{D,obs}$, with a strong preference for an adenosine at this position (Table II-2). Strikingly, binding affinity for the G(-4) substrate is decreased 20-fold relative to that of A(-4). C(-4) and U(-4) substrates result in intermediate decreases in substrate affinity. Together, these

observations indicate that the sequence specificity observed for the interaction of *B. subtilis* RNase P with substrate 5' leaders results, at least in part, from a significant preference for A over G at N(-4).

Table III-2.[iv] Effects of mutation at N(-4) and N(-5) on RNase P substrate affinity.

	B. subtilis	*E. coli*
Substrate	$K_{D, obs}$ (nM)[a]	$K_{D, obs}$ (nM)[a]
A(-5)	18 ± 4	n.d.[b]
G(-5)	32 ± 10	n.d.
UG(-5)	26 ± 6	n.d.
A(-4)	9 ± 2	35 ± 8
G(-4)	200 ± 20	170 ± 60
U(-4)	70 ± 10	100 ± 30
C(-4)	150 ± 50	54 ± 9

[a] Reaction Conditions: 2 mM $CaCl_2$, 425 mM KCl, 50 mM MES, 50 mM Tris, pH 6.0, 37˚C.
[b] Values not determined.

Comparison with N(-4) sequence preference in *E. coli*

Previously, variations in leader sequence have been reported to alter both substrate binding affinity and single turnover rates of catalysis for the *E. coli* RNase P holoenzyme [6]. We therefore also examined the effects of block mutations in the 5' leader of pre-$tRNA^{Asp}$ on binding to the *E. coli* RNase P holoenzyme. Interestingly, block mutations, including the G-tRNA, A-tRNA, and C-tRNA have no observable effect on binding under our initial experimental conditions (10 mM Ca(II)), suggesting that

interactions with the leader may differ significantly between *B. subtilis* and *E. coli* (Table 1). However, a minor preference at a specific nucleotide, such as N(-4), might be masked under these conditions. We therefore examined the possibility of a preference at N(-4) for *E. coli* RNase P at 2 mM $[Ca(II)]_f$ (Table II-2). Under these conditions, a sequence preference at N(-4) is observed for *E. coli* RNase P; however the energetic contribution of this preference to binding affinity is significantly smaller than that observed for the *B. subtilis* enzyme. At 2 mM $[Ca(II)]_f$, *E. coli* binds A(-4) and C(-4) substrates 2- to 3-fold more tightly than U(-4) and G(-4) substrates. Thus, although both *E. coli* and *B. subtilis* RNase P display sequence preferences at N(-4), they differ both in the preferred base and with respect to the magnitude of the observed preference.

Divalent metal ion dependence of *B. subtilis* nucleotide specificity at N(-4)

An important observation from the data described above is that the value of $K_{D,obs}$ for the G(-4) substrate shows a stronger dependence on $[Ca(II)]_f$ than that of the A(-4) substrate. Lowering $[Ca(II)]_f$ from 10 mM to 2 mM increases $K_{D,obs}$ for the G(-4) substrate by 40-fold, while $K_{D,obs}$ for A(-4) increases by less than 4-fold. Together, these effects increase the A / G preference at N(-4) from 2-fold at 10 mM $[Ca(II)]_f$ to 20-fold at 2 mM $[Ca(II)]_f$. To better understand this interplay between divalent metal ion binding and selectivity at N(-4), we examined the ability of the enzyme to discriminate between A(-4) and G(-4) substrates over a range of $[Ca(II)]_f$. For this experiment, binding affinities were determined using centrifuge gel-filtration columns as described above and

[iv] Data in Table II -2 collected by J.C. Kurz (*B. subtilis* A(-5), G(-5), UG(-5)); N.H. Zahler and K.S. Koutmou (*B. subtilis* A(-4), G(-4), U(-4), C(-4)); K.S. Koutmou (all *E. coli* data).

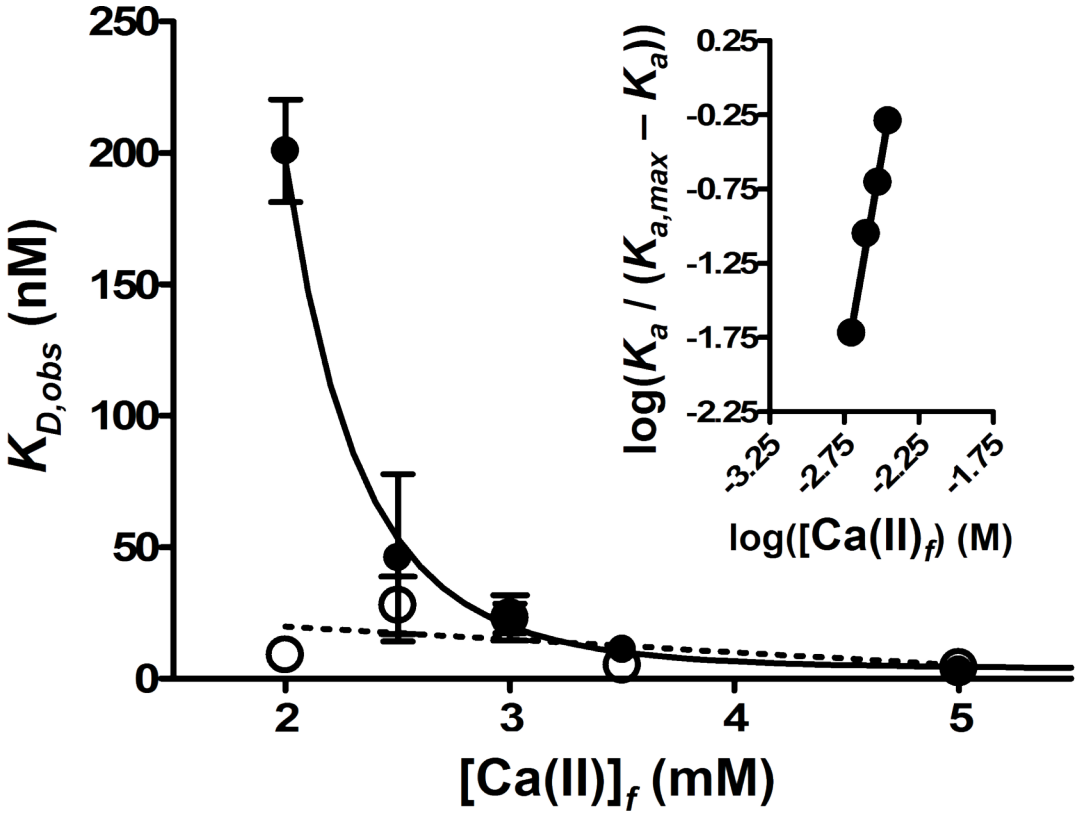

Figure III-2.[v] Dependence of A(-4) and G(-4) Substrate Affinity on Calcium Concentration. $K_{D,obs}$ values for A(-4) (open circles) and G(-4) (filled circles) substrates as a function of $[Ca(II)]_f$. Reaction conditions are 50 mM MES, 50 mM Tris, pH 6.0, 37˚C with indicated $[Ca(II)]_f$ concentrations. KCl concentrations were adjusted to maintain constant ionic strength (See Materials and Methods). Error bars represent the standard deviation of at least three or more independent trials; points with no error bar have uncertainties of less than 5 nM. The best fit of Equation 2 to the G(-4) data is shown as a solid line; a dashed line shows the best linear fit to the A(-4) data. Inset: Hill plot of data for G(-4) between 2 and 5 mM $[Ca(II)]_f$.

[v] Data in Figure II-2 collected by N.H. Zahler and K.S. Koutmou

KCl concentrations were adjusted to maintain constant ionic strength (see Materials and Methods).

Binding affinities for G(-4) and A(-4) substrates were measured at $[Ca(II)]_f$ concentrations between 2 and 10 mM (Figure II-2). $K_{D,obs}$ values for the A(-4) substrate remain relatively constant over this range of Ca(II) concentrations, with only a 4-fold change between values measured at 2 and 10 mM $[Ca(II)]_f$. Binding affinity for the G(-4) substrate, in contrast, decreases significantly at $[Ca(II)]_f$ below 5 mM. This transition shows a cooperative dependence on $[Ca(II)]_f$; fitting the G(-4) data to a cooperative binding isotherm (Equation 2) yields a Hill coefficient (n_H) of 6 ± 1 and a midpoint for the transition ($K_{1/2,Ca}$) of 3.8 ± 0.3 mM. These results indicate that the binding of multiple Ca(II) ions with dissociation constants in the mM range are required for tight binding of the G(-4) substrate. The weak dependence of $K_{D,obs}$ on $[Ca(II)]_f$ for the A(-4) substrate indicates that, if the same set of divalent ions is required for binding of this substrate, they bind to the A(-4) enzyme-substrate complex with significantly higher affinity.

The relatively minor change in the affinity of the A(-4) substrate over this range of $[Ca(II)]_f$ argues that the observed decrease in $K_{D,obs}$ at low $[Ca(II)]_f$ for the G(-4) substrate are due to a specific influence of divalent cations on enzyme-substrate interactions, and not a reduction in the fraction of correctly-folded enzyme at low $[Ca(II)]_f$. Reductions in the fraction of active enzyme would affect $K_{D,obs}$ values for both the A(-4) and G(-4) substrates equally, leading to no change in selectivity. Moreover, previous studies suggest that the *B. subtilis* RNase P holoenzyme is active and correctly folded at these divalent ion concentrations [31,39].

Identification of functional groups involved in *B. subtilis* specificity at N(-4)

To better understand the molecular interactions between P protein and the N(-4) base, and therefore the basis for the observed sequence specificity, we substituted the adenosine at the N(-4) position of the pre-tRNA substrate with a series of adenosine analogs. Specifically, we prepared substrates containing at N(-4) purine (P(-4)), 2-aminopurine (2AP(-4)) and 2,6-diaminopurine (DAP(-4)) (Figure II-3), to systematically vary the presentation of exocyclic amines along the adenosine Watson-Crick face. This series of analogs has been used previously to identify adenosine base functional groups involved in substrate binding and catalysis for P RNA and various other ribozymes [42]. The binding affinities of wild type *B. subtilis* RNase P for substrates with adenosine analogs at N(-4) were determined at 2 mM $[Ca(II)]_f$.

The binding affinities of substrates with adenosine analogue substitution indicate that recognition of adenosine at N(-4) involves two distinct functional groups (Figure II-3). First, a comparison of the affinity of RNase P for pre-tRNA containing adenosine and purine at N(-4) indicates that removal of the N6 exocyclic amine, the binding affinity decreases 3-fold. This suggests a small positive interaction, such as the formation of a hydrogen bond with N6. Second, substitution with 2,6-diaminopurine decreases the binding affinity 4-fold decrease in substrate affinity relative to adenosine, indicating the formation of a modest, unfavorable interaction, such as steric interference involving the N2 exocyclic amine of guanosine. The removal of the N6 exocyclic amine and the addition of the N2 exocyclic amine with 2-diaminopurine substitution leads to a pre-tRNA substrate with a weak affinity, $K_{D,obs}$ = 170 ± 40nM, comparable to that of pre-tRNA containing a guanosine at N(-4). Thus, the binding preference of RNase P for adenosine over guanosine at N(-4) arises from a combination of a positive interaction at

the N6 exocyclic amine in adenosine, likely hydrogen bonding, and a negative interference by the N2 exocyclic amine, likely steric hinderances, in guanosine.

Discussion

Bacterial RNase P has previously been characterized as an enzyme that relies strongly on conserved tertiary structure for substrate recognition. The data presented here, however, emphasize the growing appreciation of the contributions of sequence specificity to RNase P substrate recognition. We have demonstrated nucleotide base selectivity in substrate binding involving an interaction between RNase P and pre-tRNA 5' leader sequences at a discrete position, N(-4). Together with base pairing interactions at N(-1) [13] and with the 3' RCCA motif [16,17], a new picture is emerging in which RNase P recognizes substrates through a combination of structural recognition and sequence specificity proximal to the pre-tRNA cleavage site. Importantly, the *in vitro* measurements presented here and the previously reported genomic analyses indicate that RNase P from different species interact differently with 5' leaders. These results are consistent with the previous suggestion that there may be functional differences in the specific roles of *E. coli* and *B. subtilis* RNase P proteins [31]. When combined with previous results for naturally occurring *E. coli* substrates [6], these data also suggest a model in which RNase P and its substrate population evolve in parallel. In this model, the enzyme and substrates from a given species form a matched set, optimized for uniform substrate recognition and processing. An important implication of this model derives from the broad differences in the genomic composition of pre-tRNA leaders from divergent species. In the absence of a single overarching 5' leader recognition sequence

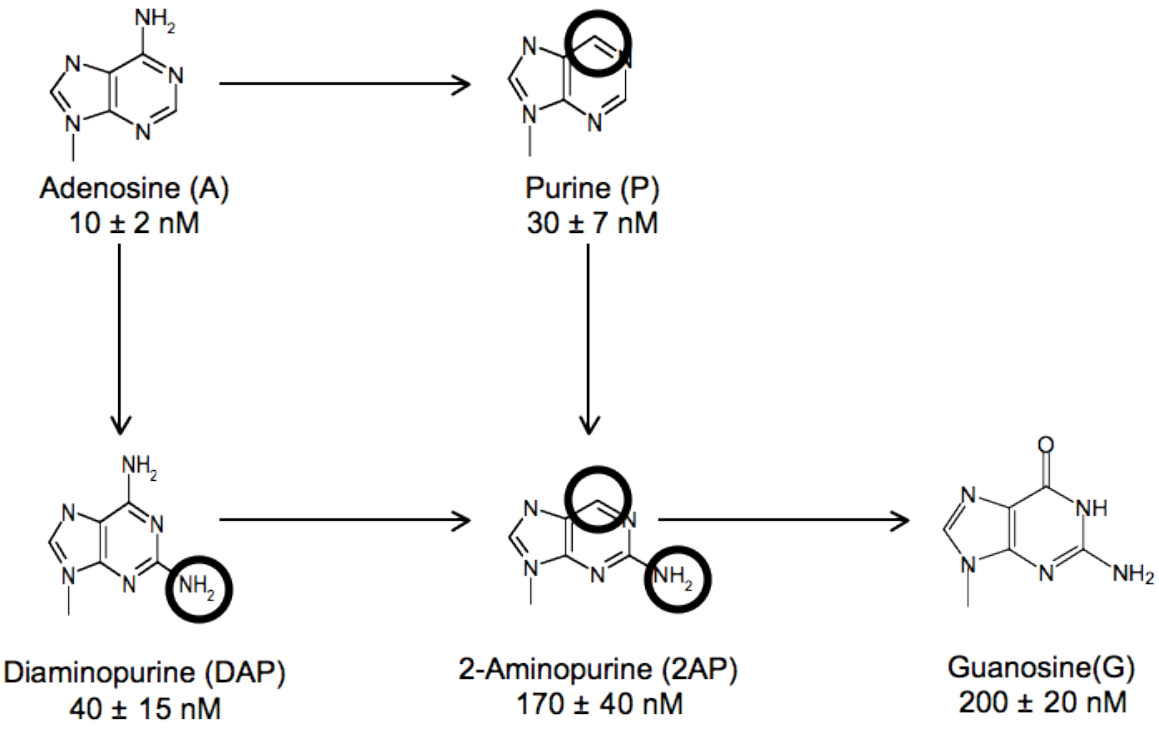

Figure III-3.[vi] Adenosine analogs at N(-4) alter the affinity of pre-tRNA for RNase P. (A) Precursor $tRNA^{Asp}$ substrate possessing a four nucleotide long 5' leader. The N(-4) position is underlined. (B) Structure of the nucleotide bases incorporated at N(-4) of pre-$tRNA^{Asp}$, including: adenosine (A(-4)), guanosine (G(-4)), purine (P(-4)), 2-aminopurine (2AP(-4)), 2,6-diaminopurine (DAP(-4)). The dissociation constants for the wild-type RNase P – substrate complex are measured using gel filtration centrifuge columns in 50 mM MES, 50 mM Tris, 425 mM KCl, 2 mM $CaCl_2$, pH 6.0 at 37°C.

[vi] Data presented in Figure II-3 collected by N.H. Zahler and K.S. Koutmou

for all Bacteria, information regarding enzyme - substrate interactions is most likely to be gained from investigations of cognate RNase P / pre-tRNA pairings using naturally occurring 5' leader sequences.

Our results indicate that RNase P from both *B. subtilis* and *E. coli* display a sequence preference at N(-4) that contributes to molecular recognition of substrates. For *B. subtilis* this interaction results in a 2 kcal / mol binding preference for A(-4) over G(-4) substrates at 2 mM $[Ca(II)]_f$, while *E. coli* shows a preference for A and C at this position. In *B. subtilis*, this sequence specificity is consistent with and explains previous analyses that implicated N(-5) in interactions with P protein [18]. Previously, substrates with 5-nucleotide leaders were shown to bind to the RNase P holoenzyme with higher affinity than those with 4-nucleotide leaders [18]. However, the sequence of 4- and 5-nucleotide 5' leaders used in the previous investigation were 5'-GCAU and 5'-GACAU, respectively, which vary the nucleobase at N(-4) from G to A. Comparison of $K_{D,obs}$ values for the G(-4), A(-4) and G(-5) substrates (Table II-2) reveals that the entirety of the previously observed binding enhancement can be accounted for by this change at N(-4). Furthermore, in the context of an A at N(-4), the addition of a G at N(-5) has a mild destabilizing, rather than a strong stabilizing, effect.

In the present study, the use of adenosine analogs at N(-4) in pre-tRNA demonstrates that *B. subtilis* RNase P forms a favorable interaction with the N6 exocyclic amine of adenosine of ~ 0.7 kcal/mol ($\Delta\Delta G^{P(-4)/A(-4)}$) and an unfavorable interaction with the N2 amine of 2-aminopurine of ~ 0.9 kcal/mol ($\Delta\Delta G^{DAP(-4)/A(-4)}$) (Figure II-3). A possible model to explain these data is the formation of a favorable hydrogen bond between the P protein and N6 exocyclic amine at N(-4) and an unfavorable steric

interaction with functional groups at C2 (amine or carbonyl). The calculated $\Delta\Delta G^{P(-4)/A(-4)}$ is consistent with previously reported ΔΔG values for the loss of a hydrogen bond between an uncharged side chain and a substrate (0.5 to 1.5 kcal/mol) [43-45]. Together, these interactions result in a 2 kcal / mol binding preference for A(-4) over G(-4) substrates at 2 mM $[Ca(II)]_f$. Identifying where N(-4) is making hydrogen bonding contacts with *B. subtilis* RNase P will be further addressed in Chapter III.

Another important conclusion from our experiments is that sequence specific interactions with the 5' leader are coupled to the binding of divalent metal ions. Binding of the G(-4) substrate shows a large (n_H = 5) dependence on $[Ca(II)]_f$ with a transition in the low mM range ($K_{1/2,Ca}$ = 3.4 + 0.3 mM). In contrast, binding of the A(-4) substrate varies little over this range of $[Ca(II)]_f$. Previously, we have shown that the Mg(II) dependence observed for RNase P single turnover rate constants varies with substrate leader length. Cleavage of substrates with short (2-nucleotide) leaders requires higher Mg(II) concentrations than the processing of substrates with longer (5-nucleotide) leaders [24]. While this previous observation linked divalent metal binding and interactions with the 5' leader, the current data demonstrate that this linkage is sequence specific, and dependent on the formation of interactions with N(-4). This coupling of sequence specificity and divalent metal binding results in a higher degree of sequence selectivity at low cation concentrations. In practical terms, this leads to an absence of selectivity at N(-4) under *in vitro* conditions commonly employed in the study of the RNase P holoenzyme, which often include 10 to 20 mM divalent metal ion [3]. In addition, the steep dependence of G(-4) binding on $[Ca(II)]_f$ suggests that interactions with the leader

sequence, and particularly with N(-4), are linked to a conformational change that results in the binding of multiple, additional divalent cations.

Previous genomic analysis of pre-tRNA genes from *B. subtilis* and *E. coli* revealed that in both of these species N(-4) is significantly enriched in nucleotides found to be favorable for binding *in vitro* [33]. This correlation is consistent with interactions with N(-4) playing a functional role in substrate recognition for both species *in vivo*. Furthermore, the agreement between sequence analysis and *in vitro* measurement at both N(-1) [13] and N(-4) demonstrates a correlation between genomic sequences and functional parameters, including substrate binding and cleavage site selection. However, unlike N(-1), the preferences observed *in vitro* at N(-4) vary markedly between *B. subtilis* and *E. coli* RNase P. These differences are reflected in the corresponding genomic analyses, representing a covariation that lends weight to the validity of this approach. A second factor lending weight to the applicability of pre-tRNA gene analysis is an increase in the number of species showing nucleotide enrichment in the 5' leader near the pre-tRNA cleavage site. This observation suggests that, while it may not be the only factor influencing 5' leader selection in a given species, substrate recognition by RNase P is a driving force in pre-tRNA gene evolution for Bacteria in general. Systematic examination of the impact of potential interactions between RNase P and additional 5' leader positions therefore remains a key goal for better understanding substrate recognition by RNase P *in vivo*.

Materials and Methods

Chemicals and Buffers

All chemicals purchased were of the highest commercially available purity. Nucleotide triphosphates were purchased from Amersham BioScience (Piscataway, NJ); calf intestinal alkaline phosphatase, T4 polynucleotide kinase, and restriction enzymes were purchased from New England Biolabs (Ipswich, MA). RNA oligonucleotides were purchased from Dharmacon Inc (Lafayette CO). All buffers were made using deionized water (Milli-Q system; Millipore Corp, Billerica, MA).

RNA and protein preparation[vii]

B. subtilis PRNA, *E. coli* M1 RNA, and pre-tRNA substrates with 5' terminal guanosine residues (G-tRNA, A-tRNA, C-tRNA, U-tRNA, AU-tRNA, GC-tRNA, G(-5) and G(-4)) were prepared by *in vitro* transcription using linearized DNA templates and T7 RNA polymerase according to standard procedures [46]. Substrates were 5' end-labeled using γ-^{32}P-ATP and T4 polynucleotide kinase [19]. Pre-tRNA substrates with 5' terminal nucleotides other than guanosine (A(-5), UG(-5), A(-4), C(-4), U(-4)) were prepared by RNA ligation. 5' oligoribonucleotides comprising the 5' leader and position +1 through +5 of pre-tRNA^{Asp} were initially 5' end-labeled using γ-^{32}P-ATP and T4 polynucleotide kinase, and ligated to a 3' tRNA fragment encoding positions +6 through +77 using splinted ligation according to standard protocols [47-49].

B. subtilis P protein was prepared as described previously [50]. P protein was expressed in *E. coli* (BL21(DE3) pLysS) grown at 37 °C to an OD_{600} of 0.6-0.8 and induced with 0.4 mM isopropylthio-β-D-galactopyranoside. P protein was purified by CM-Sepharose ion-exchange chromatography in the presence of urea [50]. *E. coli* P

protein was prepared using the Impact expression system (New England Biolabs) as described previously [51]. Prior to use, RNase P protein components were dialyzed overnight against the appropriate reaction buffer and final concentrations were determined by absorbance (*B. subtilis* P protein: $\varepsilon_{280} = 5120\ M^{-1}\ cm^{-1}$; *E. coli* C5 protein $\varepsilon_{280} = 5500\ M^{-1}\ cm^{-1}$ [50].

P RNA and pre-tRNAs were renatured by heating to 95 ˚C for 3 min in reaction buffer lacking divalent metal ions then incubated at 37 ˚C for 10 min. Divalent metals were added to the appropriate final concentration, and RNAs were incubated for 30 min. To obtain correct $[Ca(II)]_f$ in the presence of high concentrations of PRNA, we employed a buffer-exchange step in PRNA folding [24]. Briefly, PRNA was renatured as described above, then diluted into 1 to 3 ml of the appropriate final reaction buffer. The PRNA solution was then reconcentrated using Amicon ultra centrifugal filter units (10,000 molecular weight cut-off; Millipore). This process was repeated a minimum of three times. RNA concentrations were subsequently determined by absorbance and RNase P holoenzyme (0.5 to 10 μM) was formed by mixing equimolar concentrations of PRNA and P protein and incubated at 37 ˚C for a minimum of 30 minutes.

Substrate Affinity Measurements

Equilibrium binding measurements were carried out by centrifuge gel-filtration using Sephadex G-75 resin (Sigma-Aldrich) [6,19] with total substrate concentrations ($[S_{tot}]$) maintained at < 20% of the lowest total enzyme concentration in an experiment. Enzyme and substrate were renatured separately, mixed and incubated at 37 ˚C for 5 min

[vii] *E. coli* protein was prepared by F.E. Campbell

prior to loading onto pre-equilibrated columns. Columns were centrifuged at 6 krpm for 30 sec. Observed dissociation constants were determined by fitting Equation II-1 to the number of counts retained on the column, where cpm_{ret} is the number of counts retained on the column, cpm_{ft} is the number of counts in the flow through, $K_{D,obs}$ is the observed

Equation III-1

$$\frac{[ES]}{[S_{tot}]} \propto \frac{cpm_{ft}}{cpm_{ft} + cpm_{ret}} = A\frac{[E_{tot}]}{[E_{tot}] + K_{D,obs}} + B$$

dissociation constant, $[ES]$ is the concentration of bound substrate, $[S_{tot}]$ is the total substrate concentration, $[E_{tot}]$ is the total enzyme concentration, A is the amplitude of the binding curve in cpm, and B is the background number of counts that elute in the absence of enzyme. Buffer conditions for binding experiments were as indicated in the text and figure legends.

For $[Ca(II)]_f$ titration experiments, the combined contribution of $CaCl_2$ and KCl to ionic strength was held constant at 410 mM: at 2 mM $[Ca(II)]_f$, [KCl] = 405 mM; at 5 mM $[Ca(II)]_f$, [KCl] = 396 mM. For the G(-4) substrate, values for the midpoint of the transition ($K_{1/2,Ca}$) and Hill coefficients (n_H) were determined by fitting $K_{D,obs}$ values to Equation II-2, where $K_{D,\infty}$ is the dissociation constant at saturating $[Ca(II)]_f$.

Equation III-2

$$K_{D,obs} = K_{D,\infty}\left(1 + \frac{K_{1/2,Ca}^{n_H}}{[Ca(II)]_f^{n_H}}\right)$$

Single-Turnover Kinetic Measurements

Single turnover experiments were performed in 10 mM $MgCl_2$, 400 mM NH_4Cl, and 50 mM MES-Tris buffer, pH 6.0 at 37 °C using saturating RNase P holoenzyme (400 nM) as previously described [24]. Substrate and product were separated by PAGE, and quantified by PhosphorImager (Amersham Bioscience Corp, Piscataway, NJ), and observed rate constants (k_{obs}) were determined by fitting Equation II-3 to fraction cleaved (F_c), where A is the total extent of the reaction and B is the amplitude of the exponential phase.

Equation III-3

$$F_c = A - Be^{-k_{obs}t}$$

References for Chapter II

1. Smith JK, Hsieh J, Fierke CA: Importance of RNA-protein interactions in bacterial ribonuclease P structure and catalysis. *Biopolymers* 2007, 87:329-338.

2. Kirsebom LA: RNase P RNA mediated cleavage: substrate recognition and catalysis. *Biochimie* 2007, 89:1183-1194.

3. Christian EL, Zahler NH, Kaye NM, Harris ME: Analysis of substrate recognition by the ribonucleoprotein endonuclease RNase P. *Methods* 2002, 28:307-322.

4. Gossringer M, Kretschmer-Kazemi Far R, Hartmann RK: Analysis of RNase P protein (rnpA) expression in Bacillus subtilis utilizing strains with suppressible rnpA expression. *J Bacteriol* 2006, 188:6816-6823.

5. Beebe JA, Fierke CA: A kinetic mechanism for cleavage of precursor tRNA(Asp) catalyzed by the RNA component of Bacillus subtilis ribonuclease P. *Biochemistry* 1994, 33:10294-10304.

6. Sun L, Campbell FE, Zahler NH, Harris ME: Evidence that substrate-specific effects of C5 protein lead to uniformity in binding and catalysis by RNase P. *Embo J* 2006, 25:3998-4007.

7. Peck-Miller KA, Altman S: Kinetics of the processing of the precursor to 4.5 S RNA, a naturally occurring substrate for RNase P from Escherichia coli. *J Mol Biol* 1991, 221:1-5.

8. Kirsebom LA, Svard SG: The kinetics and specificity of cleavage by RNase P is mainly dependent on the structure of the amino acid acceptor stem. *Nucleic Acids Res* 1992, 20:425-432.

9. Liu F, Altman S: Differential evolution of substrates for an RNA enzyme in the presence and absence of its protein cofactor. *Cell* 1994, 77:1093-1100.

10. Loria A, Pan T: Modular construction for function of a ribonucleoprotein enzyme: the catalytic domain of Bacillus subtilis RNase P complexed with B. subtilis RNase P protein. *Nucleic Acids Res* 2001, 29:1892-1897.

11. Lowe TM, Eddy SR: tRNAscan-SE: a program for improved detection of transfer RNA genes in genomic sequence. *Nucleic Acids Res* 1997, 25:955-964.

12. Sprinzl M, Vassilenko KS: Compilation of tRNA sequences and sequences of tRNA genes. *Nucleic Acids Res* 2005, 33:D139-140.

13. Zahler NH, Christian EL, Harris ME: Recognition of the 5' leader of pre-tRNA substrates by the active site of ribonuclease P. *Rna* 2003, 9:734-745.

14. Pan T, Loria A, Zhong K: Probing of tertiary interactions in RNA: 2'-hydroxyl-base contacts between the RNase P RNA and pre-tRNA. *Proc Natl Acad Sci U S A* 1995, 92:12510-12514.

15. Zahler NH, Sun L, Christian EL, Harris ME: The pre-tRNA nucleotide base and 2'-hydroxyl at N(-1) contribute to fidelity in tRNA processing by RNase P. *J Mol Biol* 2005, 345:969-985.

16. Tallsjo A, Kirsebom LA: Product release is a rate-limiting step during cleavage by the catalytic RNA subunit of Escherichia coli RNase P. *Nucleic Acids Res* 1993, 21:51-57.

17. Kirsebom LA, Svard SG: Base pairing between Escherichia coli RNase P RNA and its substrate. *Embo J* 1994, 13:4870-4876.

18. Crary SM, Niranjanakumari S, Fierke CA: The protein component of Bacillus subtilis ribonuclease P increases catalytic efficiency by enhancing interactions with the 5' leader sequence of pre-tRNAAsp. *Biochemistry* 1998, 37:9409-9416.

19. Kurz JC, Niranjanakumari S, Fierke CA: Protein component of Bacillus subtilis RNase P specifically enhances the affinity for precursor-tRNAAsp. *Biochemistry* 1998, 37:2393-2400.

20. Niranjanakumari S, Day-Storms JJ, Ahmed M, Hsieh J, Zahler NH, Venters RA, Fierke CA: Probing the architecture of the B. subtilis RNase P Holoenzyme active site by crosslinking and affinity cleavage. *Rna* 2007, 13:512-535.

21. Niranjanakumari S, Stams T, Crary SM, Christianson DW, Fierke CA: Protein component of the ribozyme ribonuclease P alters substrate recognition by directly contacting precursor tRNA. *Proc Natl Acad Sci U S A* 1998, 95:15212-15217.

22. Rueda D, Hsieh J, Day-Storms JJ, Fierke CA, Walter NG: The 5' Leader of Precursor tRNA(Asp) Bound to the Bacillus subtilis RNase P Holoenzyme Has an Extended Conformation. *Biochemistry* 2005, 44:16130-16139.

23. Stams T, Niranjanakumari S, Fierke CA, Christianson DW: Ribonuclease P protein structure: evolutionary origins in the translational apparatus. *Science* 1998, 280:752-755.

24. Kurz JC, Fierke CA: The affinity of magnesium binding sites in the Bacillus subtilis RNase P x pre-tRNA complex is enhanced by the protein subunit. *Biochemistry* 2002, 41:9545-9558.

25. Gardiner KJ, Marsh TL, Pace NR: Ion dependence of the Bacillus subtilis RNase P reaction. *J Biol Chem* 1985, 260:5415-5419.

26. Sun L, Harris ME: Evidence that binding of C5 protein to P RNA enhances ribozyme catalysis by influencing active site metal ion affinity. *Rna* 2007.

27. Crary SM, Kurz JC, Fierke CA: Specific phosphorothioate substitutions probe the active site of Bacillus subtilis ribonuclease P. *Rna* 2002, 8:933-947.

28. Christian EL, Kaye NM, Harris ME: Helix P4 is a divalent metal ion binding site in the conserved core of the ribonuclease P ribozyme. *Rna* 2000, 6:511-519.

29. Kaye NM, Christian EL, Harris ME: NAIM and site-specific functional group modification analysis of RNase P RNA: magnesium dependent structure within the conserved P1-P4 multihelix junction contributes to catalysis. *Biochemistry* 2002, 41:4533-4545.

30. Buck AH, Kazantsev AV, Dalby AB, Pace NR: Structural perspective on the activation of RNase P RNA by protein. *Nat Struct Mol Biol* 2005.

31. Buck AH, Dalby AB, Poole AW, Kazantsev AV, Pace NR: Protein activation of a ribozyme: the role of bacterial RNase P protein. *Embo J* 2005, 24:3360-3368.

32. LaRiviere FJ, Wolfson AD, Uhlenbeck OC: Uniform binding of aminoacyl-tRNAs to elongation factor Tu by thermodynamic compensation. *Science* 2001, 294:165-168.

33. Zahler NH, Koutmou KS, Kurz JC, Sohn J, Campbell FE, Niranjanakumari S, Harris ME, Fierke CA: Sequence Preference in the Interaction of Bacterial Ribonuclease P with pre-tRNA 5' Leaders. *in preparation* 2008.

34. Loria A, Niranjanakumari S, Fierke CA, Pan T: Recognition of a pre-tRNA substrate by the Bacillus subtilis RNase P holoenzyme. *Biochemistry* 1998, 37:15466-15473.

35. Smith D, Pace NR: Multiple magnesium ions in the ribonuclease P reaction mechanism. *Biochemistry* 1993, 32:5273-5281.

36. Smith D, Burgin AB, Haas ES, Pace NR: Influence of metal ions on the ribonuclease P reaction. Distinguishing substrate binding from catalysis. *J Biol Chem* 1992, 267:2429-2436.

37. Outten CE, O'Halloran TV: Femtomolar sensitivity of metalloregulatory proteins controlling zinc homeostasis. *Science* 2001, 292:2488-2492.

38. Maguire ME, Cowan JA: Magnesium chemistry and biochemistry. *Biometals* 2002, 15:203-210.

39. Pan T, Sosnick TR: Intermediates and kinetic traps in the folding of a large ribozyme revealed by circular dichroism and UV absorbance spectroscopies and catalytic activity. *Nat Struct Biol* 1997, 4:931-938.

40. Fang XW, Pan T, Sosnick TR: Mg2+-dependent folding of a large ribozyme without kinetic traps. *Nat Struct Biol* 1999, 6:1091-1095.

41. Zarrinkar PP, Wang J, Williamson JR: Slow folding kinetics of RNase P RNA. *Rna* 1996, 2:564-573.

42. Siew D, Zahler NH, Cassano AG, Strobel SA, Harris ME: Identification of adenosine functional groups involved in substrate binding by the ribonuclease P ribozyme. *Biochemistry* 1999, 38:1873-1883.

43. Sheh-Yi Sheu D-YY, H. L. Selzle, and E. W. Schlag: Energetics of hydrogen bonds in peptides. *Proceedings of the National Academy of Sciences of the United States of America* 2003, 100:12683–12687.

44. Fersht AR SJ, Knill-Jones J, Lowe DM, Wilkinson AJ, Blow DM, Brick P, Carter P, Waye MM, Winter G: Hydrogen bonding and biological specificity analysed by protein engineering. *Nature* 1985, 314:235-238.

45. Silverman SK, Cech TR: Energetics and cooperativity of tertiary hydrogen bonds in RNA structure. *Biochemistry* 1999, 38:8691-8702.

46. Milligan JF, Uhlenbeck OC: Determination of RNA-protein contacts using thiophosphate substitutions. *Biochemistry* 1989, 28:2849-2855.

47. Moore MJ, Query CC: Joining of RNAs by splinted ligation. *Methods Enzymol* 2000, 317:109-123.

48. Moore MJ, Sharp PA: Site-specific modification of pre-mRNA: the 2'-hydroxyl groups at the splice sites. *Science* 1992, 256:992-997.

49. Loria A, Pan T: Recognition of the T stem-loop of a pre-tRNA substrate by the ribozyme from Bacillus subtilis ribonuclease P. *Biochemistry* 1997, 36:6317-6325.

50. Niranjanakumari S, Kurz JC, Fierke CA: Expression, purification and characterization of the recombinant ribonuclease P protein component from Bacillus subtilis. *Nucleic Acids Res* 1998, 26:3090-3096.

51. Guo X, Campbell FE, Sun L, Christian EL, Anderson VE, Harris ME: RNA-dependent folding and stabilization of C5 protein during assembly of the E. coli RNase P holoenzyme. *J Mol Biol* 2006, 360:190-203.

CHAPTER IV

SPECIFIC CONTACTS BETWEEN THE P PROTEIN SUBUNIT OF *BACILLUS SUBTILIS* RNASE P AND THE 5' LEADER OF PRE-TRNA CONTRIBUTE TO MOLECULAR RECOGNITION

Background

Ribonucleoprotein complexes (RNPs) are responsible for numerous essential cellular processes, including protein synthesis, mRNA splicing, and tRNA maturation [1-3]. Ribonuclease P (RNase P) is the RNP that catalyzes the cleavage of an extraneous 5' leader from all nuclear encoded precursor tRNAs (pre-tRNAs) on the pathway to forming mature tRNA required for translation; this is the only universally conserved step in tRNA maturation [4,5]. Bacterial RNase P consists of a single large RNA (P RNA, ~400 nucleotides) that is catalytically active *in vitro* and a smaller, protein subunit that is required for function *in vivo* (P protein, ~120 amino acids, Figure III-1) [6]. P RNA has two independently folding domains, the specificity and catalytic domain [7,8]. The catalytic domain contains the ribozyme portion of the molecule, and is where the bacterial protein binds to P RNA [9]. Recent crystal structures of two bacterial RNase Ps revealed a conserved catalytic core structure comprised of coaxial stacked helices P1/P4/P5, P2/P3, and P8/P9 [10-12]. The protein structure has three distinct regions: the

highly conserved RNR motif, central cleft, and metal binding loop (Figure I-3). Although not the catalytic subunit of the RNP, the P protein has a profound and vital effect on the affinity of RNase P for both metals and substrates [13-16]. However, the role of the protein in molecular recognition by RNase P has not yet been fully deciphered.

Both subunits of RNase P are important for the recognition of pre-tRNA substrates. Thus far only specific contacts between P RNA and pre-tRNA have been described [14,16-18]. P RNA recognizes the pre-tRNA T-stem loop, acceptor stem, cleavage site, N(-1) nucleotide, and the conserved terminal 3' CCA sequence [9,19-25]. In RNase P protein, residues in the central cleft and the RNR motif labeled with a cross-linker or affinity cleavage reagent interact with the leader of pre-tRNA [26-28]. Further biochemical data indicate that the bacterial P protein enhances pre-tRNA affinity through an interaction with the 5' leader [14,16,29].

There is emerging evidence that the bacterial RNase P protein recognizes the sequence of 5' leaders [29-31]. In particular, P protein enhances the binding affinity of pre-tRNA with leaders at least four nucleotides in length [16]. RNase P holoenzyme, but not P RNA alone, binds all pre-tRNAs with a fairly uniform affinity that is dependent on the sequence of both the 5' leader and the mature tRNA portions of pre-tRNA [29]. Certain 5' leader sequences specifically enhance the affinity of pre-tRNA for the holoenzyme relative to P RNA. These data suggest that sequence specific interactions between the 5' leader and the P protein subunit assist in substrate recognition by RNase P. A recent genomic analysis of the leader sequences of pre-tRNA from *B. subtilis* demonstrated a sequence preference in the leader at N(-1) (U), N(-2) (A), and N(-4) (U/A) [31]. Importantly, the relative binding affinities of RNase P for pre-tRNA

substrates varying only in the nucleotide at N(-4) where A>U>C>G, consistent with the sequence preference observed in the genomic data [31]. On a molecular level, the sequence preferences at N(-4) have been attributed to a combination of hydrogen bonding and steric interactions between the N(-4) nucleotide and *B. subtilis* RNase P protein (see Chapter II) [32].

Distance measurements using time resolved fluorescence resonance energy transfer between discrete positions on the 5' leader of pre-tRNA and multiple protein side chains suggest that the N(-4) position of the 5' leader interacts with the protein central cleft [33]. A recent current structural model of the *B. subtilis* RNase P holoenzyme•pre-tRNA complex based on affinity cleavage and cross-linking data also places the N(-4) position in close proximity to the central cleft (Figure III-1) [26,34]. However, these data do not reveal the molecular interactions between the N(-4) nucleotide and P protein that promote sequence specific recognition.

Here we alter the structure of both the base at N(-4) of pre-tRNA and the side chains in the P protein subunit to characterize contacts that lead to sequence specific recognition by RNase P. Alanine and cysteine scanning mutagenesis of the P protein identified side chains in the central cleft and RNR motif as important for high affinity binding of pre-tRNA^{Asp}. Deletion of side chains at three positions, F20, Y34, and R60, also remove the preferential binding of A(-4) pre-tRNA relative to G(-4) pre-tRNA suggesting that these groups are important for sequence specific recognition. However, structural models indicate that only F20 and Y34 are located close enough to the pre-tRNA leader in the ES complex to form a direct contact [26,33]. Deletion of a hydroxyl group in the Y34F P protein also significantly reduces sequence specific recognition in

A

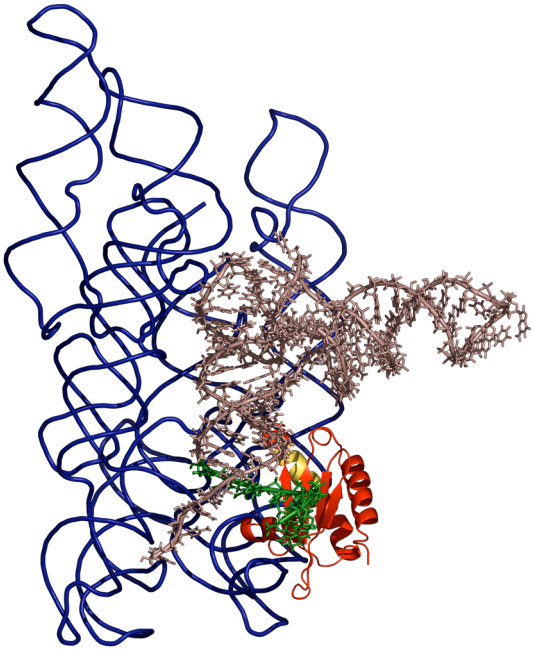

B

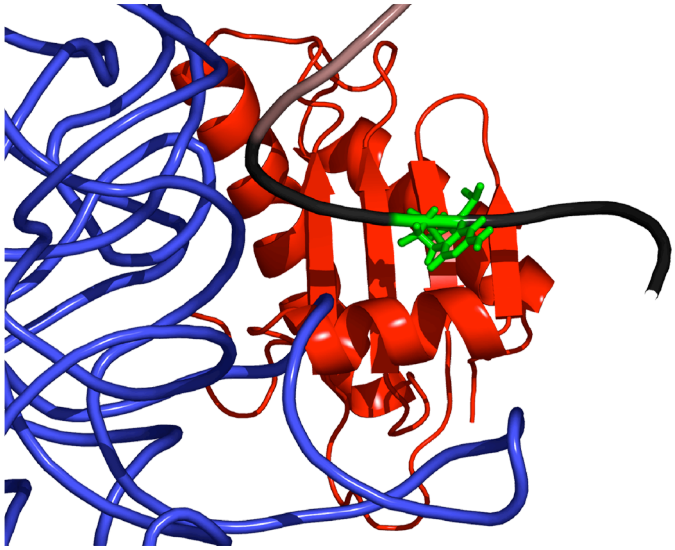

Figure IV-1. (A) Structural model of *B. subtilis* RNase P with pre-tRNA^{Asp} bound derived from affinity cleavage and cross-linking data [26]. P RNA is shown in blue, P protein in red, and tRNA^{Asp} in brown. The 5' leader of the substrate is highlighted in green. The most highly conserved protein region, the RNR motif, is in yellow. **(B)** View of *B. subtilis* RNase P protein (red) and pre-tRNA 5' leader (black) from the *B. subtilis* holoenzyme model (P RNA in blue) [35]. The N(-4) position is highlighted in green.

the mutant RNase P, suggesting that a hydrogen bond between the hydroxyl of Y34 and the base at N(-4) contributes to the recognition of adenosine at this position.

Results

Mapping the *B. subtilis* RNase P Protein Interaction with G(-4)

Structural models of the RNase P•pre-tRNA complex place the pre-tRNA leader near the P protein central cleft and RNR motif, and the 3' end of tRNA near the central cleft [26,27,33]. However, the particular interactions between the P protein and pre-tRNA that enhance binding affinity have not been characterized. Therefore, we measured the binding affinities of *B. subtilis* RNase P reconstituted with P protein containing site-specific mutants for a *B. subtilis* pre-tRNA^{Asp} substrate containing a four nucleotide long leader (G(-4)).

To begin with we used a previously prepared library of single cysteine substitutions in P protein, with mutations in three regions of the protein: central cleft, RNR motif, and metal binding loop (Table III-1, Figure III-2) [26]. These mutations were selected for study because they had been previously been shown to not disrupt the catalytic activity of RNase P [16,26]. The binding affinity was measured in the presence of 3.5 mM $[Ca(II)]_f$, where the $K_{D,obs}$ of the wild type holoenzyme for G(-4) pre-tRNA is 11 nM. Calcium was used because it substitutes for magnesium by reducing the rate of pre-tRNA cleavage by ~10^4-fold without lowering the affinity of P RNA for pre-tRNA [36]. These data (Table III-1) indicate that only mutations in the RNR motif and parts of the central cleft of P protein significantly alter the affinity (> 3- fold) of RNase P for pre-tRNA^{Asp}.

Table IV-1. Affinities of RNase P containing either a wild type or mutant P protein subunit for the G(-4) pre-tRNA.

	$K_{D,G(-4)}$ (nM)[a]	Fold Decrease
Wild Type	11 ± 3	---
K12C	61 ± 8	6
D15C	9 ± 3	---
F16C	285 ± 60	25
F20C	360 ± 100	30
S25C	14 ± 6	---
A27C	50 ± 18	5
V32C	65 ± 15	6
Q38C	12 ± 5	---
R45C	120 ± 60	11
S49C	150 ± 50	14
S51C	85 ± 15	8
A57C	12 ± 3	---
R62C	110 ± 10	10
R68C	500 ± 170	50
A70C	20 ± 7	---
I86C	105 ± 35	10
R88C	25 ± 8	---

[a] 50 mM MES, 50 mM Tris, 400 mM KCl, 3.5 mM $CaCl_2$, 37°C, pH 6.0

The magnitude of the effect of each mutation on pre-tRNA affinity was mapped onto the P protein structure to visualize regions of the protein that might contact the pre-tRNA (Figure III-2A). Cysteine substitutions that have a negligible (< 3- fold) effect on pre-tRNA affinity are located primarily on the 4th β-strand of the central cleft or in the metal binding loop. Mutations in P protein that decrease pre-tRNA binding affinity by 3 to 15-fold are located in the central cleft (K12, A27, V32, R45, S49, S51, and I86) and the RNR motif (R62) (Figure III-3A). Only three mutations increase the value of $K_{D,\,obs}$ for pre-tRNA more than 25-fold, F16C, F20C, and R68C. Both F16 and F20 are on the central cleft α-helix, and are positioned to interact with the 5' leader in structural models [26,33]. The third highly perturbing mutation, R68C, is in the RNR motif, which is near P RNA and N(-2) in the models. In summary, the affinity of RNase P for G(-4) pre-tRNA is most disrupted by side chain substitutions in the RNR motif, and the central cleft α-helix and first three beta strands, suggesting that the pre-tRNA makes energetically favorable contacts with these regions of the protein. These data are consistent with previous cross-linking, affinity cleavage, and time-resolved FRET studies suggesting that the 5' leader is located near the central cleft and RNR motif of the protein [26,33].

F20A, Y34A, and R60A P protein mutations disrupt N(-4) sequence specific recognition

To further evaluate interactions between the P protein and pre-tRNA in RNase P, we prepared single site alanine mutants in the P protein. In addition to the sites identified by the cysteine scanning mutagenesis as significantly impacting substrate affinity (F16, F20, R68, and S25), we prepared further alanine mutations in the central cleft (Y34) and

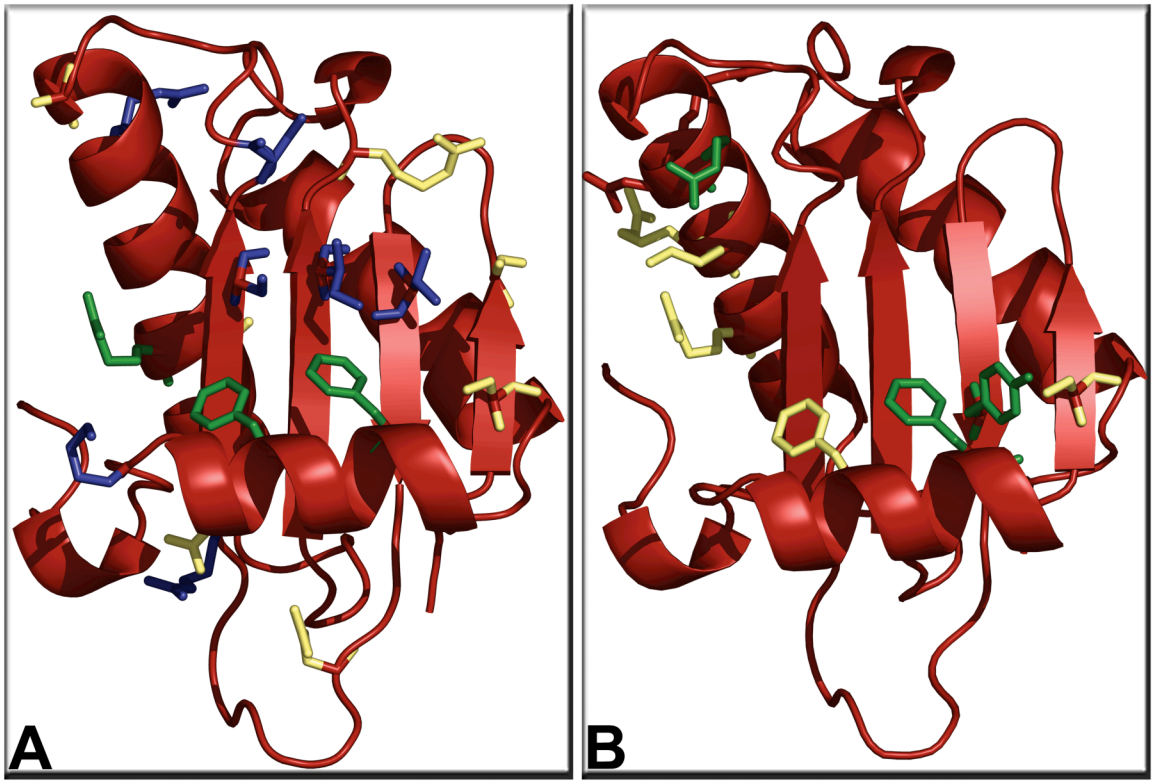

Figure IV-2. (A) Map of sites where single cysteine mutations in the *B. subtilis* P protein alter the value of $K_{D,\ obs}$ for pre-tRNA^{Asp}. The side chain color reflects the magnitude of the effect of the mutation on the value of $K_{D,\ obs}$: yellow, ≤ 3-fold increase; blue 3 to 25-fold increase; green > 25-fold increase. **(B)** *B. subtilis* P protein crystal structure with the effect of alanine mutations on the binding selectivity for A at N(-4) compared to G at this position. The residues that did not alter the binding specificity ratio when mutated to alanine are highlighted in yellow, and those that abolished the sequence preference at N(-4) are colored in green.

the RNR motif (R60, N61, K64, R65). To analyze whether these mutations affect the sequence selectivity of binding, we measured the binding affinities of the mutant RNase P enzyme with pre-tRNA containing either an A or G at the N(-4) position of the leader (Table III-2).

Table IV-2. Affinities of RNase P containing either wild type or alanine mutant P protein for the A(-4) and G(-4) pre-tRNA substrates.

	$K_{D,\,G(-4)}$ (nM)[a]	$K_{D,\,A(-4)}$ (nM)[a]	$K_{D,\,G(-4)} / K_{D,\,A(-4)}$[b]
Wild Type	11 ± 3	5 ± 1	2.1 ± 0.7
F16A	380 ± 70	260 ± 90	1.5 ± 0.6
F20A	39 ± 11	38 ± 13	1.0 ± 0.5
S25A	43 ± 16	14 ± 5	3.1 ± 1.6
Y34A	32 ± 11	57 ± 33	0.6 ± 0.4
R60A	44 ± 13	68 ± 19	0.6 ± 0.3
N61A	51 ± 21	35 ± 17	1.5 ± 0.9
K64A	60 ± 21	33 ± 12	1.8 ± 0.9
R65A	155 ± 40	73 ± 22	2.1 ± 0.8
R68A	51 ± 16	39 ± 25	1.3 ± 0.9

[a] 50 mM MES, 50 mM Tris, 400 mM KCl, 3.5 mM $CaCl_2$, 37°C, pH 6.0

The affinity of RNase P for substrates is highly dependent on the divalent ion concentration, with Hill coefficients in the range of 4 ± 1 [13,30]. Furthermore, the $K_{1/2}^{Ca2+}$ for enhancement of pre-tRNA affinity depends on both the length and sequence of the pre-tRNA leader [16,31]; the $K_{1/2}^{Ca2+}$ for G(-4) pre-tRNA is ~4 mM while the value for A(-4) pre-tRNA is < 2 mM (Figure II-2) [31]. Therefore, RNase P selectivity for the sequence of N(-4) depends on the calcium concentration; at 2 mM $[Ca(II)]_f$ $K_{D,obs\ G}/K_{D,obs\ A}$ is ~20, while at 3.5 mM this value decreases ~2 [31]. However, the pre-tRNA affinity of RNase P mutants at 2 mM $[Ca(II)]_f$ is weak, making it difficult to measure

$K_{D,obs}$ using centrifugal gel filtration. Therefore, dissociation constants were measured in 3.5 mM $[Ca(II)]_f$, where the dissociation constants for all of the mutant enzymes are measurable the two fold A(-4) / G(-4) substrate selectivity is observed [31].

Under these conditions, alanine point mutations in the P protein decrease the affinity of RNase P for both G(-4) and A(-4) pre-tRNA substrate (Table III-2). Out of the nine mutations examined, the majority decrease the affinity for pre-tRNA by < 10-fold (F20A, S25A, Y34A, R60A, N61A, K64A, and R68A). Notably, the R68A substitution had a significantly smaller effect on affinity than the R68C mutation. Only two mutations, F16A and R65A, have larger effects on binding affinity.

Alanine point mutations to seven side chains in the *B. subtilis* protein (highlighted in yellow in Figure III-2B) do not influence the sequence specific molecular recognition of pre-tRNA substrates. Compared to G(-4) pre-tRNA, all of these mutant RNase P enzymes retain a 1.5 to 2-fold preference for binding A(-4) pre-tRNA substrate. However, mutation of three protein residues, F20A, Y34A, and R60A (highlighted in green on Figure III-2B), result in a loss of sequence preference of RNase P for binding A(-4) pre-tRNA (Table III-2). The A(-4) pre-tRNA / G(-4) pre-tRNA $K_{D,obs}$ ratio decreases to ≤ 1. These data provide a qualitative identification of residues that affect sequence specificity. Mutations at F20, Y34, and R60 do not appreciably change the affinity of RNase P for G(-4) pre-tRNA. Rather, these mutations decrease the affinity for A(-4) pre-tRNA by four- to seven-fold compared to wild-type RNase P, decreasing the sequence selectivity for substrates. Thus, these data suggest that R60 in the RNR motif and the two aromatic positions in the central cleft, Y34 and F20, contribute to N(-4)

sequence selectivity. The explicit contributions of each of these three residues to the sequence specific recognition of N(-4) was further investigated.

R60 does not contact the 5' leader

R60 is the first residue in the RNR motif of P protein, a part of the protein that is not positioned near the 5' leader in structural models, while F20 and Y34 are in the central cleft near the leader [26,34]. To examine whether these two mutations specifically interact with the pre-tRNA leader, the binding affinity of RNase P reconstituted with R60A, Y34A, V32C, S51C, and I86C protein mutants for mature $tRNA^{Asp}$ was measured. Due to the weaker affinity of the RNase P for mature $tRNA^{Asp}$, these measurements were carried out at 5.0 mM $[Ca(II)]_f$. Under these conditions, RNase P binds to mature $tRNA^{Asp}$ with a $K_{D,obs}$ of 140 nM. The Y34A mutation has no effect on the affinity of RNase P for mature tRNA ($K_{D,obs}$ = 155 nM). Additional mutations in the P protein central cleft also did not alter mature tRNA binding (V32C, S51C, and I86C). While the R60A mutation decreased affinity of tRNA by > 8-fold ($K_{D,obs}$ = 1200 nM). These data suggest that the R60A mutation disrupts the affinity of RNase P for pre-tRNA by altering an interaction with tRNA, and not the 5' leader. In contrast, the data are consistent with the side chain of Y34 (and F20) interacting with the leader of pre-tRNA.

Y34 and F20 form steric and hydrogen bonding interactions with the N(-4) position of pre-tRNA

In Chapter II and above, we demonstrated that the *B. subtilis* RNase P preference for A(-4) over G(-4) has contributions from the N2 and N6 exocyclic amines of adenosine and guanosine, respectively, and the side chains of Y34 and F20 of P protein

are critical for conferring sequence specificity at N(-4) of pre-tRNA. To probe for interactions between the N(-4) base and the side chains of residues F20 and Y34, the binding affinities of RNase P reconstituted with P protein containing the F20A and Y34A mutations for pre-tRNA containing either a purine or diaminopurine at the N(-4) position at 2mM $[Ca(II)]_f$ were measured (Table III-3).

Table IV-3. Affinities of wild type, F20A, Y34A, and Y34F P protein mutants for A(-4), P(-4), DAP(-4) and G(-4) substrates.

	$K_{D,A(-4)}$ (nM)[a]	$K_{D,P(-4)}$ (nM)[a]	$K_{D,DAP(-4)}$ (nM)[a]	$K_{D,G(-4)}$ (nM)[a]
Wild Type	10 ± 2	30 ± 7	40 ± 7	200 ± 20
F20A	165 ± 25	200 ± 30	210 ± 30	400 ± 90
Y34A	140 ± 50	100 ± 25	100 ± 25	210 ± 70
Y34F	60 ± 15	50 ± 5	50 ± 10	110 ± 30

[a] 50 MM MES, 50 MM TRIS, 425 MM KCL, 2 MM $CaCl_2$, 37°C, PH 6.0

Wild type RNase P binds A(-4) pre-tRNA 3- and 4- more tightly than over P(-4) pre-tRNA and DAP(-4) pre-tRNA. F20A and Y34A mutations in P protein decrease the affinity of pre-tRNA with A, P, or DAP at N(-4) by a factor of 3 to 16-fold. However, these mutations have the largest deleterious affect on binding when N(-4) is A. Consequently, the sequence preference for binding A(-4) relative to P(-4) and DAP(-4) is lost. Futhermore, F20A and Y34A mutants in the RNase each resulted in the loss of most of the 20-fold A(-4) / G(-4) substrate selectivity observed at 2.0 mM $[Ca(II)]_f$. RNase P containing Y34A or F20A mutants retain a ≤ 2-fold selectivity. These data demonstrate that both Y34 and F20 contribute to the recognition of the nucleotide at the N(-4) position of pre-tRNA.

Sequence specific recognition at N(-4) requires the hydroxyl moiety of Y34

To investigate the potential contribution of the hydroxyl group on Y34 to N(-4) specificity, the binding affinity of RNase P containing a Y34F mutation in P protein for A(-4), G(-4), P(-4) and DAP(-4) pre-tRNA was measured at 2.0 mM $[Ca(II)]_f$. The Y34F mutation, like the F20A and Y34A mutation, causes a loss of preference for the binding of A(-4) pre-tRNA over both of the adenosine analog substrates, P(-4) and DAP(-4) pre-tRNA (Table III-3). As observed for the Y34A mutation, RNase P containing the Y34F mutation retained a 2-fold selectivity for A(-4) / G(-4). This result suggests that the hydroxyl group of Y34, not the phenyl ring leads to the sequence specific recognition of the base at N(-4) in pre-tRNA, possibly by forming a hydrogen bond.

Discussion

RNase P catalyzes the maturation of the 5' end of tRNAs and recognizes a wide variety of substrates. The protein component of the enzyme plays a large role in substrate recognition, as it increases the catalytic efficiency of the holoenzyme by 2400-fold, and the affinity of RNase P for pre-$tRNA^{Asp}$ by 10^4-fold [14,37]. This is presumably due to a direct interaction between pre-tRNA 5' leader and the central cleft region of the P protein in RNase P, as suggested by cross-linking and other biochemical studies [16,27]. Additionally, it has been reported that *B. subtilis* RNase P preferentially binds substrates with an adenosine at the fourth nucleotide from the cleavage site in the 5' leader of pre-$tRNA^{Asp}$ (N(-4) position, see Chapter II) [31]. This sequence preference hints at the possibility of a specific contact between pre-tRNA and the *B. subtilis* protein in RNase P, however the location and nature of this contact was not known.

To identify the site of the pre-tRNA / P protein interaction that leads to sequence specific recognition at N(-4), we used mutagenesis to map P protein amino acids

important for pre-tRNA affinity. These data indicate that the leader interacts with the central cleft of the P protein, consistent with crosslinking and trFRET studies [26,33]. Furthermore, these studies identified three amino acids that contribute to observed preferential binding of A(-4) over G(-4) by RNase P: R60 in the RNR motif, and the central cleft residues F20 and Y34 (Table III-2, Figure III-2B).

R60 is a completely conserved residue in the most highly conserved region of the P protein in bacteria, the RNR motif. This residue is notably the only RNR motif position essential for substrate specificity at the N(-4) position (Table III-3, Figure III-3B). The R60A mutation marginally affects the binding affinity of RNase P for G(-4), but weakens the binding of A(-4) by 6-fold. Thus, the loss of sequence preference results to a reduction in binding affinity for A(-4), and not a tightening of G(-4) affinity. The identification of R60 as important for the sequence specific recognition of the N(-4) position is unexpected because the most recent structural model of the *B. subtilis* RNase P holoenzyme•pre-tRNA complex places R60 near the mature tRNA portion of pre-tRNA substrate and distant from the leader sequence [26]. Consistent with this, the R60A mutation decreases the affinity of RNase P for mature tRNA. While the structural and biochemical data available for the positioning of R60 in RNase P argues against a direct interaction with the pre-tRNA leader, it is possible that interactions between R60 and mature tRNA facilitate the correct orientation of the 5' leader in the central cleft of the RNase P•pre-tRNA complex. Therefore, the elimination of arginine at this position could result in the misalignment of the 5' leader of pre-tRNA bound to RNase P and loss the sequence selective recognition at N(-4). However, further investigation into the position and function of R60 in the RNR motif is necessary in to delineate the role that this

residue is playing in pre-tRNA molecular recognition. The role of R60 in RNase P function will be further discussed in Chapter IV.

A common motif in the P protein subunit from bacterial RNase P is the placement of two phenylalanine residues on two adjacent alpha helical turns pointing towards the β-sheet in the central cleft (Figure III-2) [28,30]. This motif is clearly illustrated by the side chains of F16 and F20 in the *B. subtilis* P protein. F16 is the most conserved residue in the central cleft of bacterial RNase P proteins, and is also the only position that weakened both G(-4) and A(-4) pre-tRNA binding by >20-fold when mutated [28,30,38]. However, the F16A mutation decreases the affinity of RNase P for both substrates comparably (Table III-2), so it does not impact the sequence selectivity of this enzyme. Conversely, the F20A mutation significantly weakens the affinity of the enzyme for A(-4) pre-tRNA, but only decreases G(-4) pre-tRNA affinity 2-fold thereby causing a loss in sequence selectivity at N(-4). The aromatic rings of the phenylalanine protein residues could form base stacking (π-π) interactions with the aromatic rings of the pre-tRNA nucleotide base at N(-4) to enhance substrate affinity.

Consistent with this proposal, an analysis of 45 RNA-protein structures deposited in the protein data bank reveals that phenylalanine is the most common amino acid that stacks with nucleotides in RNA-protein structures, with the largest proportion of phenylalanine-nucleotide stacking interactions, 35%, observed between phenylalanine and adenosine [39]. Furthermore, aromatic amino acid-nucleotide stacking interactions are seen most frequently in RNA recognition proteins with structures similar to the RNase P protein central cleft [39]. This analysis further concluded that stacking in RNA-protein interactions are essential to forming binding pockets for proper sequence specific

recognition, which is agrees well with our model [39]. Thus, it is possible that a stacking interaction between an aromatic residue in P protein and a base in pre-tRNA could enhance sequence selectivity by properly orienting the nucleotide base for a sequence specific interaction with a second amino acid.

Tyrosine 34 is located on the third β-strand of the central cleft and points towards F20. Both the *B. subtilis* RNase P•pre-tRNA structural model and scanning mutagenesis suggest that the N(-4) base should be located near this region of the P protein (Figures II-1B, and III-2A) [26]. Tyrosine residues, unlike phenylalanine, possess both aromatic stacking, and hydrogen bonding potential due to the aryl hydroxyl group. The side chain of Y34 could contribute to both the pre-tRNA affinity and N(-4) pre-tRNA selectivity of RNase P using both hydrogen bonding to the amino functional group and base stacking. We evaluate the contribution of Y34 to substrate affinity and sequence specificity. The Y34A/F mutations do not appreciably alter the holoenzyme binding affinity for G(-4) pre-tRNA, however they significantly increase the $K_{D,obs}$ for A(-4) pre-tRNA significantly (Table III-3). These data suggest that the Y34A/F mutations eliminate a sequence specific contact with the adenosine base of A(-4). The binding data are consistent with a model in which a phenylalanine residue could act in conjunction with the functional hydroxyl group of a second tyrosine residue to confer and stabilize a sequence specific interaction.

In order to elucidate the precise roles contributed by F20 and Y34 side chains to the hydrogen bonding and steric elements of the sequence specific molecular recognition, binding studies with adenosine analogs at the N(-4) position were performed. The contributions of F20 and Y34 side chains to the steric component of the 5' leader

sequence specific interaction with the P protein were probed by measuring the binding affinities of F20A, Y34A, and Y34F mutants for DAP(-4) pre-tRNA. In the wild type portion of the study (see Chapter II), the DAP analog allowed for the determination that the additional N2 amine group in guanosine contributes to the reduced binding affinity of wild type RNase P for G(-4) pre-tRNA. DAP bases have an N6 amine, as in adenosine, and an additional N2 amine, like in guanosine. Wild type RNase P has a 4-fold preference for binding A(-4) over DAP(-4). All three P protein mutants exhibited no sequence preference for A(-4) (Table III-3). This effect could either be due to the loss of a possible hydrogen bonding interaction with Y34 because of the point mutations, or due to the addition of a steric interaction between the protein and the N2 amine in the DAP(-4) pre-tRNA. The F20A, Y34A and Y34F mutants abolish the 3-fold preference of wild type RNase P for binding A(-4) relative to P(-4) (Table III-3). Of the two positions identified as playing direct roles in sequence specificity, F20 and Y34, only the side chain of Y34 has the ability to accept a hydrogen bond from the N6 amine on adenosine. The loss of a 3-fold sequence preference for A(-4) over P(-4) with the F20A and Y34A / F mutants indicates that these residues are important for the hydrogen bonding contribution to sequence specific binding. This is consistent with a bioinformatic analysis that concluded that a large percentage of hydrogen bonds between adenosine and protein side chains, 44%, occur between the N6 amine and the protein [39].

The hydrogen bonding contribution to sequence specificity observed in wild type RNase P could result from an interaction with a protein back-bone, with the side chain of Y34, or a combination thereof. However, the loss of sequence preferential binding of A(-4) over P(-4) for the Y34F mutant suggests that the Y34 hydroxyl group forms a

hydrogen bond with the pre-tRNA leader to enhance the sequence selectivity of RNase P. From this data we propose that the hydroxyl group of Y34 forms a hydrogen bond with the adenosine at N(-4) in the 5' leader of A(-4). In this model, the role of F20 in RNase P is to properly orient the 5' leader. This model is consistent with sequence specific recognition of adenosine nucleotides in other RNAs, such as the RNA recognition motif (RRM) bound by the splicing protein Srp20 [40]. Srp20 also prefers an adenine over guanine at position A2, and solution structures of the RRM-Srp20 complex reveal that this preference is explained by a hydrogen bond between the hydroxyl moiety of a serine and the N6 amine of adenosine [40]. Another example of amino acid side chains hydrogen bonding to the N6 amine of adenosine can be seen in the co-crystal structure of PP7 bacteriophage protein and its cognate RNA [41]. Additionally, a recent study that analyzed RNA-protein structures deposited in the protein data bank concluded that hydrogen bonds between tyrosine and the adenosine base are favorable, and guanosine-tyrosine hydrogen bonding interactions are unfavorable [42]. A second possible model is that the side chains of Y34 and F20 work together to position N(-4) pre-tRNA for a hydrogen bond with the protein backbone.

A value of – 0.7 kcal/mol $\Delta\Delta G^{A(-4)\,/\,P(-4)}$ of increased binding energy for A(-4) pre-tRNA compared to P(-4) pre-tRNA can be calculated from the binding data. The Y34F mutant has a $\Delta\Delta G^{Y34F\,/\,WT}$ of –1.1 kcal/mol, also consistent with a loss of a hydrogen bond. This difference in free energy could reflect either the loss of a stacking interaction, the weakening of a backbone or Y34 hydrogen bond with the N(-4) position on the 5' leader due to a repositioning of the substrate in the central cleft, or something not yet identified. Studies of the *B. subtilis* RNase P holoenzyme has ~4 kcal/mol $\Delta\Delta G$ for

mature tRNA / precursor tRNA binding [14,43]. We propose that the free energy difference we observe for the formation of a single, sequence specific hydrogen bond between the 5' leader and the *B. subtilis* P protein could perhaps account for part of the preference seen in previous studies for pre-tRNA binding.

RNase P binds its wide variety of naturally occurring pre-tRNA substrates with uniform affinity. Harris and co-workers have shown that this uniform affinity requires contributions with both the mature tRNA and 5' leader [29]. Interestingly, certain 5' leader sequences make a larger contribution to pre-tRNA affinity, but only in the presence of the P protein. This is consistent with a sequence specific interaction between the pre-tRNA and the 5' leader, such as the one that we have shown. The interaction between the leader and the P protein in RNase P is clearly very important for substrate binding, and given the genomic data indicating sequence preferences at the N(-2), N(-3) and N(-4) in a number of species, it is likely that the more sequence specific contacts in the 5'leader exist *in vivo*.

Materials and Methods

RNase P RNA and Protein Preparation

B. subtilis P RNA was transcribed *in vitro* from a linearized plasmid template catalyzed by T7 RNA polymerase, and purified on a denaturing 8% polyacrylamide gel, as previously described [44,45]. Single alanine and phenylalanine mutations were generated using a Stratagene Quik Change Site Directed Mutagenesis Kit. All single cysteine mutations were made as reported by Niranjanakumari, *et al* [26]. The wild-type and mutant *B. subtilis* P proteins were expressed in BL21(DE3) pLysS cells and purified

with CM-sepharose chromatography as previously described [46]. P RNA concentration was quantified by absorbance at 260 nm (ε_{260} = 3.94 M^{-1} cm^{-1}) and P protein concentration was determined by absorbance at 280 nm (ε_{280} = 5500 x 10^{-6} M^{-1} cm^{-1}) [44,46].

RNase P Holoenzyme formation

The P RNA component of *B. subtilis* heated to 95°C for 3 minutes in water, incubated 37°C for 10 minutes, and folded upon the addition of buffer to a final concentration of ~2 - 10 μM P RNA, 50 mM Tris, 50 mM Mes, 400mM KCl and 2-5mM $CaCl_2$, pH 6.0 at 37°C (buffer A). The ionic strength was maintained at XX by adjusting the KCl concentration. The buffer in P RNA was exchanged using an Amicon Ultra Centrifugal Filter Unit from Millipore (10,000 MWCO). After washing the filter with buffer A, 200μL of P RNA was diluted with 5 mL of buffer A and the volume was reduced to 50-100 μL by centrifugation.

B. subtilis RNase P protein was dialyzed overnight against 250 mL of buffer A. RNase P holoenzyme (0.5-10 μM) was formed by incubating equal concentrations of P protein and P RNA together at 37 °C for 30 minutes in buffer A.

Substrate Pre-tRNA Preparation and Labeling

G(-4) pre-tRNA synthesized *in vitro* by runoff transcription catalyzed by T7 RNA polymerase [47,48]. The 5' end was labeled with ^{32}P using γ-^{32}P ATP and T4 polynucleotide kinase (PNK) and pre-tRNA was purified on a 15% denaturing polyacrylamide gel, as previously desribed [14]. The A(-4) pre-tRNA, P(-4) pre-tRNA, and DAP(-4) pre-tRNA were produced by ligating synthetic RNA oligonucleotides (5'-

ACAUGGUCC-3', 5'-PurineCAUGGUCC-3', and 5'-DiaminopurineCAUGGUCC-3' respectively) to truncated tRNA. The ribooligonucleotides were first 5' radiolabeled at the 5' end with ^{32}P and then ligated to a truncated tRNA using T4 DNA ligase with a DNA splint (5'-dCTGAACTACCGGACCATGTTTTGGGTACCA-3') [49]. The truncated tRNA was made with a runoff transcription [16].

Measurements of Dissociation Constants

To measure binding affinities, a large excess of RNase P was incubated for five minutes with < 0.2 nM pre-tRNA substrates in buffer A at 37 ^{o}C. The holoenzyme-substrate mixture was loaded onto a pre-packed G-75 Sephadex column, and the free substrate was separated from the RNase P bound substrate using centrifugational gel filtration as previously described [16,44,50]. The fraction of substrate bound ($[ES]/[S_{total}]$) was determined from scintillation counting. A standard binding isotherm was then fit to the data to calculate dissociation constants (Equation III-1).

Equation IV-1

$$[ES]/[S_{total}] = A / (1+ K_D/[E_{total}]) +B$$

A = Fraction of counts in the eluate at saturating RNase P

B = Fraction of counts in the eluate in the absence of RNase P

References for Chapter III

1. Staley JP, Guthrie C: Mechanical devices of the spliceosome: motors, clocks, springs, and things. *Cell* 1998, 92:315-326.

2. Wilson KS, Noller HF: Molecular movement inside the translational engine. *Cell* 1998, 92:337-349.

3. Guerrier-Takada C, Gardiner K, Marsh T, Pace N, Altman S: The RNA moiety of ribonuclease P is the catalytic subunit of the enzyme. *Cell* 1983, 35:849-857.

4. Kurz JC, Fierke CA: Ribonuclease P: a ribonucleoprotein enzyme. *Curr Opin Chem Biol* 2000, 4:553-558.

5. Apirion D, Miczak A: RNA processing in prokaryotic cells. *Bioessays* 1993, 15:113-120.

6. Gossringer M, Kretschmer-Kazemi Far R, Hartmann RK: Analysis of RNase P protein (rnpA) expression in Bacillus subtilis utilizing strains with suppressible rnpA expression. *J Bacteriol* 2006, 188:6816-6823.

7. Loria A, Pan T: Domain structure of the ribozyme from eubacterial ribonuclease P. *Rna* 1996, 2:551-563.

8. Pan T: Higher order folding and domain analysis of the ribozyme from Bacillus subtilis ribonuclease P. *Biochemistry* 1995, 34:902-909.

9. Loria A, Pan T: Modular construction for function of a ribonucleoprotein enzyme: the catalytic domain of Bacillus subtilis RNase P complexed with B. subtilis RNase P protein. *Nucleic Acids Res* 2001, 29:1892-1897.

10. Torres-Larios A, Swinger KK, Krasilnikov AS, Pan T, Mondragon A: Crystal structure of the RNA component of bacterial ribonuclease P. *Nature* 2005, 437:584-587.

11. Torres-Larios A, Swinger KK, Pan T, Mondragon A: Structure of ribonuclease P--a universal ribozyme. *Curr Opin Struct Biol* 2006, 16:327-335.

12. Kazantsev AV, Krivenko AA, Harrington DJ, Holbrook SR, Adams PD, Pace NR: Crystal structure of a bacterial ribonuclease P RNA. *Proc Natl Acad Sci U S A* 2005, 102:13392-13397.

13. Kurz JC, Fierke CA: The affinity of magnesium binding sites in the Bacillus subtilis RNase P x pre-tRNA complex is enhanced by the protein subunit. *Biochemistry* 2002, 41:9545-9558.

14. Kurz JC, Niranjanakumari S, Fierke CA: Protein component of Bacillus subtilis RNase P specifically enhances the affinity for precursor-tRNAAsp. *Biochemistry* 1998, 37:2393-2400.

15. Sun L, Harris ME: Evidence that binding of C5 protein to P RNA enhances ribozyme catalysis by influencing active site metal ion affinity. *Rna* 2007.

16. Crary SM, Niranjanakumari S, Fierke CA: The protein component of Bacillus subtilis ribonuclease P increases catalytic efficiency by enhancing interactions with the 5' leader sequence of pre-tRNAAsp. *Biochemistry* 1998, 37:9409-9416.

17. Loria A, Pan T: Recognition of the T stem-loop of a pre-tRNA substrate by the ribozyme from Bacillus subtilis ribonuclease P. *Biochemistry* 1997, 36:6317-6325.

18. Loria A, Niranjanakumari S, Fierke CA, Pan T: Recognition of a pre-tRNA substrate by the Bacillus subtilis RNase P holoenzyme. *Biochemistry* 1998, 37:15466-15473.

19. Kirsebom LA, Svard SG: Base pairing between Escherichia coli RNase P RNA and its substrate. *Embo J* 1994, 13:4870-4876.

20. Oh BK, Pace NR: Interaction of the 3'-end of tRNA with ribonuclease P RNA. *Nucleic Acids Res* 1994, 22:4087-4094.

21. Zahler NH, Christian EL, Harris ME: Recognition of the 5' leader of pre-tRNA substrates by the active site of ribonuclease P. *Rna* 2003, 9:734-745.

22. Brannvall M, Fredrik Pettersson BM, Kirsebom LA: The residue immediately upstream of the RNase P cleavage site is a positive determinant. *Biochimie* 2002, 84:693-703.

23. Hardt WD, Schlegl J, Erdmann VA, Hartmann RK: Kinetics and thermodynamics of the RNase P RNA cleavage reaction: analysis of tRNA 3'-end variants. *J Mol Biol* 1995, 247:161-172.

24. Hardt WD, Schlegl J, Erdmann VA, Hartmann RK: Role of the D arm and the anticodon arm in tRNA recognition by eubacterial and eukaryotic RNase P enzymes. *Biochemistry* 1993, 32:13046-13053.

25. Pan T, Loria A, Zhong K: Probing of tertiary interactions in RNA: 2'-hydroxyl-base contacts between the RNase P RNA and pre-tRNA. *Proc Natl Acad Sci U S A* 1995, 92:12510-12514.

26. Niranjanakumari S, Day-Storms JJ, Ahmed M, Hsieh J, Zahler NH, Venters RA, Fierke CA: Probing the architecture of the B. subtilis RNase P Holoenzyme active site by crosslinking and affinity cleavage. *Rna* 2007, 13:512-535.

27. Niranjanakumari S, Stams T, Crary SM, Christianson DW, Fierke CA: Protein component of the ribozyme ribonuclease P alters substrate recognition by directly contacting precursor tRNA. *Proc Natl Acad Sci U S A* 1998, 95:15212-15217.

28. Gopalan V, Baxevanis AD, Landsman D, Altman S: Analysis of the functional role of conserved residues in the protein subunit of ribonuclease P from Escherichia coli. *J Mol Biol* 1997, 267:818-829.

29. Sun L, Campbell FE, Zahler NH, Harris ME: Evidence that substrate-specific effects of C5 protein lead to uniformity in binding and catalysis by RNase P. *Embo J* 2006, 25:3998-4007.

30. Zahler NH, Sun L, Christian EL, Harris ME: The pre-tRNA nucleotide base and 2'-hydroxyl at N(-1) contribute to fidelity in tRNA processing by RNase P. *J Mol Biol* 2005, 345:969-985.

31. Zahler NH, Koutmou KS, Kurz JC, Sohn J, Campbell FE, Niranjanakumari S, Harris ME, Fierke CA: Sequence Preference in the Interaction of Bacterial Ribonuclease P with pre-tRNA 5' Leaders. *in preparation* 2008.

32. Koutmou KS, Zahler NH, Niranjanakumari S, Fierke CA: Specific Contacts between the P Protein Subunit of Bacillus Subtilis RNase P and the 5’ leader of pre-tRNA Contribute to Molecular Recognition. *in preparation* 2008.

33. Rueda D, Hsieh J, Day-Storms JJ, Fierke CA, Walter NG: The 5' Leader of Precursor tRNA(Asp) Bound to the Bacillus subtilis RNase P Holoenzyme Has an Extended Conformation. *Biochemistry* 2005, 44:16130-16139.

34. Buck AH, Kazantsev AV, Dalby AB, Pace NR: Structural perspective on the activation of RNase P RNA by protein. *Nat Struct Mol Biol* 2005.

35. Stams T, Niranjanakumari S, Fierke CA, Christianson DW: Ribonuclease P protein structure: evolutionary origins in the translational apparatus. *Science* 1998, 280:752-755.

36. Smith D, Burgin AB, Haas ES, Pace NR: Influence of metal ions on the ribonuclease P reaction. Distinguishing substrate binding from catalysis. *J Biol Chem* 1992, 267:2429-2436.

37. Kole R, Baer MF, Stark BC, Altman S: E. coli RNAase P has a required RNA component. *Cell* 1980, 19:881-887.

38. Jovanovic M, Sanchez R, Altman S, Gopalan V: Elucidation of structure-function relationships in the protein subunit of bacterial RNase P using a genetic complementation approach. *Nucleic Acids Res* 2002, 30:5065-5073.

39. Allers J, Shamoo Y: Structure-based analysis of protein-RNA interactions using the program ENTANGLE. *J Mol Biol* 2001, 311:75-86.

40. Hargous Y, Hautbergue GM, Tintaru AM, Skrisovska L, Golovanov AP, Stevenin J, Lian LY, Wilson SA, Allain FH: Molecular basis of RNA recognition and TAP binding by the SR proteins SRp20 and 9G8. *Embo J* 2006, 25:5126-5137.

41. Chao JA, Patskovsky Y, Almo SC, Singer RH: Structural basis for the coevolution of a viral RNA-protein complex. *Nat Struct Mol Biol* 2008, 15:103-105.

42. Ellis JJ, Broom M, Jones S: Protein-RNA interactions: structural analysis and functional classes. *Proteins* 2007, 66:903-911.

43. Buck AH DA, Poole AW, Kazantsev AV, Pace NR: Abstract Protein activation of a ribozyme: the role of bacterial RNase P protein. *EMBO J.* 2006, 24:3360-3368.

44. Beebe JA FC: A kinetic mechanism for cleavage of precursor tRNA(Asp) catalyzed by the RNA component of Bacillus subtilis ribonuclease P. *Biochemistry* 1994, 33:10294-102304.

45. Milligan JU, OC: Synthethesis of Small RNAs Using T7 RNA Polymerase. *Methods Enzymology* 1989, 180:51-62.

46. Niranjanakumari S, Kurz JC, Fierke CA: Expression, purification and characterization of the recombinant ribonuclease P protein component from Bacillus subtilis. *Nucleic Acids Res* 1998, 26:3090-3096.

47. Beebe JA, Fierke CA: A kinetic mechanism for cleavage of precursor tRNA(Asp) catalyzed by the RNA component of Bacillus subtilis ribonuclease P. *Biochemistry* 1994, 33:10294-10304.

48. Milligan JF, Uhlenbeck OC: Synthesis of small RNAs using T7 RNA polymerase. *Methods Enzymol* 1989, 180:51-62.

49. Moore MJ, Query CC: Joining of RNAs by splinted ligation. *Methods Enzymol* 2000, 317:109-123.

50. Penefesky HS: *Methods Enzymology* 1979, 56:527-530.

CHAPTER V

THE RNR MOTIF OF THE *B. SUBTILIS* RNASE P PROTEIN PLAYS A ROLE IN STRUCTURING THE P RNA ACTIVE SITE AND PRE-TRNA SUBSTRATE FOR INTERACTION [viii]

Background

The maturation of the 5' end of all nuclear encoded tRNAs is catalyzed by the ribonucleoprotein complex, ribonuclease P (RNase P). RNase P is an essential metal dependent enzyme comprised of a large ~400 nucleotide catalytic RNA (P RNA), and at least one protein (P protein). P RNA alone is active *in vitro* under conditions of high monovalent salt and magnesium [1]. Although the protein component does not perform the actual cleavage reaction, it is still essential for activity *in vivo* [2]. Bacterial RNase P, unlike its eukaryotic counterparts, consists of a single protein associated with its P RNA and has been recombinantly expressed and purified [3-7]. Therefore, the bacterial enzyme is the simplest and most pliable system for investigating RNase P. The function of the bacterial P RNA ribozyme alone has been extensively characterized; however, how the RNA and protein subunits work together to enhance catalysis remains less well

[viii] Work presented in this chapter is included in a manuscript of the same title by K.S. Koutmou, J. Day-Storms, and C.A. Fierke. The data displayed were collected by K.S. Koutmou and J. Day-Storms, and the specific results gathered by J. Day-Storms will be annotated.

understood. In particular, the contributions of specific regions of the protein to RNase P structure and function warrant further investigation.

Bacterial RNase P proteins, although not directly responsible for 5' leader cleavage, contribute to the catalytic efficiency of the bacterial RNase P holoenzyme. In *B. subtilis* the P protein subunit enhances k_{cat} / K_m by 2000-fold, and substrate recruitment by 10^4 - fold over cleavage of pre-tRNA^{Asp} catalyzed by P RNA alone at moderate salt concentrations [8]. Furthermore, RNase P uniformally binds and cleaves all pre-tRNAs, despite the large sequence variation between these substrates [9]. The *E. coli* P RNA subunit by itself does not bind and cleave all substrates similarly, however, when the protein is added to form the *E. coli* holoenzyme, uniform pre-tRNA recognition is restored. In fact, the *E. coli* protein enhances the cleavage rate constants for some non-canonical pre-tRNA sequences by > 900-fold [9]. Both *E. coli* and *B. subtilis* proteins also decrease the concentration of divalent metal ions required for catalysis by RNase P, and the protein subunit of RNase P has been suggested to be important for a metal stabilized conformational change of the enzyme that is important for efficient catalytic activity [9,10,11,12]. The minimal kinetic mechanism for bacterial RNase P is presented in Scheme IV-1A. In this scheme, RNase P holoenzyme undergoes two-step a binding process; substrate association, and a subsequent metal mediated conformational change prior to catalysis [12,13]. Substrate association is rapid and nearly diffusion controlled in the wild type enzyme [12]. Following irreversible 5' leader cleavage, products dissociate. The rate-limiting step is highly dependent on reaction conditions. Under single turnover conditions for wild-type RNase P, the conformational change step is partially rate limiting at high pH in magnesium, while cleavage chemistry is rate limiting

at low pH, or when magnesium is substituted for calcium (Scheme IV-1B) [12,14]. However, little is known about how the protein enhances catalytic activity in the context of this mechanism, or what regions of the protein are essential for activation.

Even though bacterial RNase P proteins are required *in vivo* and are structurally homologous, they have strikingly little sequence similarity [15]. All bacterial P proteins share a fold and structure similar to that of the *B. subtilis* protein (Figure 1A), with an overall αββββαβα topology, and two probable RNA binding regions [16-18]. The structure of a protein subunit from an archeal RNase P, a homolog of the eukaryotic RNase P protein Pop5p, is also similar to that of the bacterial P protein, suggesting an analogous functional role across all three kingdoms of life [6,19].

In the case of the bacterial protein, two RNA binding regions could interact with P RNA, pre-tRNA, or both RNA components of the system. The first region is the central cleft formed by the face of the central β-sheet and an α-helix (Figure IV-1A) [16]. Thus far, the central cleft is the only region of the protein identified as playing a specific role in RNase P function [20,21]. Time-resolved FRET (trFRET), affinity cleavage and crosslinking data provide evidence that the central cleft interacts with the 5'leader of pre-tRNA to enhance substrate recruitment and discrimination [8,22,23]. Recent biochemical studies (see Chapter III) reveal that two central cleft residues, F20 and Y34 in *B. subtilis* RNase P, have sequence specific contacts with the 5' leader position four nucleotides away from the cleavage site (N(-4)) [21,24]. The second region of the protein identified as potentially important for RNA binding is the α-helix of the unusual left-handed βαβ crossover connection between parallel β-strands of the central cleft. The α-helix portion of this region is termed the RNR motif because the first three residues are Arg-Asn-Arg,

R-N-R (Figure IV-1A). Sequence alignment studies of the bacterial proteins demonstrate that there are only 14 P protein residues with greater than 67% conservation [15]. When these residues are mapped onto the *B. subtilis* RNase P protein structure, it is evident that 6 of the 14 conserved residues are located in the RNR motif (R60, N61, R62, K64, R65, and R68), making it the most highly conserved region of bacterial P proteins (Figure 1A) [15]. However, the reasons for this sequence conservation are unknown.

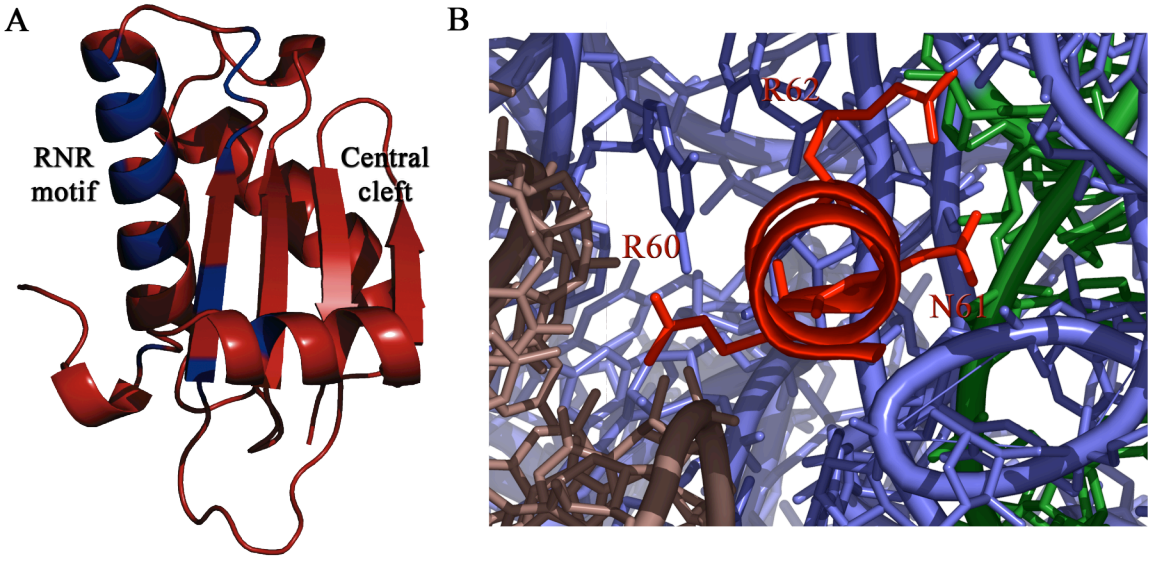

Figure V-1. Structural view of *B. subtilis* RNase P **(A)** Crystal structure of *B. subtilis* RNase P protein [16]. The 14 amino acids with >67% sequence conservation are highlighted in blue [15]. The most conserved region of the protein is termed the RNR motif, as denoted with text. **(B)** View of the location of the RNR motif in the *B. subtilis* RNase P holoenzyme model with bound pre-tRNA [22]. The protein is in red, the P RNA in blue, and the pre-tRNA in brown. Helix P4 in P RNA is highlighted in green. This figure is oriented looking down the center of the RNR motif α-helix. The first three residues (R60, N61, and R62) are shown, and sit at the interface of the P RNA and pre-$tRNA^{Asp}$.

Information regarding the structure of the RNase P holoenzyme (P RNA-P protein complex) is limited. While x-ray crystal structures of the components of the bacterial RNase P exist independently of each other, there are not yet structures available of the holoenzyme complex [16,25,26]. As such, models based on biochemical data and the

available crystal structures provide the best picture of the holoenzyme structure. The two most recent holoenzyme models with bound pre-tRNA are of *B. stearothermophilus* and *B. subtilis* RNase P (Figure I-4) [22,27]. The models share the same overall architecture, with similar P RNA structure, and the protein interacts with the same region of P RNA. However, the specific details of the structures vary. One remarkable similarity observed in both of these models is that the most conserved region of the required RNase P protein, the RNR motif is positioned at the intersection of the putative active site of P RNA and pre-tRNA (helix P4 region, which binds metals essential for catalysis) (Figure IV-1B).

A)

$$E + S \underset{k_{-1}}{\overset{k_1}{\rightleftharpoons}} ES \overset{M^{2+}}{\underset{k_{-2}}{\rightleftharpoons}} ES^* \xrightarrow{k_{chem}} EPL \xrightarrow{k_3} E + L + P \qquad K_{D,obs} = \frac{k_1}{k_2}$$

B) ***Thermodynamic constants:***

$K_{D,obs} = [E][S] / [ES] + [ES^*]$

$K_1 = [ES] / [E][S] = k_{-1} / k_1$

Overall observed rate constant:

$k_{obs} = k_{chem} k_2 / (k_{chem} + k_{-2} + k_2)$

For the wild type, in calcium at all pHs:

$k_{chem} << k_2$, therefore can assume that ES $\rightleftharpoons$ ES* are in rapid equilibrium, which reduces k_{obs} to:

$k_{obs,\,Ca} = k_{chem} / (1 + k_{-2} / k_2)$, *which because* $k_{chem} << k_2$, *and assume* $k_2 >> k_{-2}$,

$k_{obs,\,Ca} = k_{chem}$

In magnesium:

$k_{obs} = k_{chem} k_2 / (k_{chem} + k_{-2} + k_2)$

Scheme V-1. (A) The minimal kinetic mechanism for bacterial RNase P, where E is RNase P holoenzyme, S is pre-tRNA, P is mature tRNA, L is the 5' leader, E•S is the substrate bound complex, E•P•L is the enzyme•tRNA•5' leader complex [12], **(B)** Definitions of all kinetic and thermodynamic constants discussed in the text.

Given the apparent proximity of the RNR motif to the putative P RNA active site and its high level of conservation, it is positioned to perform multiple important roles. *In vivo* studies of *E. coli* RNase P with mutations in the RNR motif indicate that these mutations moderately impact pre-tRNA^{Tyr} cleavage, and severely disrupt the maturation of p4.5S RNA, a non-pre-tRNA substrate [28]. Recent *in vitro* studies of the *B. subtilis* RNR motif (see Chapter III) have shown that mutations in this region disrupt pre-tRNA^{Asp} and mature tRNA^{Asp} affinity [21]. For both the *E. coli* and *B. subtilis* enzymes, residues in the RNR motif have been proposed to stabilize binding interactions between the P RNA and P protein subunits [16,28-30]. However, the precise function of the RNR motif and the reasons for its conservation are unclear. To investigate the role of the RNR motif in *B. subtilis* RNase P, we evaluated the effects of mutations in the RNR motif on holoenzyme formation, ionic interactions between the P RNA and protein, pre-tRNA binding, and numerous steps in the kinetic mechanism (Scheme IV-1A) using a combination of binding assays, fluorescence titrations, single turnover kinetics, and stopped-flow fluorescence. Our data demonstrate that residues R60 and R62 in the RNR motif are important for holoenzyme stability, and that R60 has an ionic interaction with P RNA. Furthermore, R60, R62, R65, and R68 all contribute to the $K_{D,obs}$ for pre-tRNA^{Asp}, and R60 stabilizes the first step of substrate association, K_1. Single-turnover cleavage studies indicate that although the RNR motif does not directly contribute to cleavage chemistry (k_{chem} in Scheme IV-1A), it enhances the kinetics of the conformational change step of the minimal kinetic mechanism. These data led us to propose a model in which the RNR motif residues R60 and R62 stabilize P RNA local structure and enable the proper orientation of pre-tRNA to achieve catalysis.

Results [ix]

P protein residues R60 and R62 stabilize the formation of the *B. subtilis* holoenzyme

The formation and stability of the RNase P holoenzyme is vital to the function of the enzyme *in vivo*. However, the protein-RNA interactions that are important for the holoenzyme formation and stability have not been determined. Structural models based on cross-linking and affinity cleavage data indicate that the highly conserved RNR motif region is located close to helix P4 of P RNA, suggesting that the RNR motif may be in close proximity to the enzyme active site [22,27]. To assess the importance of the residues in the RNR motif for holoenzyme complex formation, the affinities of P RNA for the wild type protein, R60A, R62A, K64A, R65A, and R68C protein mutants were measured using a previously described magnetocapture binding assay [31]. The results are shown in Table IV-1. Of the RNR motif residues evaluated, only the R60A and R62A protein mutations impede holoenzyme complex formation and increase the $K_{D,obs}$ of P RNA for protein by greater than 20-fold compared to wild type (Table IV-1). Therefore, the first two arginines in the RNR motif play an important role in stabilizing the RNase P holoenzyme complex.

R60 has an ionic contact with P RNA

We previously reported that wild type *B. subtilis* RNase P protein makes at least four ionic interactions with P RNA based on the dependence of the binding interaction on ionic strength [31]. To evaluate if the positively charged R60 and R62 residues

[ix] Results presented in "P protein residues R60 and R62 stabilize the formation of the *B. subtilis* Holoenzyme", "R60 has an ionic contact with P RNA" were collected by JDS.

contribute to these ionic interactions, the $K_{D,obs}$ of P RNA for protein was measured as a function of ionic strength. Unfortunately, the R62A P protein mutant bound too weakly to RNase P to allow measurement of the binding affinity at elevated ionic strength. However, the R60A data revealed that this mutant protein makes only three, and not four, ionic interactions with P RNA (Table IV-1). This strongly suggests that the native R60 residue forms a salt-bridge with P RNA.

Table V-1. Binding of P RNA to P protein with RNR motif mutants, and number of ionic interactions.

	$K_{D,obs}$ (nM)[a]	Effect	Ionic Interactions (n_H)
WT	7.0 ± 0.9	1	4
R60A	170 ± 40	24 ± 6	3
R62A	230 ± 40	33 ± 7	nd[b]
K64C	7 ± 2	1 ± 0.05	nd[b]
R65C	7 ± 1	1 ± 0.02	nd[b]
R68C	11 ± 3	1.6 ± 0.05	nd[b]

[a] 50 mM Tris, 10 mM imidazole, 10 mM $MgCl_2$, 200-800 mM KCl, P protein concentrations varied from 0.1 nM – 2 μM
[b] Not determined

RNR motif affects the affinity of pre-tRNA

Previously it has been shown that the RNase P holoenzyme binds pre-tRNA 10^4-fold more tightly than P RNA alone and the binding enhancement is primarily mediated through an interaction between the P protein and the leader of pre-tRNA [32]. To determine whether the RNR motif contributes to this enhanced pre-tRNA affinity, the $K_{D,obs}$ for pre-tRNA (Scheme IV-1) of four RNase P mutants where alanine is substituted for one of the amino acids in the RNR motif was measured in buffers containing 10 mM

$CaCl_2$ (Figure IV-2A, Table IV-2). The cleavage reaction in calcium at pH 6.0 is sufficiently slow that substrate binding can be measured prior to catalysis [8,33]. $K_{D,obs}$ reflects combination of thermodynamic constants for the first two steps in the minimal kinetic mechanism (Scheme IV-1). These data indicate that the side chains of R65 and R68 decrease the pre-tRNA affinity less than 3-fold suggesting little interaction with the substrate. However, the pre-tRNA affinity decreases by at least 10-fold with the R60A and R62A mutations (Table IV-2, Figure 3A). These data demonstrate that the RNR motif stabilizes the formation of the enzyme substrate complex prior to catalysis either by stabilizing the initial substrate association complex, or altering the conformational change step in the enzyme kinetic mechanism (Scheme IV-1A).

Table V-2. RNR motif mutants affinities for pre-tRNA^{Asp} with a 5 nucleotide long 5' leader under conditions of 10 mM $CaCl_2$

	$K_{D,\,obs}$ (nM)[a]	$K_{D,\,obs,\,protein}$ / $K_{D,\,obs,\,WT}$
WT	2 ± 0.5	1
R60A	40 ± 10	20 ± 7
R62A	17 ± 5	8.5 ± 3
R65A	4 ± 0.5	2 ± 0.6
R68A	6 ± 1	3 ± 0.9

[a] 50 mM MES, 50 mM Tris, 400 mM KCl, 10mM $CaCl_2$, 37°C, pH 6.0

R60 contributes to the equilibrium of substrate association step in the kinetic mechanism (K_1)

To examine whether the disruption of pre-tRNA affinity caused by the R60A and R62A mutation can be attributed primarily to effects on substrate association or enzyme conformational change we assessed the thermodynamics of the formation of the initial

complex, K_1, for wild type and mutant RNase P enzymes. Previous studies established that in the presence of 2 mM $Co(NH_3)_6^{3+}$ and no divalent cations, the RNase P holoenzyme can form stably and can bind pre-tRNA [13]. However, divalent cations (i.e. calcium or magnesium) are required to stabilize the E•S* conformer and to activate catalysis. Therefore, in the presence of cobalt hexaammine and absence of calcium, the initial E•S complex stably forms so that the affinities (K_1) of wild type RNase P, R60A, and R62A mutants for pre-$tRNA^{Asp}$ were measured under these conditions by fluorescence titration [13]. The R62A mutation has no effect on K_1; in contrast, the R60A mutation reduces substrate affinity, and raised the value of K_1, by 6-fold compared to wild-type RNase P (Figure IV-3B, Table IV-3). These data suggest that the R60 residue stabilizes the formation of the initial E•S complex. Nevertheless, the six-fold stabilization of this complex does not fully account for the 20-fold difference seen in the affinity in calcium buffer (Table IV-2). Conversely, the R62A mutation has little or no effect on the value of K_1 suggesting that this side chain does not stabilize this E•S complex. However, this mutation causes a 9.5-fold decrease in the value of $K_{D,obs}$ (Table IV-2). Thus the side chains of R60 and R62 must contribute to the stabilization of another step prior to catalysis.

Table V-3. K_1 values measured by fluorescence titrations

	K_1 (nM)[a]	$K_{1,\,protein} / K_{1,\,WT}$
WT	33 ± 8	1
R60A	200 ± 20	6 ± 1.6
R62A	30 ± 10	1 ± 0.4

a 50 mM MES, 50 mM Tris, 180 mM KCl, 2mM [Co(NH3)6]•Cl3, 37oC, titrating to final protein concentrations between 0 – 860 nM.

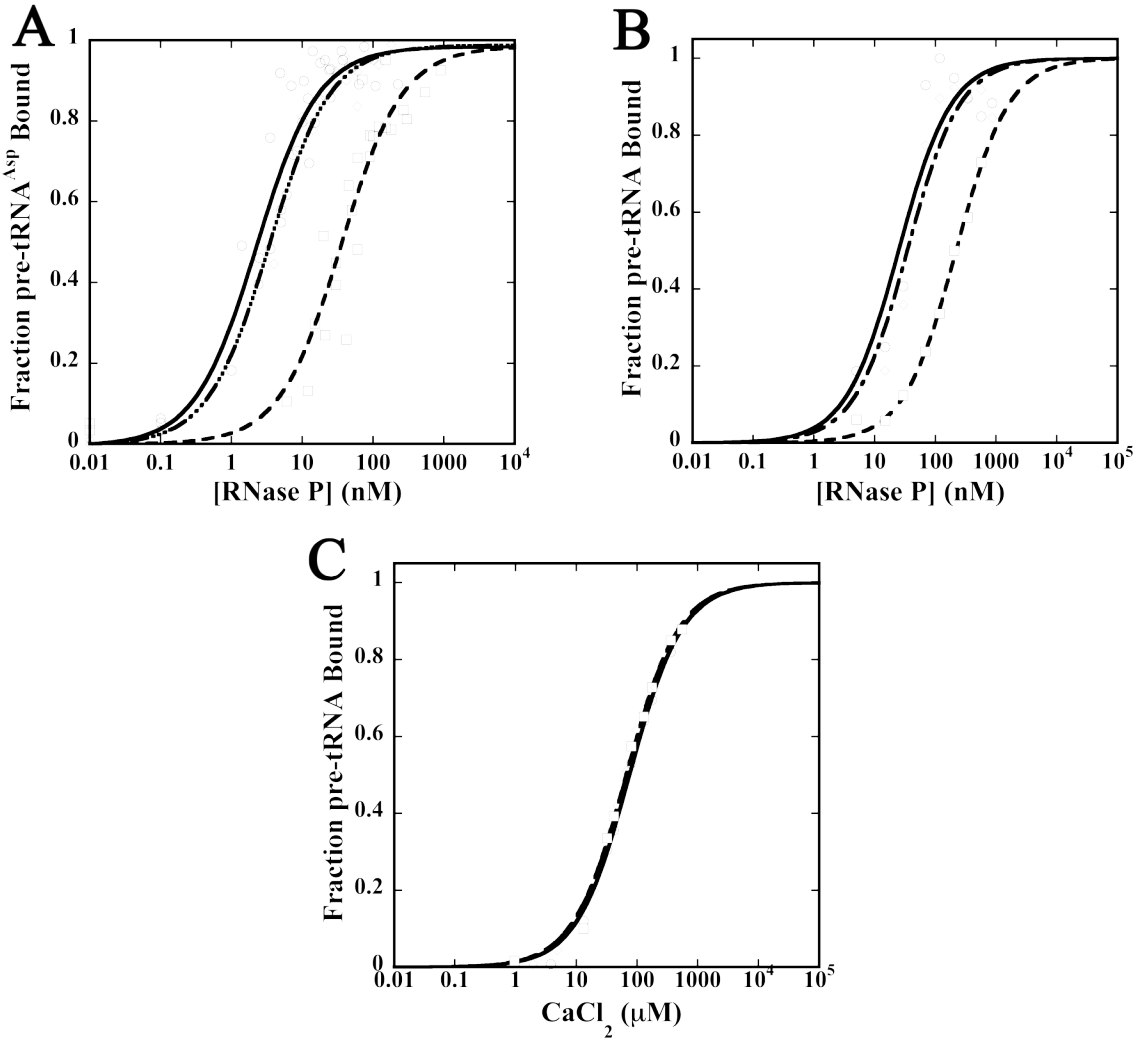

Figure V-2. (A) Binding curves for measuring $K_{D,obs}$ of ○ wild type, □ R60A, and ◇ R65A RNase P for pre-tRNA^{Asp} determined by centrifugational gel filtration in 50 mM MES, 50 mM Tris, 400 mM KCl, 10 mM $CaCl_2$, at 37°C. **(B)** Fluorescence titration data for measuring K_1 in 50 mM MES, 50 mM Tris, 180 mM KCl, 2 mM $[Co(NH_3)_6]$•Cl_3, at 37°C (○ WT, □ R60A, ◇ R62A). Data shown in Table IV-3. **(C)** Calcium dependence of pre-tRNA binding to RNase P ($K_{D,obs,Ca}$). RNase P (2μM R60A, 300 nM WT and R62A) was mixed with pre-tRNA^{Asp} (20 nM) to form E•S in 2 mM $[Co(NH_3)_6]$•Cl_3 $CaCl_2$ is titrated into the solution to stabilize the ES* complex. A single isotherm (equation 5) are fit to the data and the $K_{D,obs,Ca}$ values are listed in Table IV-4 (○ WT, □ R60A, ◇ R62A).

R60 plays a role in pre-tRNA 5' leader positioning

Previous studies (see Chapter III) proposed that the R60A mutant disrupts the orientation of the 5' leader in the central cleft of the protein [21]. Specifically, these data indicate that the R60A mutant perturbs a sequence-specific interaction between the 5' leader nucleotide at N(-4) and residues F20 and Y34 on the protein in the RNase P•pre-tRNA complex. Here we investigate the effect of the side chain of R60 on the interaction of the 5' leader with *B. subtilis* P protein using fluorescence techniques. The kinetics of binding pre-tRNA^{Asp} with a three nucleotide long leader and a fluorescein covalently attached at the 5' end (Fl-pre-tRNA^{3nt}) to RNase P were monitored by stopped-flow fluorescence in the presence of calcium so that pre-tRNA cleavage is slow. The fluorescent change observed in this assay reflects an alteration in the environment of the 5' fluorescein as a function of time due to binding to RNase P. The fluorescence time courses for binding pre-tRNA^{3nt} to wild type and R62A RNase P have two kinetic phases (Figure IV-3A). For wild-type RNase P, the first phase is associated with a decrease in fluorescence while the fluorescence signal increases in the second phase. These data are consistent with previously reported studies that assign these two phases as reflecting (a) an initial association of pre-tRNA with RNase P (fluorescence quenched phase), and (b) a conformational change step (enhanced fluorescence phase) in the kinetic mechanism (Scheme IV-1A, and Figure IV-3) [12]. Although the kinetic trace for pre-tRNA binding to RNase P containing the R60A mutation also displays two phases, both phases exhibit fluorescence enhancement in contrast to the data observed with wild type RNase P. This difference in fluorescence suggests that the environment of the fluorescein in the initial

RNase P•pre-tRNA complex is altered in the R60A mutant compared to wild type RNase P.

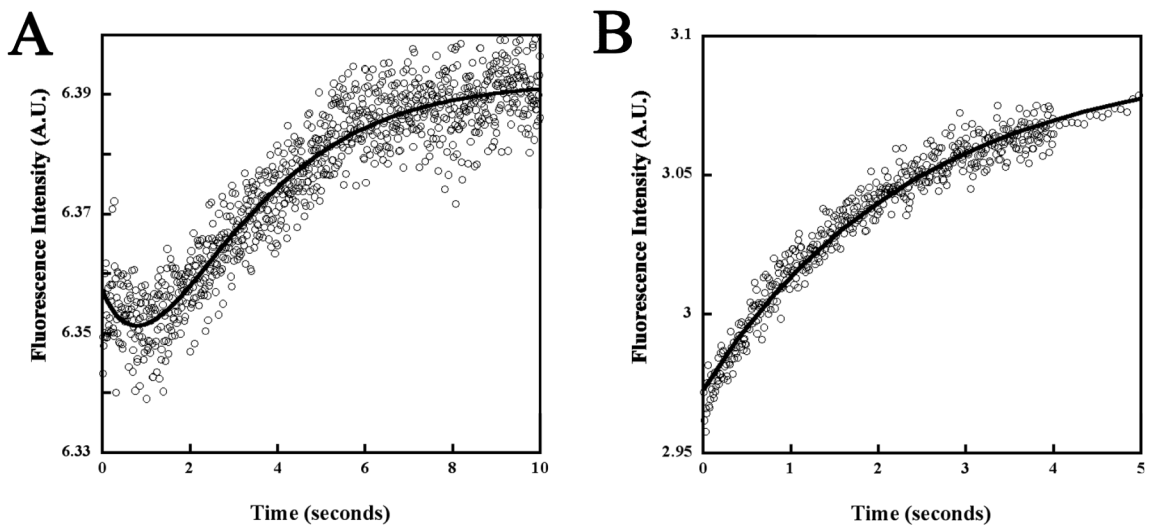

Figure V-3. Stopped flow traces of Fl-pre-tRNA^{3nt} with a three-nucleotide long leader binding to **(A)** WT RNase P and **(B)** R60A RNase . The directionality of the first phase is different for the wild type and R60A mutant, demonstrating that the fluoroscein at the 5' end of Fl-pre-tRNA^{3nt} is in a different environment.

The observed rate constants from the first stopped-flow fluorescence phase reflecting initial substrate association (k_{obs1} in Equation IV-3) was assessed as a function of RNase P concentration to calculate the substrate association rate (k_1) for wild-type, R60A, and R62A RNase P. The wild-type experiments were performed with two substrates: Fl-pre-tRNA^{3nt} and a 5' fluorescein labeled pre-tRNA^{Asp} possessing a 5 nucleotide long leader (Fl-pret-RNA^{5nt}). The k_1 values for R60A and R62A were measured with Fl-pre-tRNA^{3nt} and Fl-pre-tRNA^{5nt}, respectively. Fl-pre-tRNA^{5nt} was chosen because the binding and single turnover kinetic studies presented here were performed with a pre-tRNA^{Asp} containing a 5 nucleotide long 5' leader. However, the Fl-pre-tRNA^{5nt} substrate does not demonstrate an interpretable fluorescence signal change in the R60A mutant, so the Fl-pre-tRNA^{3nt} substrate, which clearly shows two phases

reflecting two-step binding, was used instead. For all three proteins, wild type, R60A, and R62A the pre-tRNA on rate k_1 is ~1 $\mu M^{-1}s^{-1}$ at 37°C. Therefore, these mutations do not alter the rate of pre-tRNA association. Thus, R60A must be altering the binding equilibrium, K_1, by increasing the off rate (k_{-1} in Scheme IV-1A), as opposed to decreasing the substrate association rate (k_1).

R60 and R62 do not enhance divalent metal ion binding after ES formation

Scheme IV-1A depicts a minimal kinetic mechanism for RNase P. However, previous kinetic studies indicate that the E•S* complex is stabilized by divalent cations; this minimal mechanism therefore can be expanded into a more complete mechanism as illustrated in Scheme IV-2A [13]. The M^{2+} ion in the expanded kinetic mechanism represents a divalent cation that makes an inner-sphere contact with P RNA to stabilize a conformational change prior to catalysis [13]. The site of this metal binding to P RNA is unknown, although it has been hypothesized to bind in helix P4 [13,34]. To address whether the RNR motif enhances the affinity of this divalent metal, the effect of mutations in the RNR motif on the observed equilibrium ($K_{D,obs,Ca}$) for formation of E•S*-M^{2+} (E•S + M^{2+} $\rightleftharpoons$ E•S-M^{2+} $\rightleftharpoons$ E•S*-M^{2+}) was assessed (Scheme IV-2A).

Table V-4. Values for the apparent calcium affinity ($K_{D,obs,Ca}$) measured by fluorescence titrations

	$K_{D,obs,Ca}$ (μM)[a]	Mutant $K_{D,obs,Ca}$ / WT $K_{D,obs,Ca}$
WT	60 ± 5	1
R60A	40 ± 6	0.7 ± 0.1
R62A	64 ± 7	1.1 ± 0.1

a 50 mM MES, 50 mM Tris, 180 mM KCl, 2mM $[Co(NH_3)_6]•Cl_3$, 37°C, titrating to final $CaCl_2$ concentrations between 0 – 200 μM.

To test this, the enzyme-substrate (E•S) complex was pre-formed in 2 mM $Co(NH_3)_6^{3+}$ at a saturating RNase P concentration, then calcium was titrated into the reaction and the change in fluorescence resulting from the conformational change occurred was measured. The value for $K_{D,obs,Ca}$ was calculated from the fit of a single binding isotherm to the data (Scheme IV-2B). Since the reaction is done under saturating conditions, the starting reactant is E•S. Therefore, the $K_{D,obs,Ca}$ value reflects a combination of both the K_3 and K_5 steps in the expanded mechanism shown in Scheme IV-2A. $K_{D,obs,Ca}$ values were measured for wild type, R60A and R62A using previously

A)

$$\begin{array}{ccccccc} E + S + M^{2+} & \overset{K_1}{\rightleftharpoons} & ES + M^{2+} & & & & \\ K_2 \updownarrow & & \updownarrow K_3 & & & & \\ E - M^{2+} + S & \overset{K_4}{\rightleftharpoons} & ES\text{-}M^{2+} & \overset{K_5}{\rightleftharpoons} & ES^*\text{-}M^{2+} & \xrightarrow{k_{chem}} & EPL \longrightarrow E + P + L \end{array}$$

B) $K_{D,\,obs,\,Ca} = [ES][M^{2+}] / [ES\text{-}M^{2+}] + [ES^*\text{-}M^{2+}]$

$K_1 = [E][S] / [ES]$

$K_2 = [E][M^{2+}] / [E\text{-}M^{2+}]$

$K_3 = [ES][M^{2+}] / [ES\text{-}M^{2+}]$

$K_4 = [E\text{-}M^{2+}][S] / [ES\text{-}M^{2+}]$

$K_5 = [ES\text{-}M^{2+}] / [ES^*\text{-}M^{2+}]$

Scheme V-2 (A) The expanded minimal kinetic mechanism. Where E is RNase P holoenzyme, S is pre-tRNA substrate, M^{2+} is divalent metal **(B)** Equilibrium constant expressions to define the terms in (A).

described fluorescence titrations [35]. Neither the R60A or the R62A mutation significantly altered the affinity of RNase P for calclium; the value of $K_{D,obs,Ca}$ was altered < 1.5 – fold with respect to the wild type RNase P (Figure IV-4C, Table IV-4). These data argue that neither R60 nor R62 significantly affect the value of either K_3 reflecting calcium affinity or K_5, reflecting the conformation change. Alternatively,

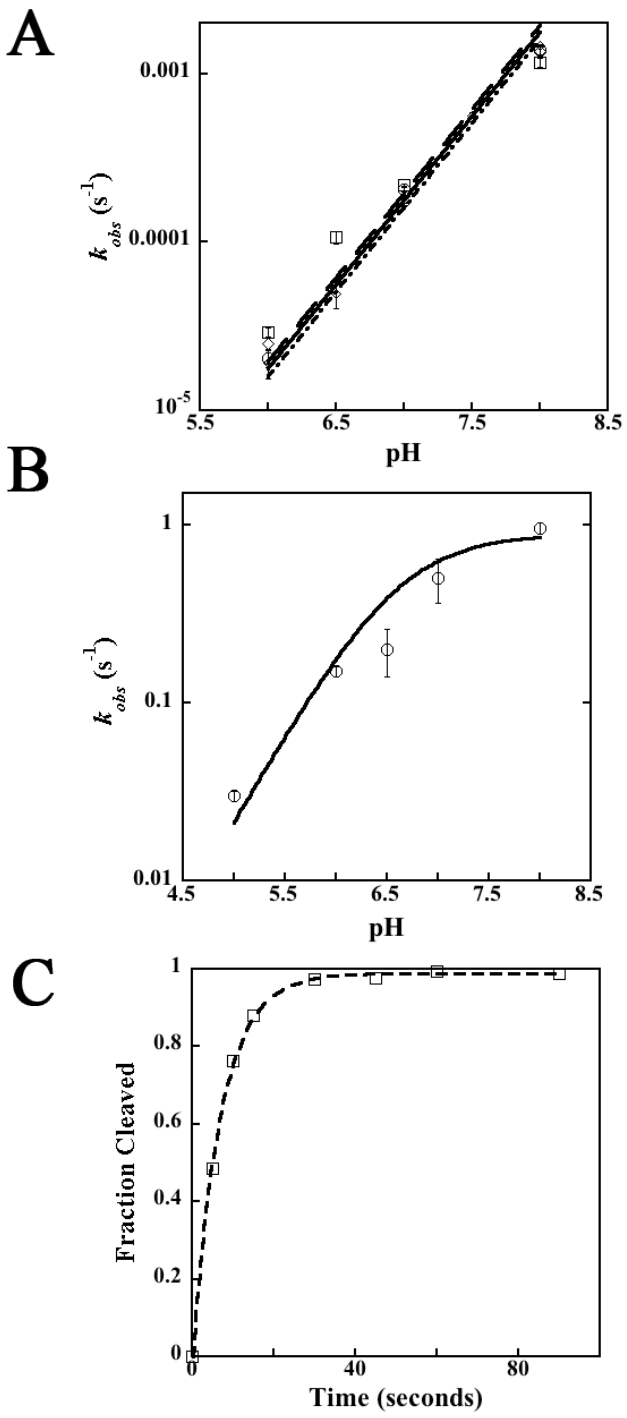

Figure V-4. (A) pH dependence of wild type, R60A, and R62A cleavage rates in 50 mM MES, 50 mM Tris, 180 mM KCl, 10 mM $CaCl_2$, 37°C, pH 5-8, **(B)** pH dependence of wild type cleavage rates cleavage rates in 50 mM MES, 50 mM Tris, 180 mM KCl, 10 mM $MgCl_2$, 37°C, pH 5-8, **(C)** Single-turnover time course for R60A in 50 mM MES, 50 mM Tris, 180 M KCl, 10 mM $MgCl_2$, 37°C, pH 6.0.

amine functionality in $Co(NH_3)_6^{3+}$ could effectively compensate for the deleted side chain (R60 or R62) to restore wild-type affinity for calcium.

RNR motif does not play a role in pre-tRNA cleavage step

To identify whether the side chains of the RNR motif contribute to the stabilization of the transition state for cleavage step (k_{chem}) we measured the single turnover cleavage rate constant in calcium (Table IV-5, Figure IV-4B). RNase P catalyzes cleavage of the 5' leader from pre-tRNA in a pH and metal dependent manner [10]. In calcium, the observed rate constants for product formation ($k_{obs,Ca}$) under single turnover conditions exhibit a log-linear dependence on pH, reflecting mainly the rate constant of the cleavage step (k_{chem}) because $k_{chem} << k_2$ under these conditions (Scheme IV-1B, Figure 4A) [33].

Table V-5. Single turnover rate constants under varying pH and divalent metal conditions

	WT	R60A	R62A
Mg^{2+}, pH 5.0[a] k_{obs} (s^{-1})	$0.03 \pm 2 \times 10^{-3}$	$0.03 \pm 7 \times 10^{-3}$	$0.03 \pm 2 \times 10^{-3}$
Mg^{2+}, pH 6.0[a] k_{obs} (s^{-1})	0.15 ± 0.01	0.1 ± 0.01	0.2 ± 0.01
Mg^{2+}, pH 6.5[a] k_{obs} (s^{-1})	0.2 ± 0.06	0.2 ± 0.2	0.1 ± 0.3
Mg^{2+}, pH 7.0[a] k_{obs} (s^{-1})	0.5 ± 0.14	0.5 ± 0.16	0.2 ± 0.05
Mg^{2+}, pH 8.0[a] k_{obs} (s^{-1})	0.96 ± 0.07	0.5 ± 0.09	0.2 ± 0.05
Ca^{2+}, pH 8.0[b] $k_{obs,\ Ca}$ (s^{-1})	$2 \times 10^{-3} \pm 2 \times 10^{-4}$	$1 \times 10^{-3} \pm 8 \times 10^{-5}$	$1 \times 10^{-3} \pm 5 \times 10^{-5}$
Mg^{2+} pK_a	6.6 ± 0.05	6.2 ± 0.06	5.8 ± 0.06

[a] 50 mM MES, 50 mM Tris, 180 mM KCl, 10 mM $MgCl_2$, 37°C
[b] 50 mM MES, 50 mM Tris, 180 mM KCl, 10 mM $CaCl_2$, 37°C.

To evaluate whether the RNR motif has a role in stabilizing the cleavage step catalyzed by RNase P, single turnover rate constants catalyzed by wild type RNase P, and R60A and R62A RNase P mutants in the presence of 10 mM calcium were measured. Neither R60A, nor R62A mutations significantly alter the value of $k_{obs,Ca}$ at any pH (Figure IV-4A, Table IV-5). These data indicate that the RNR motif does not directly stabilize the transition state of the cleavage reaction catalyzed by RNase P, which is unsurprising given that P RNA alone retains catalytic activity.

R60A and R62A mutations effect the E•S to E•S* conformational change.

In magnesium, the rate-determining step for wild type RNase P is not always the cleavage step (k_{chem}), as is the case in calcium (Scheme IV-1B). Under single turnover conditions the rate-limiting step for the reaction depends upon the pH of the reaction: chemistry is rate-limiting a low pH but not at high pH. As such, the observed pK_a of RNase P-catalyzed cleavage in magnesium is not a thermodynamic pK_a, but a kinetic pK_a that reflects this change in rate limiting step. The pH dependence of RNase P-catalyzed cleavage under single turnover conditions was measured for the wild type, R60A, and R62A RNase P in 10 mM $MgCl_2$. For the wild type enzyme at low pH, the rate constant is linearly dependent on the concentration of protons suggesting that the rate-limiting step is cleavage, and the value of k_{obs} reflects k_{chem} under saturating conditions (Scheme IV-1B). As pH increases the value of k_{chem} increases and approaches the value of k_2; therefore, k_{obs} reflects a combination of both the conformational change and substrate cleavage steps (Scheme IV-1B) and the value of the observed pK_a of 6.6 ± 0.05 mainly reflects this change in rate-limiting steps [12].

We find that the mutants in the RNR motif decrease the value of the observed pK_a for single turnover cleavage; the pK_a of R60A RNase P is lowered by less than half a pH unit to 6.2 ± 0.2 (Figure IV- 4B and C, Table IV-5). In contrast, the observed pK_a of R62A RNase P is lowered by almost a full pH unit to 5.8 ± 0.06. These shifts in the value of the pK_a means that the change in rate limiting steps occurs at a lower pH either due to an increase in the apparent rate constant for the pH dependent cleavage step or a decrease in the rate constants describing the pH independent conformational change. This latter effect could be accomplished either by decreasing the value of k_2 or altering the equilibrium concentration of E•S* by increasing the value of k_{-2}. In other words, the side chain of R62 (and R60 to a lesser extent) enhances the kinetics of the conformational change in RNase P prior to substrate cleavage.

Discussion

RNase P proteins, although functionally and structurally homologous, share very little sequence conservation. A comparison of RNase P protein sequences revealed that only ~10% of the amino acids in bacterial P proteins have conserved identities [15]. Almost half of these residues (R60, N61, R62, K64, R65, R68 in *B. subtilis*) are found on a single α-helix termed the RNR motif (Figure IV-1A). Two of these positions, R60 and R65, are invariant in all bacterial RNase P proteins, and a third position, R68, is conserved >80% of the time. Mutation of the RNR motif disrupts RNase P function *in vivo,* yet the exact structural and functional roles of the RNR motif have not been well understood [15,28]. In an effort to identify some of the reasons for this conservation, we investigated the precise contributions of RNR motif residues to the kinetic mechanism of

the enzyme. Our data demonstrate that the RNR motif influences a conformational change in the enzyme prior to catalysis, likely by stabilizing local RNA structure.

Photocrosslinker or affinity cleavage reagents covalently attached to P protein at residues in the RNR motif (R60, N61, R62, K64, R65 and R68) were previously reported to cleave or cross-link to the P RNA subunit, suggesting that the RNR motif might form a portion of the RNA-protein subunit interface [22]. Our findings confirm this hypothesis, as our data demonstrate that the side chains of two residues, R60 and R62, stabilize the holoenzyme by ~2 kcal/mol each at moderate salt concentrations (Table IV-1). Furthermore, a comparison of the ionic strength dependence of the binding affinity for wild-type and the R60A mutant P protein indicates that the positively charged R60 side chain makes an ionic contact with the negatively charged P RNA to stabilize the P RNA-protein complex (Table IV-1). The association rate of *E. coli* P protein was previously reported to be 10 to 100-fold slower than expected for diffusion controlled binding, suggesting that a conformational change occurs upon the formation of the P RNA•protein complex, as observed in the assembly of other RNPs including the ribosome and signal recognition particle [36,37]. Phosphorothioate iodine structure mapping are in good agreement with this hypothesis because they suggest that structural changes around the P RNA helix P4 may accompany protein binding [27]. Structure probing studies place both R60 and R62 near the presumed active site (P2, P3, P4 and P19) and in close proximity to the cleavage site and 5' leader of the pre-tRNA substrate [22,27]. Therefore, the side chains R60 and R62 in P Protein potentially stabilize not only holoenzyme formation, but also the structure of the RNase P RNA near the active site [22].

In the recent *B. subtilis* holoenzyme structural model, the RNR motif is located at the interface of the P RNA and the pre-tRNA substrate (Figures IV-1B), suggesting that the interactions with both P RNA and bound pre-tRNA [22,27]. The affinity of wild type RNase P for pre-tRNA^{Asp} is highly dependent on both the concentration of divalent (i.e. $CaCl_2$) and monovalent cations [21,24,35]. At saturating calcium concentrations (10 mM), the affinity of RNase P for pre-tRNA^{Asp} increases by 5-fold relative to the affinity at 2 mM $CaCl_2$. The $K_{D,obs}$ values measured here in saturating (10 mM) $CaCl_2$ for the R60A, R62A, R65A, and R68A P protein mutants (Figure IV-3A, Table IV-2) agree well with previously reported data (see Chapter III) measured at low (2 - 3.5 mM) $CaCl_2$ concentrations demonstrating that RNR motif mutants (R60A, R60C, N61A, R62A, K64C, R65C, R68A, R68C) decrease the affinity of the RNase P holoenzyme for pre-tRNA^{Asp} by 4 to 20-fold compared to wild-type RNase P [21]. All $K_{D,obs}$ values measured in calcium reflect a combination of the equilibria for the first two mechanistic steps shown in Scheme IV-1: pre-tRNA association with RNase P followed by a metal-dependent conformational change. These binding data demonstrate that the side chains of R60, R62, and R65 in the RNase P holoenzyme complex must contribute to the stability of one or both of the first two steps in the minimal kinetic mechanism.

Previous stopped-flow kinetic studies in buffer with $Co(NH_3)_6^{3+}$ showed that the holoenzyme can form stably and bind substrate, but that the subsequent E•S $\rightleftharpoons$ E•S* conformational step does not occur (Scheme IV-1) [13]. Thus, the formation of the E•S complex can be analyzed in this $Co(NH_3)_6^{3+}$ buffer system to determine whether R60, and R62 contribute to the first step in the minimal kinetic mechanism. Even though the R62A and R60A P protein mutants respectively increase the $K_{D,obs}$ for RNase P binding

pre-tRNA by 9 and 20 – fold compared to the wild type RNase P, only the R60A mutant exhibits a modest 1.1 kcal/mol destabilization of the first step of substrate association, K_1 (Figures IV-3B, Table IV-3).

Thus, the question arises; how do the R60 and R62 P protein mutants perturb $K_{D,obs}$ more than K_1? This is possible only if these mutants disrupt the conformational change step prior to catalysis (E•S $\rightleftharpoons$ E•S*) in the complex with RNase P (Scheme IV-1). Although the equilibrium for this step is not directly measurable, additional binding and single turnover kinetic studies strongly suggest that the RNR motif lowers the energetic barrier for this step.

The expanded kinetic mechanism shown in Scheme IV-2 better describes the metal-dependent conformational change than the mechanism in Scheme IV-1. Scheme IV-2 highlights the fact that the metal ion required for the conformational change could associate with RNase P either before or after substrate binding. As already described, the E•S complex can be formed in $Co(NH_3)_6^{3+}$ without divalent metals present. If calcium is then titrated into the E•S solution, the apparent affinity of RNase P for pre-tRNA increases and an apparent equilibrium constant for stabilization of the complex by calcium can be measured ($K_{D,obs,Ca}$). This constant reflects a combination of the equilibrium constants K_3 and K_5 in Scheme IV-2. The measured $K_{D,obs,\ Ca}$ values for RNase P containing either the R60A, or R62A mutation are both within error of wild type RNase P (Figure IV-2C, Table IV-4). These data suggest that these two arginines do not specifically stabilize the steps reflected by $K_{D,obs,Ca}$ (K_3 and K_5). Alternatively, $Co(NH_3)_6^{3+}$, which is more highly charged than calcium, can mimic the arginine side chain in these mutant RNase P•pre-tRNA complexes to stabilize the formation of E•S

and/or E•S* pathway resulting in an unchanged $K_{D,obs,Ca}$. In summary, the equilibrium data demonstrate that R60A and R62A have large impacts on $K_{D,obs}$, but have either no or moderate effect on K_1, and do not alter $K_{D,obs,Ca}$. By elimination, these data suggest that the side chairs of R60 and R62 stabilized the conformational change of E•S to E•S*.

To further probe whether the side chains of R60 and R62 contribute to the conformational change in the RNase P mechanism, single-turnover kinetic studies were undertaken to probe specific steps in the kinetic pathway. The finding that these residues do not alter the single turnover cleavage rate constants in calcium, and therefore do not participate in the cleavage reaction (k_{chem}), is unsurprising given that P RNA is the catalytic subunit of the holoenzyme (Table IV-5, Figure IV-4A) [1]. The observation that R60 and R62 alter the values of the single turnover rate constants in magnesium, where rate constants prior to chemistry become kinetically significant, agrees with both our binding data and previously reported binding data, providing further evidence that these residues contribute to a step in the kinetic mechanism prior to catalysis (Figure IV-4B, Table IV-5) [21]. R60A does not change the pK_a of the reaction as much as R62A, however it does reduce the k_{obs} values at high pH by at 2 - fold. At high pH in wild-type RNase P, the rate-limiting step in k_{obs} is no longer k_{chem}, but a combination of the rate constants for cleavage and conformational change (k_{chem}, k_2 and k_{-2}). The R62A mutant dramatically lowered pK_a in magnesium, shifting the pK_a by almost a full pH unit. Together, these data suggest that in the R60A and R62A mutants, k_2, k_{-2}, and k_{chem} are closer in magnitude at low pH, not because k_{chem} is smaller, but because k_2 and k_{-2} are altered. In summary, all of the data are consistent with mutations at R60 and R62 altering

the rate constant for the conformational change that occurs after substrate binding and prior to cleavage in the RNase P•pre-tRNA complex.

Now that we have established which step in the kinetic mechanism the RNR motif contributes to, the question remains as to how this portion of the P protein stabilizes the conformational change in the RNase P•pre-tRNA complex? Melting, binding, and folding studies of *E. coli* and *B. subtilis* RNase P suggest that bacterial proteins stabilize local P RNA structure [38]. Footprinting studies of the *E. coli* and *B. stearothermophilus* P RNAs complexed with *E. coli*, *B. stearothermophilus* and *B. subtilis* protein revealed that all three bacterial proteins protect the same region of P RNA; helices P3, P3, and P4 [27]. Furthermore, binding of P protein appears to influence the conformation of *E. coli* and *B. stearothermophilus* P RNA regions flanking helix P4. In the holoenzyme complex, the RNR motif is in close proximity to the P RNA helix P4, and we propose that the RNR motif functions by stabilizing the P RNA conformation in the putative active site helix P4 following substrate binding to enhance catalysis. The ionic interaction identified between R60 and P RNA is an example of one way that the RNR motif could fulfill such a role (Table IV-1). Several examples of arginines stabilizing RNA conformations can be found in the literature. For example, arginine residues in the human immunodeficiency virus (HIV) Tat and Rev proteins stabilize conformations of HIV RNA [39] [40,41].

A further role for the universally conserved first RNR motif residue, R60, can also be suggested. Previous studies proposed that in R60A RNase P the interaction between the 5' leader and the P protein is altered [21]. Stopped-flow fluorescence data provides further evidence for this (Figure IV-3). Therefore the side chain of R60 could

stabilize the active conformations of both the P RNA subunit and pre-tRNA substrate in the E•S* complex to bring them both together in the proper orientation for efficient cleavage.

In conclusion, the most highly conserved region of bacterial RNase P proteins, the RNR motif, is important for RNase P complex formation, and substrate association. Two residues, R60 and R62 also have roles in the kinetic mechanism of the *B. subtilis* enzyme, and stabilize a conformational change step (Scheme IV-1A). We propose that the positively charged RNR motif stabilizes the local structure of the nearby P RNA helix P4 to enhance substrate binding and catalysis.

Materials and Methods

Preparation of RNA and protein

All RNAs were transcribed from linearized plasmid digested with a restriction enzyme as templates for *in vitro* transcription catalyzed by T7 RNA polymerase, as previously described [42,43]. The *B. subtilis* P RNAs used in the magnetocapture assays and the *B. subtilis* pre-tRNA^{Asp} containing a five nucleotide leader (ptR5) used in the kinetic assays were prepared using excess guanosine to form RNA transcripts containing a 5' hydroxyl and were subsequently labeled at the 5' terminus with ^{32}P-γ-ATP (MP Life Technologies) catalyzed by T4 polynucleotide kinase (New England Biolabs) as previously described [44]. All RNAs were purified by electrophoresis on an 8 – 12% polyacrylamide denaturing gel.

The wild-type *B. subtilis* P protein and the N-terminal His-tagged *B. subtilis* P protein were expressed and purified as previously described [7,31]. Single alanine point

mutations were made using megaprimer PCR amplification and were cloned into either pET28b or pET8c vectors (Novagen) as previously described [7,22]. The recombinant *B. subtilis* P protein was expressed in BL21(DE3)pLysS *E. coli* containing plasmids encoding the variant P proteins grown at 37°C followed by induction by isopropylthio-β-D-galactopyranoside. The protein was purified using CM-sepharose chromatography, and the concentration was determined by absorbance at 260 nm (ε_{260} = 5120 M^{-1} cm^{-1}) [7].

Substrate Preparation and ^{32}P Labeling

The pre-tRNA^{Asp} substrate with a five-nucleotide long leader was synthesized *in vitro* by run-off transcription. The 5' end was radioactively labeled with ^{32}P using γ-^{32}P ATP and T4 polynucleotide kinase (PNK), followed by purification on a 12% denaturing polyacrylamide gel as previously described [8].

P RNA – P protein K_D determination by magnetocapture assay

Trace concentrations of 5' 32P- end labeled P RNA were denatured by heating at 95 °C for three minutes and were refolded at 25 °C in buffer containing 50 mM Tris (pH 8), 10 mM imidazole, 10 mM MgCl2, and 200 mM KCl. Holoenzyme complex was formed by incubating the radiolabeled P RNA with an excess of P protein (0.1 nM – 2 μM) at 25 °C for thirty minutes. Magnetic beads (10 – 20 μL) were added and the solution was agitated for an hour, as described previously [31]. An external magnet was used to separate the magnetic beads from the bulk solution, and the bound RNA was eluted from the beads in 100 mM EDTA, 2% (v/v) sodium dodecyl sulfate at 95°C for five minutes. The radioactivity in the supernatant (free RNA) and the eluate (bound

RNA) was measured by Cerenkov scintillation counting. The fraction bound was determined by ([Protein•RNA]/[RNATotal]) = (cpmeluate - cpmbackground) /(cpmendpoint - cpmbackground) where cpmbackground is the radioactivity bound in the absence of protein and cpmendpoint is that bound at saturating concentrations of protein [31] [8]. Equation IV-1 was fit to the data using Kaleidagraph (Synergy Software) curve-fitting program.

Equation V-1

$$\frac{[\mathrm{RNA \bullet Protein}]}{[\mathrm{RNA_{Total}}]} = \frac{1}{\left[1 + \left(\frac{\mathrm{K_{D,\,app}}}{[\mathrm{Protein}]}\right)\right]}$$

The dependence of the $K_{D,obs}$ dissociation constant on ionic strength was determined by varying the concentration of KCl (500 – 800 mM). At high ionic strength, the $K_{D,obs}$ is approximated by $\log K_{D,obs} = m'\psi \log [Z] - m'\psi \log K_3$ where m' is the number of ionic interactions and ψ is the thermodynamic value (0.89) for the proportion of phosphates with a metal bound [31]. The ionic strength was determined from Equation IV-2 where $[I_i]$ is the concentration of ion I_i, and Z_i is the ionic charge of ion i.

Equation V-2

$$\text{Ionic strength} = 0.5\left[\sum_i [I_i](Z_i)^2\right]$$

Stopped-flow fluorescence assays

Both P RNA and pre-tRNA were folded by incubating in 1 mM TE at 90°C for 3 minutes, followed by incubation at 37°C for 10 minutes. Buffer was then added to a final

concentration of 50 mM MES, 50 mM Tris, 180 mM KCl, 10 mM $CaCl_2$ at pH 6.0, and the solution was incubated for an additional 30 minutes at 37°C. The stopped flow assays were run under single turnover conditions, 0-2μM RNase P, and 50 nM Fl-pre-tRNA^{5nt} and Fl-pre-tRNA^{3nt}. The reactions were performed at 25°C and 37°C in a KinTek stopped flow. Equation IV-3 was fit to the data where A_1 and A_2 are amplitude terms, $k_{1,obs}$ and $k_{2,obs}$ are rate constants and C is the value of the starting fluorescence.

Equation V-3

$$\text{Fluorescence} = A_1e^{-k1,obs(t)} + A_2e^{-k2,obs(t)} + C$$

Measurement of $K_{D,obs}$

P RNA and pre-tRNA were folded as described above. After P RNA was folded, a 1:1.1 ratio of the appropriate P protein was added, and the solution was incubated at 37°C for an additional 30 minutes. Control experiments with ratios of 1:5 and 1:10 P RNA to R60A and R62A P protein were performed, and the data were not changed within the limitation of error for this technique (2-fold). These experiments indicate that the holoenzyme formed for all of the RNR motif mutants.

To measure $K_{D,obs}$, a >10-fold excess of RNase P was incubated for five minutes with ^{32}P 5' end labeled pre-tRNA substrates in the buffer described above at 37 °C. The concentration of RNase P holoenzyme ($[E_{total}]$) was varied (0 to 900 nM) for this experiment. The holoenzyme-substrate mixture was loaded onto a pre-packed G-75 Sephadex column, and the unbound substrate was separated from the RNase P-bound substrate via centrifugational gel filtration as previously described [32,43]. The fraction of substrate bound ($[ES]+[ES^*]/[S_{total}]$) was determined using scintillation counting. A

standard binding isotherm was then fit to the data to calculate dissociation constants (Equation IV-4).

Equation V-4

$$[ES]/[S_{total}] = 1 / (1+ K_{D,\,obs}/[E_{total}])$$

Fl-pre-tRNA^{3nt} and Fl-pret-RNA^{5nt} synthesis and labeling

Substrates containing a 5′-monothiophosphate was prepared by *in vitro* transcription using T7 RNA polymerase in the presence of GMPS (4 mM ATP, CTP, UTP, and GMPS, 0.8 mM GTP, 0.1 μg/μL T7 RNA polymerase, 0.1 μg/μL linearized DNA template, 28 mM $MgCl_2$, 1 mM spermidine, 5 mM DTT, and 50 mM Tris-HCl, pH 8.0, incubated at 37 °C for 4 h). Transcription reactions were terminated by addition of 30 mM EDTA, and the RNA was concentrated 10-fold and exchanged into TE buffer (10 mM Tris-HCl, pH 7.0, and 2 mM EDTA) by centrifugal filtration. A 10-fold molar excess of 5-IAF dissolved in DMSO was added to the pre-tRNA solution and incubated overnight in the dark at 4 °C, and terminated upon the addition of DTT or 2-mercaptoethanol (10 mM). The Fl-pre-tRNA^{3nt} and Fl-pret-RNA5nt labeled substrates were purified by denaturing gel electrophoresis (15%polyacrylamide, 8 M urea).

Fluorescence titration measurements of K_1

Fl-pre-tRNA^{5nt} was prepared as described above [23]. RNase P holoenzyme and pre-tRNA were folded as outlined above for $K_{D,obs}$ measurements, the only difference is that cobalt hexaammine is substituted for calcium in the buffer (50 mM MES, 50 mM Tris, 400 mM KCl, 2 mM $Co(NH_3)_6^{3+}$). Fl-pre-tRNA^{5nt} was incubated in buffer in a fluorescence cuvette at 37^{o}C for five minutes. Fluorescein was excited at 485 nm, and

fluorescent emission was collected at 535 nm. RNase P holoenzyme (0 – 860 nM) was titrated into the fluorescence cuvette, and the observed changes in fluorescence were plotted as a function of holoenzyme concentration. The data were fit with a quadratic binding isotherm, equation IV-5 [23]. The values measured in this study reflect K_1 in Schemes 1B and 2B.

Equation V-5

$$\Delta F = \Delta F_o + (\Delta F_{max} - \Delta F_o)((K_1 + E_o + S_o) - [(K_1 + E_o + S_o)^2 + 4E_oS_o / 2S_o)]^{1/2})$$

ΔF = Observed fluorescence enhancement

ΔF_o = Fluorescence in the absence of enzyme

ΔF_{max} = Fluorescence at enzyme saturation

Fluorescence titration measurements of $K_{D,obs,Ca}$

Pre-tRNA and RNase P holoenzyme were folded as outlined above in the following buffer: 50 mM MES, 50 mM Tris, 400 mM KCl, 2 mM $Co(NH_3)_6^{3+}$. 20 nM fluorescein-labeled pre-$tRNA^{Asp}$ and 30 nM wild-type or R62A RNase P holoenzyme, or 200 nM R60A RNase P, were incubated together in a fluorescence cuvette at 37°C for five minutes. Fluorescein was excited at 485 nm, and emissions were collected at 535 nm,. $CaCl_2$ (up to 200 μM) was titrated into the fluorescence cuvette, and the observed changes in fluorescence were plotted as a function of holoenzyme concentration. The data were fit with a quadratic binding isotherm equation IV-5. The values measured in this study reflected $K_{D,obs,Ca}$ in Scheme IV-2B.

Single turnover experiments

Experiments measuring single turnover cleavage were performed using excess holoenzyme concentrations ([E]/[S] >> 5; [E] = 0.4 – 2 μM; [S] ≤ 0.1 nM) with radiolabelled pre-tRNA^{Asp} with a five nucleotide long 5' leader at 37°C in two different conditions. Condition 1: 10 mM $CaCl_2$, 50 mM MES, 50 mM Tris, ~ 200 mM KCl (pH 5 to 8), ionic strength maintained at 0.639 with KCl. Condition 2: 10 mM $MgCl_2$, 50 mM MES, 50 mM Tris, ~200 mM KCl (pH 5 to 8). All reactions were quenched with an equal volume of buffer containing 8 M urea, 100 mM EDTA, and 0.05% (w/v) each of xylene cyanol and bromophenol blue. The 5' leader product was separated from the pre-tRNA substrate on a 20 % denaturing polyacrylamide urea gel. The gels were scanned using a PhosphorImager. All kinetic data were well-described by a single exponential (equation IV-6) [43]. All time points less than 3 seconds were measured on a KinTek quench flow apparatus.

Equation V-6

$$[P] = [P]_{\infty}\left(1 - e^{-k_{obs}t}\right)$$

References for Chapter IV

1. Guerrier-Takada C, Gardiner K, Marsh T, Pace N, Altman S: The RNA moiety of ribonuclease P is the catalytic subunit of the enzyme. *Cell* 1983, 35:849-857.

2. Gossringer M, Kretschmer-Kazemi Far R, Hartmann RK: Analysis of RNase P protein (rnpA) expression in Bacillus subtilis utilizing strains with suppressible rnpA expression. *J Bacteriol* 2006, 188:6816-6823.

3. Hall TA, Brown JW: Archaeal RNase P has multiple protein subunits homologous to eukaryotic nuclear RNase P proteins. *Rna* 2002, 8:296-306.

4. Jarrous N: Human ribonuclease P: subunits, function, and intranuclear localization. *Rna* 2002, 8:1-7.

5. Chamberlain JR, Lee Y, Lane WS, Engelke DR: Purification and characterization of the nuclear RNase P holoenzyme complex reveals extensive subunit overlap with RNase MRP. *Genes Dev* 1998, 12:1678-1690.

6. Walker SC, Engelke DR: Ribonuclease P: the evolution of an ancient RNA enzyme. *Crit Rev Biochem Mol Biol* 2006, 41:77-102.

7. Niranjanakumari S, Kurz JC, Fierke CA: Expression, purification and characterization of the recombinant ribonuclease P protein component from Bacillus subtilis. *Nucleic Acids Res* 1998, 26:3090-3096.

8. Kurz JC, Niranjanakumari S, Fierke CA: Protein component of Bacillus subtilis RNase P specifically enhances the affinity for precursor-tRNAAsp. *Biochemistry* 1998, 37:2393-2400.

9. Sun L, Campbell FE, Zahler NH, Harris ME: Evidence that substrate-specific effects of C5 protein lead to uniformity in binding and catalysis by RNase P. *Embo J* 2006, 25:3998-4007.

10. Kurz JC, Fierke CA: The affinity of magnesium binding sites in the Bacillus subtilis RNase P x pre-tRNA complex is enhanced by the protein subunit. *Biochemistry* 2002, 41:9545-9558.

11. Sun L, Harris ME: Evidence that binding of C5 protein to P RNA enhances ribozyme catalysis by influencing active site metal ion affinity. *RNA* 2007.

12. Hsieh J, Niranjanakumari S, Fierke CA: Conformational change follows precursor tRNA binding to the B. subtilis RNase P holoenzyme. *in preparation* 2008.

13. Hsieh J, Rueda D, Walter NG, Fierke CA: A High-affinity Inner-sphere Divalent Cation Stabilizes Conformational Change in the B. subtilis RNase P Holoenzyme•pre-tRNA Complex. *in press* 2008.

14. Smith D, Burgin AB, Haas ES, Pace NR: Influence of metal ions on the ribonuclease P reaction. Distinguishing substrate binding from catalysis. *J Biol Chem* 1992, 267:2429-2436.

15. Jovanovic M, Sanchez R, Altman S, Gopalan V: Elucidation of structure-function relationships in the protein subunit of bacterial RNase P using a genetic complementation approach. *Nucleic Acids Res* 2002, 30:5065-5073.

16. Stams T, Niranjanakumari S, Fierke CA, Christianson DW: Ribonuclease P protein structure: evolutionary origins in the translational apparatus. *Science* 1998, 280:752-755.

17. Kazantsev AV, Krivenko AA, Harrington DJ, Carter RJ, Holbrook SR, Adams PD, Pace NR: High-resolution structure of RNase P protein from Thermotoga maritima. *Proc Natl Acad Sci U S A* 2003, 100:7497-7502.

18. Spitzfaden C, Nicholson N, Jones JJ, Guth S, Lehr R, Prescott CD, Hegg LA, Eggleston DS: The structure of ribonuclease P protein from Staphylococcus aureus reveals a unique binding site for single-stranded RNA. *J Mol Biol* 2000, 295:105-115.

19. Wilson RC, Bohlen CJ, Foster MP, Bell CE: Structure of Pfu Pop5, an archaeal RNase P protein. *Proc Natl Acad Sci U S A* 2006, 103:873-878.

20. Niranjanakumari S, Stams T, Crary SM, Christianson DW, Fierke CA: Protein component of the ribozyme ribonuclease P alters substrate recognition by directly contacting precursor tRNA. *Proc Natl Acad Sci U S A* 1998, 95:15212-15217.

21. Koutmou KS, Zahler NH, Niranjanakumari S, Fierke CA: Specific Contacts between the P Protein Subunit of Bacillus Subtilis RNase P and the 5' leader of pre-tRNA Contribute to Molecular Recognition. *in preparation* 2008.

22. Niranjanakumari S, Day-Storms JJ, Ahmed M, Hsieh J, Zahler NH, Venters RA, Fierke CA: Probing the architecture of the B. subtilis RNase P Holoenzyme active site by crosslinking and affinity cleavage. *RNA* 2007, 13:512-535.

23. Rueda D, Hsieh J, Day-Storms JJ, Fierke CA, Walter NG: The 5' Leader of Precursor tRNA(Asp) Bound to the Bacillus subtilis RNase P Holoenzyme Has an Extended Conformation. *Biochemistry* 2005, 44:16130-16139.

24. Zahler NH, Koutmou KS, Kurz JC, Sohn J, Campbell FE, Niranjanakumari S, Harris ME, Fierke CA: Sequence Preference in the Interaction of Bacterial Ribonuclease P with pre-tRNA 5' Leaders. *in preparation* 2008.

25. Torres-Larios A, Swinger KK, Krasilnikov AS, Pan T, Mondragon A: Crystal structure of the RNA component of bacterial ribonuclease P. *Nature* 2005, 437:584-587.

26. Kazantsev AV, Krivenko AA, Harrington DJ, Holbrook SR, Adams PD, Pace NR: Crystal structure of a bacterial ribonuclease P RNA. *Proc Natl Acad Sci U S A* 2005, 102:13392-13397.

27. Buck AH, Kazantsev AV, Dalby AB, Pace NR: Structural perspective on the activation of RNase P RNA by protein. *Nat Struct Mol Biol* 2005.

28. Gopalan V, Baxevanis AD, Landsman D, Altman S: Analysis of the functional role of conserved residues in the protein subunit of ribonuclease P from Escherichia coli. *J Mol Biol* 1997, 267:818-829.

29. Gopalan V, Golbik R, Schreiber G, Fersht AR, Altman S: Fluorescence properties of a tryptophan residue in an aromatic core of the protein subunit of ribonuclease P from Escherichia coli. *J Mol Biol* 1997, 267:765-769.

30. Koutmou KS, Day-Storms J, Fierke CA: The RNR Motif of B. subtilis RNase P Plays a Role in Structuring the P RNA Active Site and pre-tRNA Substrate for Interaction. *in preparation* 2008.

31. Day-Storms JJ, Niranjanakumari S, Fierke CA: Ionic interactions between PRNA and P protein in Bacillus subtilis RNase P characterized using a magnetocapture-based assay. *Rna* 2004, 10:1595-1608.

32. Crary SM, Niranjanakumari S, Fierke CA: The protein component of Bacillus subtilis ribonuclease P increases catalytic efficiency by enhancing interactions with the 5' leader sequence of pre-tRNAAsp. *Biochemistry* 1998, 37:9409-9416.

33. Smith D, Pace NR: Multiple magnesium ions in the ribonuclease P reaction mechanism. *Biochemistry* 1993, 32:5273-5281.

34. Koutmou KS, Getz MM, Pazicni S, Casiano-Negroni A, Penner-Hahn JE, Al-Hashimi HM, Fierke CA: Identification and characterization of a tightly bound metal in the P4 helix of the metallo-ribozyme ribonuclease P. *in preparation* 2008.

35. Hsieh J, Fintushel S, Hewlett N, Walter NG, Fierke CA: Concerted Conformational Change in the B. subtilis Holoenzyme•pre-tRNA Complex Requires Contribution from Both PRNA and P Protein interaction with Pre-tRNA. *in preparation* 2008.

36. Talbot SJ, Altman S: Kinetic and thermodynamic analysis of RNA-protein interactions in the RNase P holoenzyme from Escherichia coli. *Biochemistry* 1994, 33:1406-1411.

37. Williamson JR: Induced fit in RNA-protein recognition. *Nat Struct Biol* 2000, 7:834-837.

38. Buck AH, Dalby AB, Poole AW, Kazantsev AV, Pace NR: Protein activation of a ribozyme: the role of bacterial RNase P protein. *Embo J* 2005, 24:3360-3368.

39. Tan R, Frankel AD: Costabilization of peptide and RNA structure in an HIV Rev peptide-RRE complex. *Biochemistry* 1994, 33:14579-14585.

40. Tan R, Frankel AD: Circular dichroism studies suggest that TAR RNA changes conformation upon specific binding of arginine or guanidine. *Biochemistry* 1992, 31:10288-10294.

41. Hermann T, Patel DJ: RNA bulges as architectural and recognition motifs. *Structure* 2000, 8:R47-54.

42. Milligan JF, Uhlenbeck OC: Determination of RNA-protein contacts using thiophosphate substitutions. *Biochemistry* 1989, 28:2849-2855.

43. Beebe JA, Fierke CA: A kinetic mechanism for cleavage of precursor tRNA(Asp) catalyzed by the RNA component of Bacillus subtilis ribonuclease P. *Biochemistry* 1994, 33:10294-10304.

44. Ziehler WA, Day JJ, Fierke CA, Engelke DR: Effects of 5' leader and 3' trailer structures on pre-tRNA processing by nuclear RNase P. *Biochemistry* 2000, 39:9909-9916.

CHAPTER VI

IDENTIFICATION AND CHARACTERIZATION OF A TIGHTLY BOUND METAL IN A MODEL OF THE P4 HELIX OF THE METALLO-RIBOZYME RIBONUCLEASE P [x]

Introduction

Ribonuclease P (RNase P) is the ribonucleoprotein complex that catalyzes the metal dependent maturation of the 5' end of tRNAs. Bacterial RNase P enzymes have two components; a large RNA (P RNA, ~400 nucleotides), and a small associated protein (P protein, ~120 amino acids) (Figure V-1A). P RNA alone can catalyze the cleavage of the 5' end of pre-tRNAs in the presence of high salt and divalent metal ion concentrations, making RNase P a ribozyme [1]. *In vivo* the metal requirement is most likely fulfilled by magnesium ions, which facilitate not only P RNA folding, but are also proposed to directly participate in catalysis [2]. RNase P catalyzes the cleavage of a specific phosphodiester bond that produces 5' phosphate and 3' hydroxyl end groups (Figure V-1B) [3-7]. Although magnesium is the metal cofactor *in vivo*, the enzyme is

[x] Work presented in this chapter is included in a manuscript of the same title by M. Getz, K.S. Koutmou, S. Pazicni, A.J. Andrews, A. Negroni-Casiano, J.E. Penner-Hahn, H. Al-Hashimi, and C.A. Fierke. The data displayed were collected by K.S. Koutmou (material preparation and XAS experimental design), S. Pazicni (XAS), and M.M. Getz (NMR). K.S. Koutmou was responsible for coordinating the integration of the biology with the biophysics aspects of the project, and wrote the introduction, and discussion portions of the manuscript. The results section drafts were written by M. Getz and S. Pazicni, and edited by K.S. Koutmou.

active in the presence of other divalent metal ions, including calcium, manganese and zinc, *in vitro* [8-10]. The divalent metal binding sites essential for catalysis have not yet been clearly delineated in RNase P RNA; although several sites have been implicated in metal binding, these sites have not been well characterized [11,12].

Divalent metals associated with RNA can have structural, catalytic, and co-catalytic roles. Examples of metal ions bound to RNA are available in the crystal structures of tRNA[13], hammerhead ribozyme [14,15], group I intron [16,17], and the ribosome [18]. In RNase P metal ions stabilize the folded P RNA structure, enhance the affinity of RNase P for ligands, and stabilize the transition state for cleavage [2,19-23]. For the purposes of this discussion, we define catalytic metals as directly participating in the cleavage reaction, while co-catalytic metals are required for catalysis, but are not involved in the actual reaction. Many large ribozymes, such as group I and II introns and RNase P, require both catalytic and co-catalytic metals [24]. There are at least two catalytic or co-catalytic metal ions required for RNase P catalysis; however, details of where and how these ions are bound is lacking, leaving many questions regarding the molecular mechanism of the enzyme [24] [25,26]. Divalent metals ion contact RNA via either an outer- or inner-sphere interactions [2,4,5,24,27-30]: outer-sphere interactions are water-mediated, whereas inner-sphere interactions involve direct coordination of metal ions by RNA functional groups [31]. Inner-sphere metals bound to P RNA stabilize the catalytic transition state ion [32] [33]. Kinetic isotope effect studies of *E. coli* P RNA suggest that a metal ion directly coordinates a water molecule that functions as the nucleophile in the hydrolysis reaction; this interaction is proposed to enhance catalysis by lowering the pK_a of the metal-water to form the more reactive metal-

hydroxide and by stabilizing the developing negative charge in the transition state [20]. A majority (> 90%) of the roughly 150 divalent metal ions associated with P RNA are estimated to bind non-specifically to the polyelectrolyte via electrostatic interactions [2,34]. Discerning where and how the few divalent ions that interact with a specific site in P RNA is a major challenge to understanding the RNase P mechanism.

Helix P4 is the most highly conserved region of the catalytic P RNA, possessing 11 of the 21 universally conserved nucleotides in P RNA (Figures V-1C and V-1D) [35]. Although there are substantial differences between bacterial P RNAs and their archeal and eucaryal counterparts, P RNAs from all three domains of life possess homologs of the P4 helix [36] [37-39]. Hydroxyl radical-mediated footprinting, and affinity cleavage studies demonstrate that both the *E. coli* and *B. subtilis* P proteins are located near helix P4 in the holoenzyme complex. Moreover, cross-linking and affinity cleavage data reveal that pre-tRNA is also in close proximity to the helix in *E. coli* and *B. subtilis* RNase P [11,40,41]. Additionally, helix P4 is positioned at the core of the enzyme in both the P RNA crystal structures and the holoenzyme structural models, and is ideally situated to interact with both the P protein and substrate simultaneously [19,40,42,43] (Figure V-1A). Mutation of single nucleotides in the P4 helix reduces RNase P activity by > 100-fold *in vitro*, and inhibits cell growth *in vivo* under conditions of magnesium starvation [44-47]. Modifications of non-bridging oxygens that can disrupt metal ion coordination in the P4 helix from either *E. coli* or *B. subtilis* P4 helix result in large (1,000 to 10,000-fold) defects in RNase P catalytic activity [26,46,48]. Some of these catalytic defects can be rescued by addition of manganese, suggesting that metal ions form an inner sphere contact with the phosphodiester backbone in the P4 helix [7]. For

example, sulfur substitution at the non-bridging oxygens of the phosphodiester bonds in P4 helix of nucleotides A49 and A50 in *B. subtilis* RNase P (A67 and A68 in *E. coli*) decreases the cleavage rate constant enormously without affecting the affinity of pre-tRNA; these effects can be partially or wholly rescued by substitution of magnesium with manganese as the catalytic metal ion [11,46,48]. Crosslinking studies of *E. coli* RNase P RNA examining the position of pre-tRNA cleavage site relative to helix P4 suggest that metal binding in helix P4 leads to specific but indirect stabilization of catalytic metal ions at the scissile phosphate [11]. Thus, helix P4 has been identified as a likely region for catalytic and/or co-catalytic metal ion binding, and contains at least a portion of the putative active site of the enzyme [11,45,46,48,49]. Although biochemical evidence suggests that several divalent metal binding sites that enhance catalysis are located in P4, thus far it has been impossible to characterize the structure of these sites on a molecular level.

Here we combine nuclear magnetic resonance (NMR) and x-ray absorption (XAS) spectroscopic techniques to identify and characterize inner-sphere metal ions binding sites in a stem-loop that serves as a model for the *B. subtilis* RNase P helix P4 (corresponding to nucleotides 48-57 and 391-398 in the full-length *B. subtilis* enzyme). These two biophysical techniques complement each other, as NMR spectroscopic methods can identify nucleotides that are located near metals, while XAS provides information about the average ligand environment of a metal of interest, in this case zinc. Our NMR studies reveal a single high affinity divalent metal binding site located near G22 and G23 in the *B. subtilis* P4 helix mimic (G378 and G379 in full-length *B. subtilis*). XAS studies of this site indicate that the metal ion binds to the P4 helix mimic with a six-

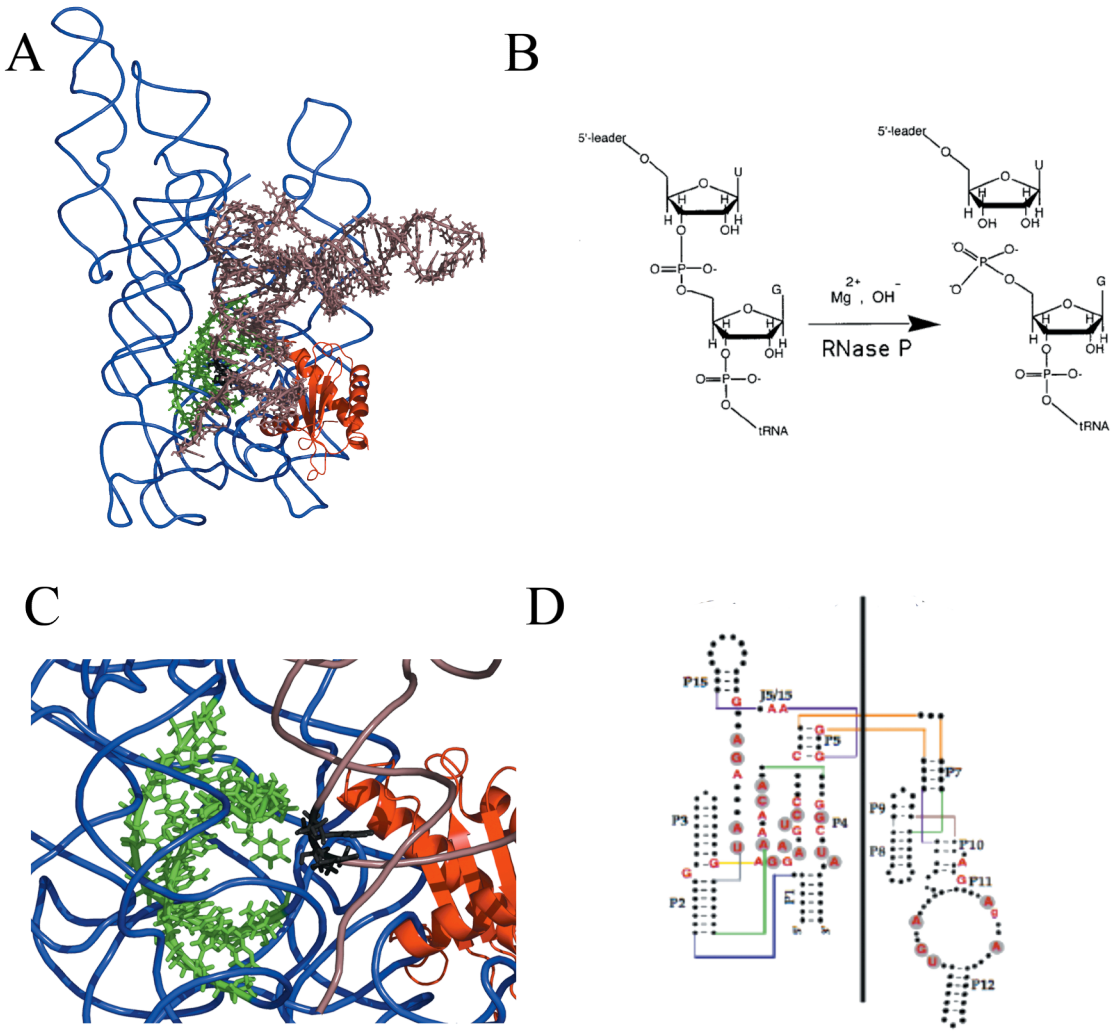

Figure VI-1. RNase P structure, reaction, and conservation **(A)** Structural model of the *B. subtilis* RNase P holoenzyme. P RNA is shown in blue, RNase P protein is red, and pre-tRNA substrate is shown in brown. The P4 helix in PRNA is highlighted in green, and the pre-tRNA cleavage site is denoted in black. **(B)** Schematic of the RNase P reaction. **(C)** A close-up view of the P4 helix (green) in P RNA (blue). This figure demonstrates that P4 is located near the pre-tRNA cleavage site (black) and the RNase P protein (red) in the holoenzyme model. **(D)** Secondary structure of bacterial P RNAs. All nucleotide that have conserved sequences are de-noted with letter.

coordinate geometry and an average Zn^{2+}– O/N bond distances of ~ 2.08 Å, indicative of inner sphere metal coordination. The NMR and XAS data together suggest a model for the metal environment of a tightly bound metal in the putative active site of the metallo-ribozyme RNase P. The work presented herein represents the successful combination of NMR and XAS for studying metal coordination by RNA, and should be applied to the study other metal-requiring ribozymes. Furthermore, this work identifies an inner-sphere metal binding site in helix P4, and provides the first molecular characterization of the environment of a catalytic and/or co-catalytic metal ion important to RNase P catalysis.

Results

Preparation of helix P4 for NMR and EXAFS studies[xi]

Helix P4 samples (Figure V-2D) for NMR EXAFS studies were prepared by *in vitro* transcription reactions using T7 RNA polymerase, and synthetic DNA templates containing the T7 promoter and sequence of interest [50]. Conditions were optimized for transcription (48 mM $MgCl_2$, 6 mM ATP/GTP /CTP/UTP, 0.08% w/v polyethylene glycol 8,000 MW, RNase inhibitor, pyrophosphatase, 20 pM DNA template, 50 mM Tris, 1 mM spermidine, 5 mM DTT, 0.35 μg / μL T7). All transcription volumes were ≤ 1 mL, and up to 5 transcriptions were run simulanteously. RNA transcripts were purified on 20% denaturing polyacrylamide gels containing 8 M urea/1x TBE. RNA was recovered from gels by soaking overnight in buffer (10 mM Tris, pH 8.0, 1 mM EDTA, 0.1%

[xi] "Preparation of helix P4" was performed by K.S. Koutmou; K.S. Koutmou and S. Pazicni designed XAS experiments; S. Pazicni collected XAS data; M.M. Getz conducted NMR experiments; A. Casiano made Figure V-2.

sodium dodecyl phosphate (SDS), 500mM NaCl), buffer exchanged into TE (10 mM Tris, pH 8.0, 1 mM EDTA) with Amicon Ultra-Concentrators (5,000 MWCO), and then ethanol precipitated. The RNA pellet was dried in a speed-vac, dissolved in water, and added to the appropriate buffer (each P4 preparation yielded final concentrations typically around 50-100uL of 9-12 mM RNA).

Resolving inner from outer-sphere interactions: $Co(NH_3)_6^{3+}$/ Zn^{2+} induced changes in chemical shift

Previous NMR studies on the *B. subtilis* RNase P P4 helix stem-loop model indicated that magnesium ion induces chemical shift changes at a number of positions, including G22 and G23 (Figure V-2D) [12]. However, chemical shift changes are very sensitive to the chemical environment, making it difficult to distinguish if they result from metal ion binding either proximal or distal to the altered site. An aim of this study was to distinguish between inner-sphere or outer-sphere interactions of divalent metals with functional groups in the P4 mimic. Towards that aim $Co(NH_3)_6^{3+}$, with its kinetically stable ligands, and Zn^{2+} were employed to mimic outer-sphere and inner-sphere interactions of Mg^{2+}, respectively [51]. Although RNase P has no activity in the presence of $Co(NH_3)_6^{3+}$ alone and decreased activity in Zn^{2+} alone, in the presence of both cations the catalytic activity of RNase P is comparable to the activity in magnesium [8,21,34]. Therefore, this combination of metal ions are particularly relevant for analyzing metal binding in the P4 helix mimic [8]. To distinguishing inner- and outer-sphere metals bound to helix P4, we conducted chemical shift titrations using $Co(NH_3)_6^{3+}$, Zn^{2+}, or both. Comparison of chemical shifts in $Co(NH_3)_6^{3+}$ and $Co(NH_3)_6^{3+}$ / Zn^{2+} reveal two nucleotides (G22 and G23 in Figure V-2D) that have inner-sphere

interactions with Zn^{2+}, as described below, suggesting that these nucleotides make similar contacts with Mg^{2+}.

In comparison to previous NMR studies of the *B. subtilis* P4 helix mimic, significantly less $Co(NH_3)_6^{3+}$ (0.5 mM) is needed relative to Mg^{2+} (15 mM) to induce chemical shift changes of similar magnitude [12]. This is unsurprising because $Co(NH_3)_6^{3+}$ is more positively charged than Mg^{2+} and is generally observed to bind to RNA with higher affinity than magnesium. In the previously reported *B. subtilis* P4 helix stem-loop structure Mg^{2+} showed two distinct binding regions, one above and one below the bulged U7 (U51 in *B. subtilis*). In contrast, titration of $Co(NH_3)_6^{3+}$ induces additional shifts in the P4 helix mimic in a continuous region above and below the U7 bulge [12]. Residues A10 and G23 exhibit the clearest differences in the direction that the chemical shift moves. To confirm that the mode of binding is different for Mg^{2+} and for $Co(NH_3)_6^{3+}$, the directions of chemical shift changes in the 2D HSQC spectra were compared. These results suggest different modes of metal binding at these sites.

One possible explanation for the differences in the direction of the chemical shifts is that Mg^{2+} interacts at these sites via inner shell interactions that cannot be accomplished by $Co(NH_3)_6^{3+}$. To test this hypothesis, we examined the alterations in the chemical shifts upon addition of 1 mM Zn^{2+} to the P4-$Co(NH_3)_6^{3+}$ sample. The RNase P holoenzyme retains high catalytic activity under similar conditions (1:4 $Co(NH_3)_6^{3+}$ to Zn^{2+}; Figure V-2B) [8]. Furthermore, zinc is an ideal metal for XAS studies, and was therefore also used in the NMR studies for consistency. Under these conditions, significant chemical shift changes are observed at a number of sites, including G23. Interestingly, a majority of the chemical shift changes upon addition of Zn^{2+} to the P4-

$Co(NH_3)_6^{3+}$ sample cause the peaks to shift back towards where their position in the absence of Zn^{2+}, $Co(NH_3)_6^{3+}$, or Mg^{2+} ions alone, indicating that Zn^{2+} is displacing $Co(NH_3)_6^{3+}$ at these positions. Two sites, G23 (N1H1) and G22 (C8H8), the addition of Zn^{2+} causes the chemical shift to change from a unique value in $Co(NH_3)_6^{3+}$ towards the position observed in Mg^{2+} (Figure V-2B).

In order to determine where Zn^{2+} binds in the absence of $Co(NH_3)_6^{3+}$, 16 mM $ZnCl_2$ was added to a sample of 0.1 mM P4 RNA. In contrast to the results upon addition of Mg^{2+} or $Co(NH_3)_6^{3+}$, the majority of peaks do not shift significantly upon addition of Zn^{2+} alone. The one exception to this is residue G22 where the C8H8 (black), and N1H1/N3H3 (yellow) resonances shift by > 0.05 ppm (Figure V-2A and 2B). These shifts in the nucleobase resonances are particularly significant because they are in close proximity to the functional groups that typically coordinate divalent metal ions, namely O6 and N7 in purines [12]. Smaller changes are seen in the imino peaks of U11, U21, G23 and U26 perhaps due to secondary binding effects of neighboring residues (Figure V-2A). In summary, the sites that shift the most in both $Co(NH_3)_6^{3+}/Zn^{2+}$ and Zn^{2+} alone are G22 and G23, suggesting inner sphere coordination at this site.

Probing P4 metal localization using Mn^{2+} paramagnetic line broadening

We sought to confirm sites of metal localization by a method that relies on detection of resonance linewidths and intensities rather than chemical shifts. We chose to examine the changes in linewidth / intensities as a function of the manganese (Mn^{2+}) concentration to detect sites of localization within P4. Manganese is a paramagnetic ion and it induces distance-dependent ($\propto r^{-6}$) line broadening in the resonances located near

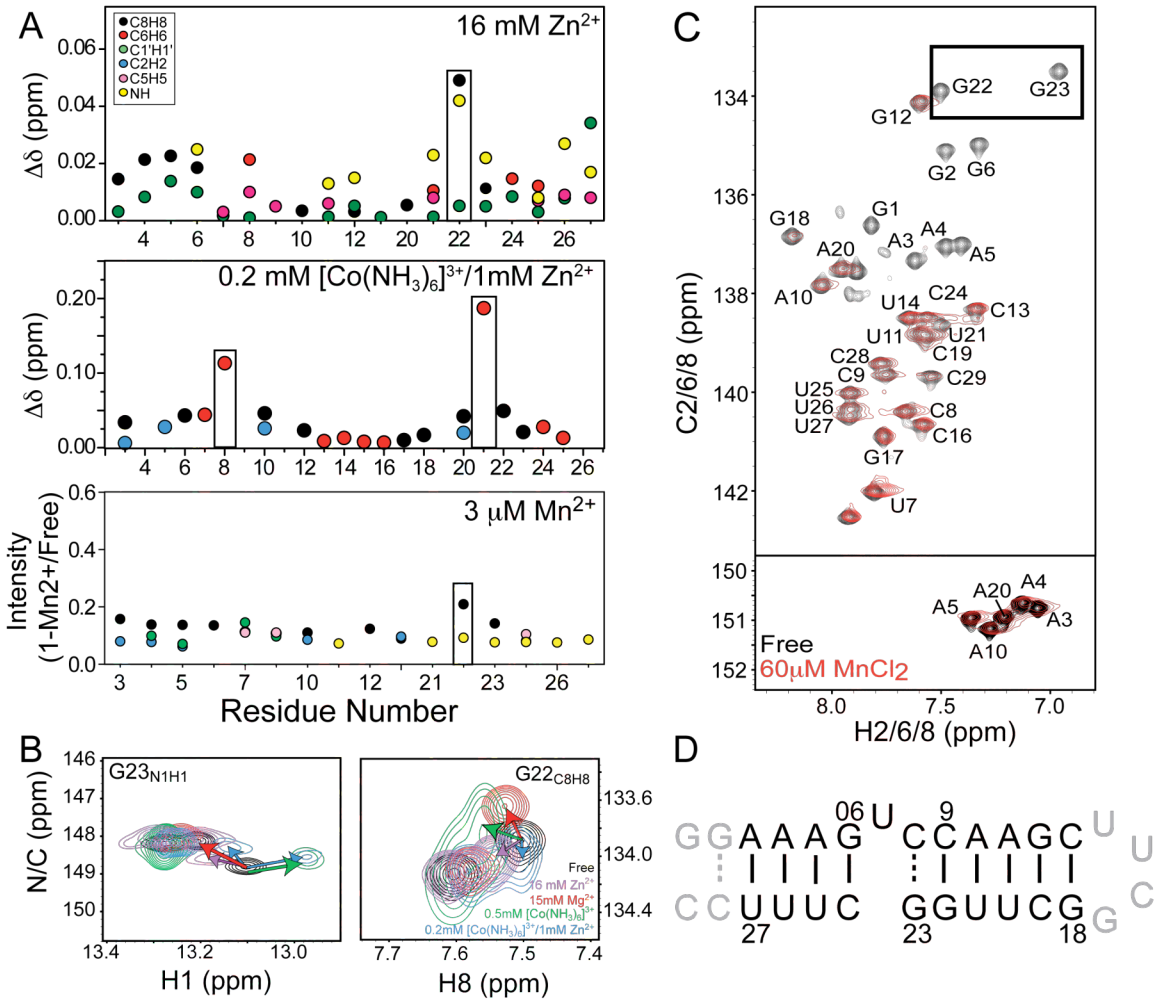

Figure VI-2. Metal localization and detection of inner sphere binding sites in P4 detected by Mn^{2+} and a combination of $Co(NH_3)_6^{3+}/Zn^{2+}$. **(A)** Chemical shift changes upon addition of 16 mM Zn^{2+}, 0.2mM $Co(NH_3)_6^{3+}$/ 1mM Zn^{2+} and normalized intensities (=1-I_M/I_F) upon addition of 3 μM Mn^{2+} are shown as a function of residue number for the following vectors: C8H8 (black), C6H6 (green), C1'H1' (red), C5H5 (blue) and C2H2 (pink), N1H1/N3H3 (yellow). **(B)** Sites in P4 with unique chemical shift environments measured in 15 mM Mg^{2+} (red), 0.5 mM $Co(NH_3)_6^{3+}$ (green), 0.2 mM $Co(NH_3)_6^{3+}$/1 mM Zn^{2+} (blue), and 16 mM Zn^{2+} (purple). **(C)** The aromatic region of a 2D HSQC experiment on the P4 construct both in the absence (black) and in the presence of 60 M Mn^{2+} (red). Highlighted by a black box is the main site for metal binding. **(D)** Secondary structure of P4.

the metal ion. This method has been used in other RNA systems including the hairpin ribozyme, varkud satellite ribozyme, and adenine sensing riboswitch, to identify nucleotides that directly coordinate divalent metals [52-54].

Spectra were recorded following the addition of Mn^{2+} to the P4 stem-helix RNA. 2D HSQC experiments were recorded on ^{13}C / ^{15}N labeled P4 samples in the presence of 3 μM, 6 μM, 12 μM, 24 μM, and 60 μM $MnCl_2$. The degree of line broadening was computed and compared qualitatively from 1- (I_M/ I_F) in which I_M and I_F are the resonance intensities observed in the presence and absence of Mn^{2+}. Increasing the concentration of Mn^{2+} (3 to 6 μM) resulted in an increase in the line broadening at G22 and G23, which showed the greatest broadening of any resonances at all concentrations of Mn^{2+} (Figures V-2B and V-2C). A secondary site appears at higher (12 μM) Mn^{2+} concentrations at residues A3-A5 and to a lesser extent G6 (Data not shown). These two groups of broadened resonances correspond to largest chemical shift perturbations upon addition of Mg^{2+} ions suggesting metal binding sites at these positions [12]. Weak broadening was also observed at higher Mn^{2+} concentrations (60 μM) at residues C9, U11, U21, C24, U25, U26, and U27 which correspond to sites adjacent to the proposed binding sites that are, as expected, affected to a lesser extent by localization of the paramagnetic metal (Figure V-2C).

The results from Mn^{2+} line broadening experiments combined with the data from the $Co(NH_3)_6^{3+}$ / Zn^{2+} induced changes in chemical shift studies suggest the identity of nucleotides in the P4 helix mimic that make inner-sphere contacts with divalent metals (Zn^{2+} and Mn^{2+}). Interestingly, only G22 and G23 exhibit line broadening at low Mn^{2+} concentrations, and were identified in the chemical shift mapping studies as having inner-

sphere contacts with Zn^{2+}. We conclude from these data that G22 and G23 comprise a single site in the P4 helix that directly coordinates divalent metal ions.

Characterization of the tightly bound divalent site

X-ray Absorption Near Edge Structure (XANES) and Extended X-ray Absorption Fine Structure (EXAFS) are metal-specific techniques that provide information about the average ligand environment of a metal of interest, in this case, the divalent metal that binds to G22 and G23 in helix P4. In general, large RNAs bind multiple metal ions, a situation that renders XANES and EXAFS uninformative, because XAS data provide information about an average metal environment. However, the NMR data indicate that the P4 helix mimic contains a single, high affinity inner-sphere metal site that can be uniquely populated at low concentrations of metal ions. Therefore, XANES and EXAFS can be used to provide structural information for this critical metal-binding site in the P4 mimic. These techniques are especially useful for obtaining information about the structures of zinc and other d^{10} metals, which are silent in other spectroscopic methods [55]. Although EXAFS can distinguish between atoms in different rows of the periodic table, it cannot distinguish between atoms of similar atomic number, such as nitrogen and oxygen. EXAFS can also provide information beyond the first coordination sphere of the metal, details which can potentially be useful in distinguishing between coordination of a metal by the phosphodiester backbone versus a ribonucleotide base of an RNA molecule. This work demonstrates that EXAFS, a method regularly applied to metalloproteins, can be used together with NMR to investigate the structure of metal ions bound to RNA. We used these biophysical techniques to characterize the inner-sphere metal site from the perspective of the metal ion, instead of the RNA.

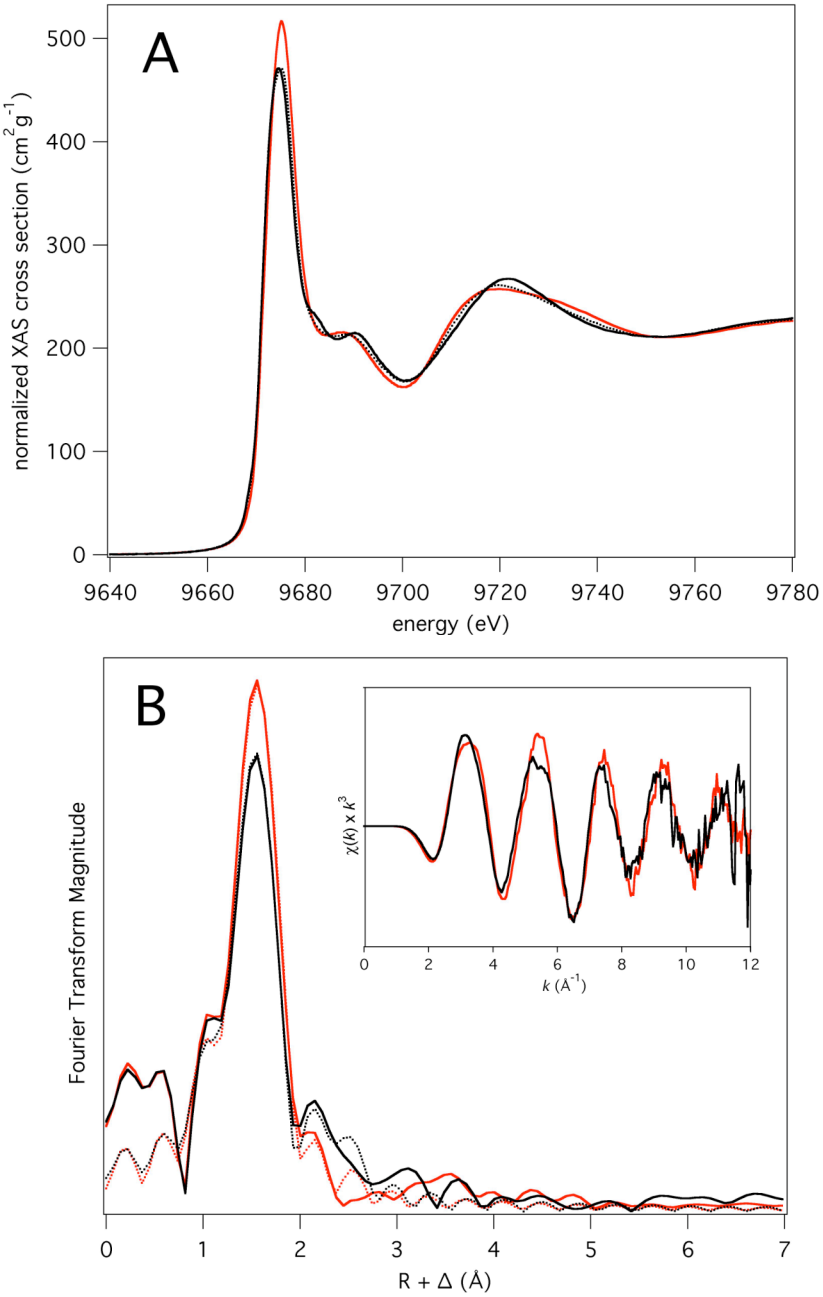

Figure VI-3. (A) Normalized XANES spectra of zinc-RNA samples: 1 mM Zn^{2+} + 4 mM P4 (black, solid), 2 mM Zn^{2+} + 2 mM $Co(NH_3)_6^{3+}$ + 4 mM P4 (black, dashed), and 2 mM Zn^{2+} (red, solid). All samples were 10 mM in MES, 10 mM in $NaNO_3$, 30% glycerol, pH ~ 6. **(B)** Fourier transform (k = 2.55-10.8 Å^{-1}) of the k^3-weighted EXAFS data showing (in black) the first and second shell scattering peaks for Zn^{2+} in the presence of RNA and $Co(NH_3)_6^{3+}$ and (in red) the first shell scattering peak for Zn^{2+} in a buffer control sample. Dashed lines represent the best fits to these data: (black) 6 N/O scatterers and 6 C scatterers, and (red) 6 N/O scatterers. (inset) k^3-weighted EXAFS spectra of Zn^{2+} with (black, also contains $Co(NH_3)_6^{3+}$) and without (red) P4 construct.

Figure V-3A shows a comparison of the normalized XANES spectra for Zn^{2+} samples in the presence and absence of RNA, illustrating the changes that occur when Zn^{2+} binds to the P4 construct. Data were collected on three different samples: 1) helix P4 mimic in Zn^{2+}; 2) helix P4 mimic in $Co(NH_3)_6^{3+}$ and Zn^{2+}; 3) Zn^{2+} alone. To maximize the population of zinc bound to the high affinity site, the data measured in Zn^{2+} and $Co(NH_3)_6^{3+}/Zn^{2+}$ were collected with excess RNA (RNA:Zn stoichiometry = 4 mM : 2 mM) . While the XANES spectra of the Zn^{2+} in the presence of P4 appear very similar to that of the Zn^{2+}–MES control, subtle differences exist suggesting that the P4 construct perturbs the coordination environment of zinc relative to the buffer control. The most striking alteration is the difference in the normalized edge intensity between Zn^{2+} samples with and without RNA; the Zn^{2+}–MES control exhibits an ~ 50 cm^2g^{-1} higher K-edge intensity than do either of the Zn^{2+}–P4 samples (Figure V-3A). In addition, the post-edge (EXAFS) oscillations of the Zn^{2+}–MES control spectrum are out-of-phase with those of the Zn^{2+}–P4 spectra (Figure V-3A). Slight differences in the EXAFS oscillations of the Zn^{2+}–P4 samples are also observed, likely because the presence of $Co(NH_3)_6^{3+}$ further decreases any potential outer-sphere contact of zinc with the RNA molecule. The Zn^{2+}–P4 sample with $Co(NH_3)_6^{3+}$, therefore, represents the Zn^{2+} – RNA sample with the more homogeneous zinc coordination environment. That the Zn^{2+}–P4 sample with $Co(NH_3)_6^{3+}$ is notably different than the Zn^{2+} only control sample and similar to the P4 - Zinc sample can be taken as strong evidence that zinc is binding preferentially to a high-affinity site on the RNA molecule.

Figure V-3B shows the EXAFS data, the Fourier transforms of the EXAFS data, and the fits to these data. The EXAFS data confirm the observation that zinc binds to the

P4 RNA construct and that the coordination environment of the zinc ion is perturbed relative to the Zn^{2+}–MES control sample. The EXAFS spectra of the Zn^{2+}–P4 with $Co(NH_3)_6^{3+}$ and Zn^{2+}–MES control samples display subtle differences, including the phase shift of the Zn^{2+}–MES control sample relative to the Zn^{2+}–P4 with $Co(NH_3)_6^{3+}$ sample mentioned above. Moreover, the Fourier transform of the Zn^{2+}–P4 with $Co(NH_3)_6^{3+}$ EXAFS data is notably different than that of the Zn^{2+}–MES control sample in two ways. First, the first-shell scattering peak (at $R + \alpha = \sim 1.5$ Å) of the Zn^{2+}–MES control sample is more intense than that of the Zn^{2+}–P4 with $Co(NH_3)_6^{3+}$ sample. Second, the Zn^{2+}–P4 sample with $Co(NH_3)_6^{3+}$ exhibits a greater Fourier transform intensity beyond the first-shell scattering peak (at $R + \alpha = \sim 2.2$ Å) than does the control. Both of these observations suggest that there is some type of outer-shell scattering occurring in the Zn^{2+}–P4 sample with $Co(NH_3)_6^{3+}$ that is not occurring in the Zn^{2+}–MES control sample. This is consistent with the fits to the data shown in Figure V-3B and summarized in Table 1. The best fits for the Zn^{2+}–P4 samples, with and without $Co(NH_3)_6^{3+}$, show the immediate coordination environment of zinc to be hexacoordinate of O/N scatterers. The best fit of Zn^{2+}–MES control sample also shows the first-shell coordination of zinc to be 6 O/N, albeit with slightly shorter average Zn^{2+}–O/N distances. The distinct difference between the Zn^{2+}–MES control sample and the Zn^{2+}–P4 sample samples, though, lies in the fitting of second shell scatters. The fits of the Zn^{2+}–P4 samples are significantly improved with the addition of a second shell composed of either six carbon or two phosphorous scatters, as judged by the reduced chi-squared statistic ξ'. Carbon and phosphorous are arguably the only relevant atoms with which to model the second shell of a zinc coordinated to the P4 construct and cannot with confidence be

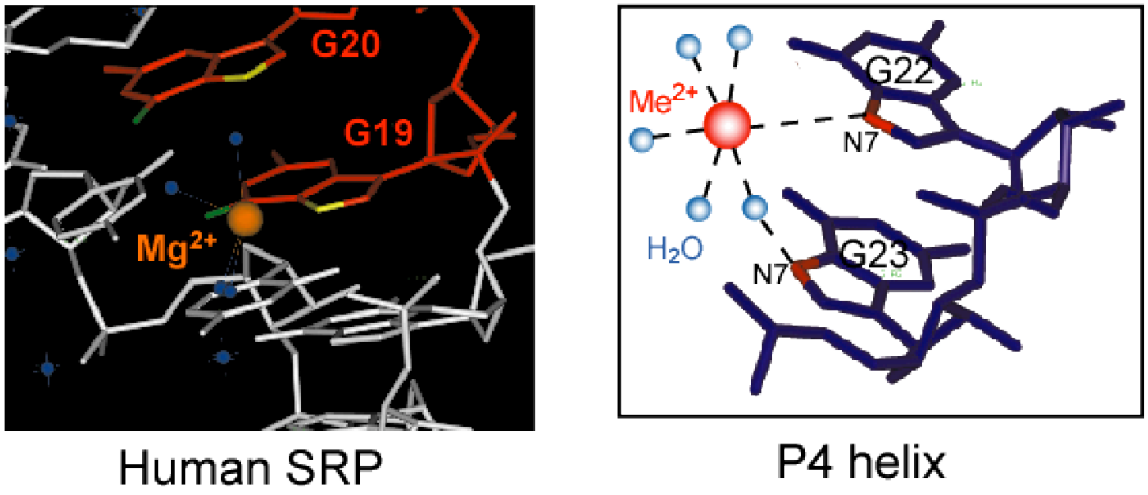

Figure VI-4. Inner sphere binding observed in SRP crystal structure and proposed in P4. Crystal structure of Human SRP at 2.0 Å resolution (PDB ID#1D4R) showing tandem guanine residues binding Mg^{2+} with inner and outer sphere coordination[41]. Proposed model of inner sphere binding with the bases of P4, an inner sphere contact in G22 and an outer sphere contact in G23.

distinguished from each other by these fits. The fit of Zn^{2+}–MES control sample, however, is not improved significantly by the addition of a second shell of P/C scatters, as judged by both ξ' and by the refined Debye-Waller factors. The requirement of second-shell P/C scatterers at an average distance of ~ 3 Å to accurately fit the EXAFS data of the Zn^{2+}–P4 samples strongly suggests that zinc is coordinating to a specific site in the P4 mimic in a six-coordinate fashion with average Zn^{2+}– O/N bond distances of ~ 2.08 Å. Combining the EXAFS and NMR spectroscopic data indicates that the zinc ion forms an inner sphere metal site at G22 and G23 in the P4 helix construct.

Discussion

RNase P is a metal dependent ribozyme required by all organisms. Metals play multiple essential roles in RNase P, including P RNA folding, conformational change stabilization, and pre-tRNA cleavage [2,22,56,57]. Although the metal requirement of RNase P is well documented, the P RNA nucleotides that have inner-sphere interactions with metals, and the nature of these interactions has not been clear. The aim of this study was to probe inner-sphere metal ions that interact with helix P4, and to characterize the environment of the these site(s) in an effort to better understand how metal ions enhance the RNase P cleavage reaction. These investigations successfully identified a potential catalytic / co-catalytic metal binding site in helix P4, and provide insight into the how metals interact with this essential helix to facilitate catalysis.

NMR structures of helix P4 mimics from *E. coli* (residues 63-73, and 354-36) and *B. subtilis* (residues 48-57 and 391-398) are currently available [12,58,59]. The structures of the *E. coli* and *B. subtilis* P4 helices are in good agreement with one another, indicating that this region of P RNA is conserved in both sequence and structure.

Moreover, the reported *B. subtilis* NMR structure of the P4 helix exhibits only small differences in inter-helical angles relative to the P4 helix in the crystal structure of the full-length *B. stearothermophilus* ribozyme [12,42]. These data suggest that the information ascertained about the P4 structure from studying the truncated helix is useful in the context of the entire P RNA.

The studies reported here also examined the *B. subtilis* P4 helix residues 48-57 and 391-398. The nucleotides we report to directly coordinate divalent metal ions (G22 and G23 in Figure V-2D) were previously identified as metal binding sites in the initial NMR structures of helix P4 from *E. coli* and *B. subtilis*. However, because the first structures were solved in the presence of either Mg^{2+} or $Co(NH_3)_6^{3+}$ ions, but not the presence of both $Co(NH_3)_6^{3+}$ and divalent ions, it had not been not possible to distinguish which metal binding sites were inner-sphere or outer-sphere sites in the initial structures.

The identification of G22 and G23 as an inner-sphere metal binding site is consistent with other metal sites observed in RNA, where metals bind tandem purines. For example, metals binding tandem purines are seen in crystal structures of human SRP, hammerhead ribozyme, leadzyme, and the 50S ribosomal subunit [60-63]. Figure V-4 highlights the crystal structure of the RNA from the human signal recognition particle showing a magnesium ion coordinating two tandem guanines (G19, and G20, Figure V-4A). This structure shows one visible inner-sphere coordination to the N7 of G19 and other outer sphere interactions with the O6 of G19 and the N7 and O6 of G20 through the four visible water molecules surrounding the metal. Such a mode of binding is consistent with our results in P4, which suggest at least one inner-sphere binding site in the G22-G23 region.

A working model for this metal site contains a direct coordination of magnesium to the N7 of G22, based on the large chemical shift changes in zinc in the C8H8 and N1H1 atom pairs, but other binding sites are possible such as the O6 in G22 and G23 about which no information was obtained in this study (Figure V-4). This model is also in agreement with XAS data collected on Zn^{2+} – P4 samples, which predict a hexacoorindate Zn^{2+} bound by O / N atoms at an average distance of 2.08 Å. Moreover, the fact that the Zn^{2+} – P4 EXAFS outer-shell scattering can be fit to a moderate number of carbon atoms at an average distance ~ 3 Å is also consistent with a working model of metal binding to a ribonucleotide pocket formed by G22-G23, with the remainder of zinc coordination sites filled by water molecules. A Zn^{2+}–N distance of 2.08 Å and Zn^{2+}–C distances of ~ 3 Å are indeed consistent with Zn^{2+} coordination to various nucleotides, including guanine. However, other alternative sources for the observed Zn^{2+} – P4 outer-shell scattering intensity, such as phosphorous atoms from the RNA phosphodiester backbone, cannot conclusively be ruled out at this time. This is the first time that these two methods have been combined to look at metals in RNA, and can be further applied to other systems such as group I and II introns.

There are a number of potential roles for the identified inner-sphere metal binding site at nucleotides G22 and G23. Given that P4 is the P RNA helix that binds metals required for catalysis, and it is not yet known where the catalytic metal binds in RNase P, it is possible that this is the catalytic metal site [48]. However, it is equally as likely that the site we have identified is a co-catalytic metal site, and that the inner-sphere associated metal ion stabilizes P RNA in the active conformation. Phosphorothioate rescue and cross-linking studies in *E. coli* P RNA indicate that a P4 helix-metal mediated interaction

with pre-tRNA helps to set-up the active site for coordination of the catalytic metal ion [11]. Additionally, Hsieh and Fierke recently demonstrated that a tightly bound metal ion in *B. subtilis* RNase P stabilizes a substrate induced conformational change in the enzyme required for catalysis [64]. Thus, the G22 / G23 metal site could be helping to set up the active site following substrate binding. Regardless of which role the inner-sphere metal ion fulfills, this tightly bound metal certainly contributes to the RNase P catalytic mechanism in a significant way.

We have seen that P4 has the potential to bind both outer and inner sphere metals which makes it a possible candidate for the catalytic metal site, based on the binding properties of the site deduced by biochemical data. NMR chemical shift mapping using the combination of Mn^{2+}, $Co(NH_3)_6^{3+}$ and Zn^{2+}, together with EXAFS promises to be a ubiquitous method for assigning and characterizing outer- and inner-sphere metal binding sites in a variety of RNAs.

Materials and Methods

Preparation and purification of $^{13}C/^{15}N$ labeled RNA

P4 samples (Figure V-2D) for NMR studies were prepared by *in vitro* transcription reactions using T7 RNA polymerase, uniformly $^{13}C/^{15}N$ labeled (Spectra Stable Isotopes, Inc.), and synthetic DNA templates (Integrated DNA Technologies, Inc.) containing the T7 promoter and sequence of interest [50]. RNA transcripts were purified on 15% (w/v) denaturing polyacrylamide gels containing 8 M urea/1x TBE. RNAs were recovered from gels by passive electroelution followed by ethanol precipitation. The RNA pellet was dissolved and repeatedly exchanged into NMR buffer (10 mM sodium

chloride, 10 mM sodium phosphate, pH ~ 6.2) using a Centricon Ultracel YM-3 concentrator (Millipore Corp). The final RNA concentration in the NMR samples was between 0.1 mM and 0.5 mM.

Preparation and purification of RNA for EXAFS

P4 samples (Figure V-2D) for EXAFS studies were prepared by *in vitro* transcription reactions using T7 RNA polymerase, and synthetic DNA templates (Integrated DNA Technologies, Inc.) containing the T7 promoter and sequence of interest [50]. RNA transcripts were purified on 20% (w/v) denaturing polyacrylamide gels containing 8 M urea/1x TBE. RNAs were recovered from gels by soaking overnight in buffer (TE, 0.1% sodium dodecyl phosphate (SDS), 500mM NaCl), buffer exchanged into TE, concentrated in Amicon Ultra-Concentrators (5,000 MWCO), then ethanol precipitated. The RNA pellet was dissolved in water and added to the appropriate EXAFS buffer ($Buffer_{1,\ EXAFS}$: 10 mM MES, 10 mM $NaNO_3$, X mM $ZnSO_4$, 30% glycerol, pH ~ 6; $Buffer_{2,\ EXAFS}$: 10 mM MES, 10 mM $NaNO_3$, 1 mM $Co(NH_3)_6^{3+}$, X mM $ZnSO_4$, 30% glycerol, pH ~ 6). The final RNA concentration in all of the EXAFS samples was 4 mM.

NMR spectroscopy

Metal binding experiments were carried out on an Avance Bruker 600 MHz NMR spectrometer equipped with a triple-resonance 5 mm cryogenic probe at 298 K. Sample volumes of ~300 µL in Shigemi tubes were used in all experiments. 2D ^{13}C–^{1}H S^3E HSQC experiments [65,66] were used to monitor chemical shift changes with the following carrier frequencies: ^{1}H 4.69 ppm, $^{13}C1'$ 89.50 ppm, $^{13}C5$ 99.00 ppm, and ^{15}N

154 ppm. NMR spectra were processed using NMRPipe/NMRDraw [67], analyzed using NMRView [68], and overlaid using SPARKY 3.

Detection of metal association by chemical shift mapping

Changes in chemical shift upon addition of $Co(NH_3)_6^{3+}$ and Zn^{2+} were quantified using the equation $\Delta\delta = \sqrt{(\Delta\delta_H)^2 + (\alpha\Delta\delta_X)^2}$, where $\Delta\delta_H$ and $\Delta\delta_X$ are the changes in proton and carbon/nitrogen chemical shift and α is the ratio of the C/N and H gyromagnetic ratio. The most significant changes for each vector type are highlighted on the P4 secondary structure (Figures V-2A, V-2D). The terminal and loop residues were excluded from the analysis.

Mn^{2+} peak broadening

The intensity for each type of C–H and N-H spin measured in Mn^{2+} was normalized to = $1-I_M/I_F$ (where I_M is peak intensity with Mn^{2+}, I_F is peak intensity without Mn^{2+}) so that a higher normalized value means a greater extent of peak broadening (identical experiments were used to record without and with Mn^{2+} so no other normalization was necessary, Figure V-2B).

XAS Spectroscopy and Data Analysis

Samples were prepared as detailed above and loaded into Lucite cuvettes with 40 μm Kapton windows and rapidly frozen in liquid nitrogen. XAS data were collected at SSRL on beamline 9-3 (3 GeV, ~ 90 mA), using a Si(220) double-crystal monochromator with a Rh-coated mirror upstream of the monochromator for harmonic rejection. The sample temperature was held at 7.5 K in an Oxford liquid He flow cryostat during data

collection. Spectra were measured using 10 eV increments in the pre-edge region (9430-9630 eV), 0.2 eV for the edge region (9630-9700 eV), 0.05 $Å^{-1}$ increments for the early EXAFS region (2.29 – 7.5 $Å^{-1}$), and 0.04 $Å^{-1}$ increments for the late EXAFS region (7.5 – 12 $Å^{-1}$) with integration times of 1s in the pre-edge and edge regions and 5-25 s (k^3 weighted) in the EXAFS region for a total scan time of ~ 45 min. For all samples, energy calibration was performed using a zinc foil as an internal standard, with the first inflection point of the foil spectrum defined as 9659 eV.

XAS data were collected as fluorescence excitation spectra using a thirty-element Ge solid-state detector array, equipped with a 3 μm Cu filter and Soller slits focused on the Ge detector. The integrated count rate for each channel held below ~90 kHz to avoid detector saturation. The windowed Zn Kα count rates were ~ 7-8 kHz in the EXAFS region, giving a total of ~ 5×10^6 useful counts per scan at k = 12 Å. For all samples, each channel of each scan was examined independently for glitches and good channels (27 per scan) were averaged to give the final spectrum. Average files for Zn-RNA and Zn-MES samples were calculated using 4 scans and 1 scan, respectively.

XANES data were normalized by fitting data to the McMaster absorption coefficients below and above the edge using a single background polynomial and scale factor. The EXAFS background correction was performed by fitting a three region cubic spline for all samples. The data were then converted to k-space using

$$k = \sqrt{\frac{2m_e\left(E - E_0\right)}{\hbar^2}}$$

Where E_0 = 9664 eV for Zn, which was calibrated by fitting EXAFS data for model compounds of known. Fourier transforms were calculated using k^3 weighted data over a range of 2.55-10.8 $Å^{-1}$ for all samples.

EXAFS data can be described by the following equation:

$$\chi(k) = \sum_s \frac{N_s S_s(k) A_s(k)}{k R_{as}^2} \exp\left(-2k^2\sigma_{as}^2\right) \exp\left(\frac{-2R_{as}}{\lambda}\right) \sin\left(2kR_{as} + \phi_{as}(k)\right),$$

where $\chi(k)$ is the fractional modulation in the absorption coefficient above the edge; Ns is the number of scatters at a distance R_{as}; $A_s(k)$ is the backscattering amplitude; σ_{as}^2 is the root-mean-square variation in R_{as}; $\phi_{as}(k)$ is the phase shift experienced by the photoelectron wave in passing through the potentials of the absorbing atom; λ is the mean free path of the photoelectron and backscattering atoms; and $S_s(k)$ is a scale factor specific to the absorber-scatterer pair. The sum is taken over all scattering interactions. The program Feff version 7.02 was used to calculate amplitude and phase functions, $A_s(k)\exp(-2R_{as}/\lambda)$ and $\phi_{as}(k)$ for a zinc-oxygen interaction at 2.0 Å, and zinc-phosphorus and zinc-carbon interactions at 3.0 Å. Data were analyzed in k-space using the program EXAFSPAK. For all data, S_s was fixed at 0.9 based on fits to the EXAFS data for structurally characterized model complexes.

References for Chapter IV

1. Guerrier-Takada C, Gardiner K, Marsh T, Pace N, Altman S: The RNA moiety of ribonuclease P is the catalytic subunit of the enzyme. *Cell* 1983, 35:849-857.

2. Beebe JA, Kurz JC, Fierke CA: Magnesium ions are required by Bacillus subtilis ribonuclease P RNA for both binding and cleaving precursor tRNAAsp. *Biochemistry* 1996, 35:10493-10505.

3. Hanna R, Doudna JA: Metal ions in ribozyme folding and catalysis. *Curr Opin Chem Biol* 2000, 4:166-170.

4. DeRose VJ: Two decades of RNA catalysis. *Chem Biol* 2002, 9:961-969.

5. Doudna JA, Cech TR: The chemical repertoire of natural ribozymes. *Nature* 2002, 418:222-228.

6. Hsieh J, Andrews AJ, Fierke CA: Roles of protein subunits in RNA-protein complexes: lessons from ribonuclease P. *Biopolymers* 2004, 73:79-89.

7. Harris ME, Christian EL: Recent insights into the structure and function of the ribonucleoprotein enzyme ribonuclease P. *Curr Opin Struct Biol* 2003, 13:325-333.

8. Cuzic S, Hartmann RK: Studies on Escherichia coli RNase P RNA with Zn2+ as the catalytic cofactor. *Nucleic Acids Res* 2005, 33:2464-2474.

9. Brannvall M, Kirsebom LA: Manganese ions induce miscleavage in the Escherichia coli RNase P RNA-catalyzed reaction. *J Mol Biol* 1999, 292:53-63.

10. Smith D, Burgin AB, Haas ES, Pace NR: Influence of metal ions on the ribonuclease P reaction. Distinguishing substrate binding from catalysis. *J Biol Chem* 1992, 267:2429-2436.

11. Christian EL, Smith KM, Perera N, Harris ME: The P4 metal binding site in RNase P RNA affects active site metal affinity through substrate positioning. *Rna* 2006, 12:1463-1467.

12. Getz MM, Andrews AJ, Fierke CA, Al-Hashimi HM: Structural plasticity and Mg2+ binding properties of RNase P P4 from combined analysis of NMR residual dipolar couplings and motionally decoupled spin relaxation. *Rna* 2007, 13:251-266.

13. Quigley GJ, Seeman NC, Wang AH, Suddath FL, Rich A: Yeast phenylalanine transfer RNA: atomic coordinates and torsion angles. *Nucleic Acids Res* 1975, 2:2329-2341.

14. Rueda D, Wick K, McDowell SE, Walter NG: Diffusely bound Mg2+ ions slightly reorient stems I and II of the hammerhead ribozyme to increase the probability of formation of the catalytic core. *Biochemistry* 2003, 42:9924-9936.

15. Hammann C, Norman DG, Lilley DM: Dissection of the ion-induced folding of the hammerhead ribozyme using 19F NMR. *Proc Natl Acad Sci U S A* 2001, 98:5503-5508.

16. Russel R, Herschlag D: Probing the folding landscape of the Tetrahymena ribozyme: commitment to form the native conformation is late in the folding pathway. *Journal of Molecular Biology* 2001, 308:839-851.

17. Woodson SA: Structure and assembly of group I introns. *Current Opinions in Structural Biology* 2005, 15:324-330.

18. Ban N, Nissen P, Hansen J, Moore PB, Steitz TA: The complete atomic structure of the large ribosomal subunit at 2.4 A resolution. *Science* 2000, 289:905-920.

19. Buck AH, Kazantsev AV, Dalby AB, Pace NR: Structural perspective on the activation of RNase P RNA by protein. *Nat Struct Mol Biol* 2005.

20. Cassano AG, Anderson VE, Harris ME: Analysis of solvent nucleophile isotope effects: evidence for concerted mechanisms and nucleophilic activation by metal coordination in nonenzymatic and ribozyme-catalyzed phosphodiester hydrolysis. *Biochemistry* 2004, 43:10547-10559.

21. Brannvall M, Mikkelsen NE, Kirsebom LA: Monitoring the structure of Escherichia coli RNase P RNA in the presence of various divalent metal ions. *Nucleic Acids Res* 2001, 29:1426-1432.

22. Fang XW, Pan T, Sosnick TR: Mg2+-dependent folding of a large ribozyme without kinetic traps. *Nat Struct Biol* 1999, 6:1091-1095.

23. Warnecke JM, Held R, Busch S, Hartmann RK: Role of metal ions in the hydrolysis reaction catalyzed by RNase P RNA from Bacillus subtilis. *J Mol Biol* 1999, 290:433-445.

24. Pyle AM: Metal ions in the structure and function of RNA. *J Biol Inorg Chem* 2002, 7:679-690.

25. Brannvall M, Kirsebom LA: Metal ion cooperativity in ribozyme cleavage of RNA. *Proc Natl Acad Sci U S A* 2001, 98:12943-12947.

26. Harris ME, Pace NR: Identification of phosphates involved in catalysis by the ribozyme RNase P RNA. *Rna* 1995, 1:210-218.

27. Sigel RK, Vaidya A, Pyle AM: Metal ion binding sites in a group II intron core. *Nat Struct Biol* 2000, 7:1111-1116.

28. Kurz JC, Niranjanakumari S, Fierke CA: Protein component of Bacillus subtilis RNase P specifically enhances the affinity for precursor-tRNAAsp. *Biochemistry* 1998, 37:2393-2400.

29. Beebe JA, Fierke CA: A kinetic mechanism for cleavage of precursor tRNA(Asp) catalyzed by the RNA component of Bacillus subtilis ribonuclease P. *Biochemistry* 1994, 33:10294-10304.

30. Misra VK, Draper DE: A thermodynamic framework for Mg2+ binding to RNA. *Proc Natl Acad Sci U S A* 2001, 98:12456-12461.

31. Misra VK, Draper DE: On the role of magnesium ions in RNA stability. *Biopolymers* 1998, 48:113-135.

32. Draper DE, Grilley D, Soto AM: Ions and RNA folding. *Annu Rev Biophys Biomol Struct* 2005, 34:221-243.

33. Juneau K, Podell E, Harrington DJ, Cech TR: Structural basis of the enhanced stability of a mutant ribozyme domain and a detailed view of RNA--solvent interactions. *Structure (Camb)* 2001, 9:221-231.

34. Kurz JC, Fierke CA: The affinity of magnesium binding sites in the Bacillus subtilis RNase P x pre-tRNA complex is enhanced by the protein subunit. *Biochemistry* 2002, 41:9545-9558.

35. Frank DN, Pace NR: Ribonuclease P: unity and diversity in a tRNA processing ribozyme. *Annu Rev Biochem* 1998, 67:153-180.

36. Forster AC, Altman S: External guide sequences for an RNA enzyme. *Science* 1990, 249:783-786.

37. Tranguch AJ, Engelke DR: Comparative structural analysis of nuclear RNase P RNAs from yeast. *J Biol Chem* 1993, 268:14045-14055.

38. LaGrandeur TE, Darr SC, Haas ES, Pace NR: Characterization of the RNase P RNA of Sulfolobus acidocaldarius. *J Bacteriol* 1993, 175:5043-5048.

39. Nieuwlandt DT, Haas ES, Daniels CJ: The RNA component of RNase P from the archaebacterium Haloferax volcanii. *J Biol Chem* 1991, 266:5689-5695.

40. Niranjanakumari S, Day-Storms JJ, Ahmed M, Hsieh J, Zahler NH, Venters RA, Fierke CA: Probing the architecture of the B. subtilis RNase P Holoenzyme active site by crosslinking and affinity cleavage. *Rna* 2007, 13:512-535.

41. Biswas R, Ledman DW, Fox RO, Altman S, Gopalan V: Mapping RNA-protein interactions in ribonuclease P from Escherichia coli using disulfide-linked EDTA-Fe. *J Mol Biol* 2000, 296:19-31.

42. Kazantsev AV, Krivenko AA, Harrington DJ, Holbrook SR, Adams PD, Pace NR: Crystal structure of a bacterial ribonuclease P RNA. *Proc Natl Acad Sci U S A* 2005, 102:13392-13397.

43. Torres-Larios A, Swinger KK, Krasilnikov AS, Pan T, Mondragon A: Crystal structure of the RNA component of bacterial ribonuclease P. *Nature* 2005, 437:584-587.

44. Rasmussen TA, Nolan JM: G350 of Escherichia coli RNase P RNA contributes to Mg2+ binding near the active site of the enzyme. *Gene* 2002, 294:177-185.

45. Frank DN, Pace NR: In vitro selection for altered divalent metal specificity in the RNase P RNA. *Proc Natl Acad Sci U S A* 1997, 94:14355-14360.

46. Crary SM, Kurz JC, Fierke CA: Specific phosphorothioate substitutions probe the active site of Bacillus subtilis ribonuclease P. *Rna* 2002, 8:933-947.

47. Waugh DS, Pace NR: Gap-scan deletion analysis of Bacillus subtilis RNase P RNA. *Faseb J* 1993, 7:188-195.

48. Christian EL, Kaye NM, Harris ME: Helix P4 is a divalent metal ion binding site in the conserved core of the ribonuclease P ribozyme. *Rna* 2000, 6:511-519.

49. Kaye NM, Christian EL, Harris ME: NAIM and site-specific functional group modification analysis of RNase P RNA: magnesium dependent structure within the conserved P1-P4 multihelix junction contributes to catalysis. *Biochemistry* 2002, 41:4533-4545.

50. Milligan JF, Uhlenbeck OC: Determination of RNA-protein contacts using thiophosphate substitutions. *Biochemistry* 1989, 28:2849-2855.

51. Cowan JA: Metallobiochemistry of RNA. Co(NH3)6(3+) as a probe for Mg2+(aq) binding sites. *J Inorg Biochem* 1993, 49:171-175.

52. Noeske J, Schwalbe H, Wohnert J: Metal-ion binding and metal-ion induced folding of the adenine-sensing riboswitch aptamer domain. *Nucleic Acids Res* 2007, 35:5262-5273.

53. Butcher SE, Allain FH, Feigon J: Determination of metal ion binding sites within the hairpin ribozyme domains by NMR. *Biochemistry* 2000, 39:2174-2182.

54. Campbell DO, Bouchard P, Desjardins G, Legault P: NMR structure of varkud satellite ribozyme stem-loop V in the presence of magnesium ions and localization of metal-binding sites. *Biochemistry* 2006, 45:10591-10605.

55. de Groot F: High-resolution x-ray emission and x-ray absorption spectroscopy. *Chemical Reviews* 2001, 101:1779-1808.

56. Qu X, Smith GJ, Lee KT, Sosnick TR, Pan T, Scherer NF: Single-molecule nonequilibrium periodic Mg2+-concentration jump experiments reveal details of the early folding pathways of a large RNA. *Proc Natl Acad Sci U S A* 2008, 105:6602-6607.

57. Hsieh J, Niranjanakumari S, Fierke CA: Conformational change follows precursor tRNA binding to the B. subtilis RNase P holoenzyme. *in preparation* 2008.

58. Schmitz M, Tinoco I, Jr.: Solution structure and metal-ion binding of the P4 element from bacterial RNase P RNA. *Rna* 2000, 6:1212-1225.

59. Schmitz M: Change of RNase P RNA function by single base mutation correlates with perturbation of metal ion binding in P4 as determined by NMR spectroscopy. *Nucleic Acids Res* 2004, 32:6358-6366.

60. Wedekind JE, McKay DB: Crystal structure of the leadzyme at 1.8 A resolution: metal ion binding and the implications for catalytic mechanism and allo site ion regulation. *Biochemistry* 2003, 42:9554-9563.

61. Klein DJ, Moore PB, Steitz TA: The roles of ribosomal proteins in the structure assembly, and evolution of the large ribosomal subunit. *J Mol Biol* 2004, 340:141-177.

62. Wild K, Weichenrieder O, Leonard GA, Cusack S: The 2 A structure of helix 6 of the human signal recognition particle RNA. *Structure* 1999, 7:1345-1352.

63. Markley JC, Godde F, Sigurdsson ST: Identification and characterization of a divalent metal ion-dependent cleavage site in the hammerhead ribozyme. *Biochemistry* 2001, 40:13849-13856.

64. Hsieh J, Rueda D, Walter NG, Fierke CA: A High-affinity Inner-sphere Divalent Cation Stabilizes Conformational Change in the B. subtilis RNase P Holoenzyme•pre-tRNA Complex. *in press* 2008.

65. Meissner A, Sorensen OW: Optimization of three-dimensional TROSY-type HCCH NMR correlation of aromatic (1)H-(13)C groups in proteins. *J Magn Reson* 1999, 139:447-450.

66. Meissner A, Duus JO, Sorensen OW: Integration of spin-state-selective excitation into 2D NMR correlation experiments with the heteronuclear ZQ/2Q pi rotations for 1JXH- resolved E.COSY-type measurements of heteronuclear coupling constants in proteins. *J Biomol NMR* 1997, 10:89-94.

67. Delaglio F, Grzesiek S, Vuister GW, Zhu G, Pfeifer J, Bax A: NMRPipe: a multidimensional spectral processing system based on UNIX pipes. *J Biomol NMR* 1995, 6:277-293.

68. Johnson BA, Stevens SP, Williamson JM: Determination of the three-dimensional structure of margatoxin by 1H, 13C, 15N triple-resonance nuclear magnetic resonance spectroscopy. *Biochemistry* 1994, 33:15061-15070.

CHAPTER VII

CONCLUSIONS AND FUTURE DIRECTIONS

Overview

The goal of the work presented here was to advance our understanding of how the RNA, protein, and metal components of bacterial RNase P work synergistically to catalyze an essential biological reaction. My findings highlight the importance of RNA-protein interactions in the molecular recognition of pre-tRNA, identify specific roles for conserved residues of the essential protein in the RNase P kinetic pathway, and characterize a divalent metal binding site in the conserved P RNA helix P4. This work emphasizes the cooperative nature of the RNase P subunits, and demonstrates how the required P RNA cofactors, protein and metal, contribute to RNase P function.

Conclusions

Recognition of the pre-tRNA nucleotide N(-4) by bacterial RNase P

RNase P substrate recognition has been attributed to the tertiary structure of pre-tRNAs, with the sequence of the substrate 5' leader playing no role. However, genomic analyses indicate a preference for particular nucleotides at specific locations in the 5' leader of bacterial pre-tRNAs suggesting the possibility of sequence specific interactions

between RNase P and pre-tRNA 5' leaders. My work established that *B. subtilis* and *E. coli* RNase P prefer to bind substrates with an adenosine located four nucleotides on the 5' of the cleavage site in their 5' leaders (N(-4) position, Figure II-3). Binding studies reveal that *B. subtilis* RNase P has a 20-fold tighter affinity for substrates with an adenosine instead of guanosine at the N(-4) position arising from a positive hydrogen bonding contribution with the N6 exocyclic amine of adenosine, and a negative contribution from the N2 exocyclic amine of guanosine. These findings redefine and expand the current model for pre-tRNA recognition by RNase P, demonstrating the significance of the pre-tRNA 5' leader sequence to substrate recognition.

Specific contacts between the P protein Subunit of Bacillus subtilis RNase P and the 5' leader of pre-tRNA contribute to molecular recognition

Structural models of the RNase P•pre-tRNA complex indicate that the 5' leader of pre-tRNA is located near the protein subunit of the RNP [1,2]. The contribution of protein•leader interactions to sequence specific substrate recognition was examined. A combination of site-directed mutagenesis and substrate affinity measurements demonstrated that specific amino acids in the RNR motif and central cleft regions of the protein are important for substrate affinity. Additionally, three protein residues (F20, Y34, and R60) were identified as contributing to the enhanced affinity of pre-tRNA with an adenosine at the N(-4) nucleotide, thus resulting in a sequence specific recognition of this position. The role of the hydroxyl group on one of the three implicated residues, Tyr34, was further explored, and a model was proposed in which this functional group participates in a hydrogen bonding interaction between the protein and pre-tRNA substrate at the N(-4) position. We propose that this hydroxyl group forms a hydrogen

bond with the N6 exocyclic amine of adenosine to enhance the binding affinity of pre-tRNA. These unexpected findings provide the first example of a sequence specific interaction between the P protein and pre-tRNA substrate. They also emphasize the importance of RNA-protein interactions in the molecular recognition of pre-tRNAs by *B. subtilis* RNase P protein.

The RNR motif of B. subtilis RNase P stabilizes RNA-protein interactions in the holoenzyme

Although the RNase P protein is required for enzyme activity *in vivo*, the contributions of the protein to the RNase P mechanism have not been extensively characterized [3]. The most highly conserved region of the protein, the RNR motif, is at the interface of the P RNA and pre-tRNA in structural models (Figure III-1), but no direct function has yet been ascribed to it. A combination of site directed mutagenesis, binding measurements, single turnover and stopped-flow kinetics were utilized to investigate the role of the RNR motif. These studies show that the RNR motif is important for both holoenzyme formation (P RNA•P protein complex) and pre-tRNA binding. They also reveal which step in the RNase P kinetic mechanism is stabilized by side chains in the RNR motif. Specifically, these data demonstrate that the conserved RNR region in P protein enhances a metal mediated conformational change in the RNase P•pre-tRNA complex prior to the substrate cleavage step.

Identification and characterization of a tightly bound metal in the P4 helix of the metallo-ribozyme ribonuclease P

A strategy was presented that employs a combination of nuclear magnetic resonance (NMR), and x-ray absorption (XAS) spectroscopic techniques to locate and

characterize metal ions making inner-sphere contacts with a stem-loop that serves as a model for *B. subtilis* RNase P helix P4 (residues 48-57 and 391-398 in the full-length *B. subtilis* enzyme). Our NMR studies reveal a single high affinity divalent metal binding site located near G22 and G23 in the *B. subtilis* P4 helix mimic (G378 and G379 in full-length *B. subtilis*). XAS studies of this site indicates that the metal ion binds to the P4 helix mimic with a six-coordinate geometry and an average Zn^{2+}– O/N bond distances of ~ 2.08 Å, indicative of inner sphere metal coordination. The NMR and XAS data together suggest a model for the metal environment of a tightly bound metal in the putative active site of the metallo-ribozyme RNase P (Figure V-4). The work presented represents the successful combination of NMR and XAS for studying metal coordination by RNA, and should be applied to the study other metal-requiring ribozymes. Furthermore, this study identifies an inner-sphere metal binding site in helix P4, and provides the first molecular characterization of the environment of a catalytic and/or co-catalytic metal ion important to RNase P catalysis.

Future Directions

RNase P is one of the best characterized large RNPs, in spite of this, numerous questions central to understanding the function of this enzyme still remain. Below is a brief discussion of some of the major questions remaining in the field, and brief proposals on how I would approach answering them. Specifically, strategies for investigating RNase P holoenzyme structure, substrate molecular recognition, P RNA-metal interactions, and kinetic mechanism will be addressed.

RNase P Holoenzyme Structure

Although structures of each of the components of RNase P (P RNA, P protein, tRNA) exist independently of one another, there is no x-ray structure of the RNase P holoenzyme complex [4]. As such, structural knowledge of the complex is limited to models derived from biochemical data. In lieu of an x-ray structure, current holoenzyme models can be further refined with constraints from published crystal structures of the three components, biochemical data that indicate where pre-tRNA nucleotides N(-1), N(-4), and the 3' CCA end interact with RNase P, and trFRET distance measurements between the P RNA, protein, and substrate. Furthermore, because of the inherent problems in characterizing large RNAs with NMR, structures of truncated P RNA constructs, such as the catalytic domain, that are active and bind protein can alternatively be pursued using this technique. Both the model refinement and NMR approaches for investigating RNase P structure are currently being pursued in the Fierke lab along with their collaborators in the Al-Hashimi lab (see Appendix B for more information on the NMR study).

Small angle x-ray scattering (SAXS) can be applied to probing the global conformation of RNase P under different solution conditions. SAXS has been successfully employed to examine RNase P holoenzyme dimer formation in the presence and absence of pre-tRNA substrate [5] [6]. The published SAXS studies were conducted prior to the release of the P RNA crystal structures, when it not possible to assign regions of the SAXS model to specific P RNA helices. Although this technique only permits the observation of relatively large structural rearrangements, these conformational changes can be given a physical meaning, because regions of the SAXS model can be assigned to specific RNase P RNA helices using the published x-ray structures. Thus, SAXS can be

further exploited to examine helical movements upon protein, substrate, metal, or inhibitor binding to obtain additional structural information about conformational changes in the enzyme.

RNase P undergoes at least one conformational change during the catalytic cycle (Scheme I-1). Monitoring these structural changes on a short timescale provides a challenge for understanding the RNase P structure/function relationship. Two strategies that are currently being used to monitor the folding of large RNAs can potentially be applied to RNase P to observe structural changes during catalysis. The first method is time resolved hydroxyl radical foot-printing, which uses hydroxyl radicals generated with a synchrotron x-ray beam to detect RNA secondary and tertiary structure and protein interactions on a time scale of 10 milliseconds to 100 seconds [7,8]. In this method, a ribose sugar interacts with hydroxyl radicals, causing the cleavage of the RNA backbone. The reactivity of the polynucleotide backbone to hydroxyl radicals is proportional to its solvent accessibility and is independent of the base sequence. Thus, hydroxyl radical cleavage can yield information on the structure of a nucleic acid with single-nucleotide resolution [7,9]. This method would allow us to monitor transient conformational states in real time; the estimated lifetime of the enzyme-substrate complex prior to the conformational change is between 0.1 to > 20 seconds depending on solution conditions. Additionally, it may also allow for the mapping of P RNA *in vivo*, a study by Woodson and co-worker applied an *in vivo* variant of this technique to *E. coli* P RNA, and demonstrated that it is possible to carry out these types studies with RNase P [10].

A second technique based on a similar principle, time resolved selective 2'-hydroxyl acylation analyzed by primer extension (SHAPE), could also be employed to

monitor secondary and tertiary changes in P RNA structure during catalysis [11]. In this method, flexible nucleotides are reactive toward hydroxyl-selective electrophiles. Time resolved SHAPE chemistry permits the study of RNA in ~1 second snapshots. It has already been employed to follow the time-dependent folding of the *B. subtilis* RNase P RNA specificity domain [11]. Both of these techniques are currently being used to answer RNA folding questions, but there is no reason that they could not be applied to monitoring how the RNA structure in RNase P changes during catalysis.

Molecular Recognition

RNase P binds and processes substrates with both canonical and non-canonical sequences with uniform efficiency [12]. However, the precise contributions of the pre-tRNA sequence to uniform substrate recognition have not been explored in detail. In Chapters II and III we characterized a sequence specific interaction between RNase P and the 5' leader nucleotide at N(-4). However, as discussed in Chapter II, most bacterial genomes also exhibit sequence preferences at the N(-2) and N(-3) positions in their 5' leaders. Therefore, binding and mutagenesis studies similar to those performed in Chapters II and III need to be undertaken to evaluate the interactions between these 5' leader positions and RNase P. The investigation of the N(-2) nucleotide is currently being undertaken by Wan Lim in the Fierke lab. These studies are particularly important to firmly establish a direct link between the genomic sequence preferences and molecular recognition of substrates by RNase P.

The extensive level of post-transcriptional modification is one of the most unique features of tRNA structure *in vivo*. However, studies of RNase P molecular recognition *in vitro* have utilized pre-tRNA substrates transcribed by T7 polymerase, which

synthesizes pre-tRNAs lacking post-transcriptional modifications. Investigation of amino acylated-tRNAs (aa-tRNAs) demonstrated that post-transcriptional modifications contribute to the kinetic and thermodynamic uniformity in translation [13], and recent studies of *E. coli* RNase P molecular recognition have suggested that there are striking similarities between aa-tRNAs recognition by EfTu, and pre-tRNA recognition by RNase P [12]. Furthermore, a study by Söll in co-workers in 1973 observed that post-transcriptional modifications in pre-tRNA^{Tyr} impact the rate of RNase P catalyzed pre-tRNA cleavage [14]. Thus, this is a potentially important aspect of pre-tRNA molecular recognition that warrants investigation. In the past, these modifications may not have been well studied due to the difficulty of synthesizing post-transcriptionally modified precursor tRNAs. However, there are now enzymatic and chemical methods available to synthesize and incorporate modified nucleotides into RNA [15,16]. Therefore it is feasible to study post-transcriptional modified pre-tRNAs *in vitro*, and to assess their contributions to substrate recognition and cleavage by utilizing binding and pre-steady state kinetic measurements. These studies will provide a better understanding of RNase P action *in vivo* where post-transcriptional modifications are always present.

Mechanism

Although an expanded minimal kinetic mechanism has recently been proposed by our lab (Scheme IV-I), a number of fundamental questions regarding the mechanism of RNase P still remain [17]. For example, is the mechanism of the eukaryotic, organellar, and archeal enzymes the same as that of the bacterial? How do aminoglycoside inhibitors function on a molecular level? What is the chemical mechanism of the cleavage step and how do active site nucleotides stabilize this reaction? How does RNase P recognize and

cleave non pre-tRNA substrates? Are there further intermediate kinetic steps that we have not been able to see with our current techniques?

RNase P has been shown to recognize and cleave a number of non pre-tRNA substrates including *E. coli* pre-4.5S RNA, OLE RNA, vitamin B_{12} riboswitches, and tmRNA [18-20]. Cross-linking, hydroxyl radical footprinting, mutagenesis, and substrate binding studies are required to characterize how RNase P recognizes these non pre-tRNA substrates. Furthermore, steady state and pre-steady state kinetic investigations will need to be employed to probe if RNase P uses the same mechanism of action to cleave these substrates, as it does for pre-tRNA substrates. These data will be essential to understanding all of the roles of RNase P *in vivo*.

Recently the first detailed kinetic study of a eukaryotic RNase P mechanism was published [21]. This study determined that the minimal kinetic mechanism for *S. cerevisiae* RNase P is almost identical to the kinetic mechanism of the bacterial enzyme. However, these studies do not address the underlying question of why the eukaryotic RNase P requires multiple proteins to function, while bacterial RNase P enzymes require only a single protein cofactor. Therefore, further studies of eukaryotic RNase P need to be undertaken to establish why these enzymes evolved to have such a different architecture. Specifically, careful mutagenesis of the yeast enzyme, and evaluation of how these mutants impact the kinetic mechanism is warranted. However, it must be acknowledged this will be difficult until a recombinant eukaryotic RNase P is available.

Recent studies have revealed previously unobserved intermediates in the RNase P kinetic pathway [22]. Scheme IV-2 demonstrates that there are two potential pathways for the E•S to E•S* transition following substrate binding. Single molecule studies can

be used to distinguish which pathway is more probable in the wild type enzyme (K_2 or K_3 in Scheme IV-2), as well as allow us to probe for additional intermediates in the kinetic mechanism. The major advantage of single molecule over bulk kinetic studies is that this technique permits the dissection of heterogeneous populations of molecules. Instead of just seeing how an overall factory works (bulk solution kinetic studies), single molecule studies allow the interrogation of the contributions of each individual worker to a factory's production to provide a better molecular level understanding of production. Single molecule studies will provide a better understanding of the conformational changes in RNase P following substrate binding, and perhaps reveal new kinetic intermediates. Preliminary single molecule studies are being carried out as a collaboration between the Fierke and Walter labs.

Metals in RNase P

Metals play numerous vital roles in RNase P, and are required for P RNA folding, substrate binding, and pre-tRNA cleavage [23-26]. However, due to the large number of divalent metals associated with the large negatively charged P RNA, characterizing individual metals and assigning roles to metals coordinated to the enzyme at specific sites has proven difficult. A natural extension of the work presented in Chapter V would be to undertake further NMR and XAS studies to determine which functional groups in the helix P4 residues G22 and G23 coordinate to the divalent metal. This could be accomplished by inserting phosphorothioates and guanosine analogs at these sites in the RNA, and performing a similar series of experiments as the ones described here. The added advantage of these experiments is that these same analogs could be inserted into the entire RNase P to evaluate the effects on catalytic activity.

Human Mitochondrial RNase P

Excitingly, last month the first all protein RNase P was reported by Rossmanith and co-workers [27]. This proteinaceous RNase P was recombinantly purified from human mitochondria, cloned, and reconstituted *in vitro* from three separate proteins. It will be of great interest to characterize the structure, molecular recognition, and kinetic mechanism of this non-ribozyme RNase P. An unlimited number of possibilities exist for studying this newly discovered RNase P, ranging from utilizing x-ray crystallography and NMR spectroscopy to elucidate the structure, performing cross-linking studies with pre-tRNA to establish which regions of the substrate are recognized by the protein enzyme, labeling protein components with FRET pairs to observe domain movements during catalysis, to undertaking steady state and pre-steady state kinetic studies of pre-tRNA cleavage to investigate the enzyme mechanism. Comparing human mitochondrial RNase P with bacterial RNase P will provide a glimpse into how nature has evolved two very different molecules for performing the exact same task.

References for Chapter VI

1. Niranjanakumari S, Day-Storms JJ, Ahmed M, Hsieh J, Zahler NH, Venters RA, Fierke CA: Probing the architecture of the B. subtilis RNase P Holoenzyme active site by crosslinking and affinity cleavage. *Rna* 2007, 13:512-535.

2. Buck AH, Kazantsev AV, Dalby AB, Pace NR: Structural perspective on the activation of RNase P RNA by protein. *Nat Struct Mol Biol* 2005.

3. Gossringer M, Kretschmer-Kazemi Far R, Hartmann RK: Analysis of RNase P protein (rnpA) expression in Bacillus subtilis utilizing strains with suppressible rnpA expression. *J Bacteriol* 2006, 188:6816-6823.

4. Smith JK, Hsieh J, Fierke CA: Importance of RNA-protein interactions in bacterial ribonuclease P structure and catalysis. *Biopolymers* 2007, 87:329-338.

5. Barrera A, Fang X, Jacob J, Casey E, Thiyagarajan P, Pan T: Dimeric and monomeric Bacillus subtilis RNase P holoenzyme in the absence and presence of pre-tRNA substrates. *Biochemistry* 2002, 41:12986-12994.

6. Fang XW, Yang XJ, Littrell K, Niranjanakumari S, Thiyagarajan P, Fierke CA, Sosnick TR, Pan T: The Bacillus subtilis RNase P holoenzyme contains two RNase P RNA and two RNase P protein subunits. *Rna* 2001, 7:233-241.

7. Woodson SA, Deras ML, Brenowitz M: Time-resolved hydroxyl radical footprinting of RNA with X-rays. *Curr Protoc Nucleic Acid Chem* 2001, Chapter 11:Unit 11 16.

8. Sclavi B, Sullivan M, Chance MR, Brenowitz M, Woodson SA: RNA folding at millisecond intervals by synchrotron hydroxyl radical footprinting. *Science* 1998, 279:1940-1943.

9. Brenowitz M, Chance MR, Dhavan G, Takamoto K: Probing the structural dynamics of nucleic acids by quantitative time-resolved and equilibrium hydroxyl radical "footprinting". *Curr Opin Struct Biol* 2002, 12:648-653.

10. Adilakshmi T, Lease RA, Woodson SA: Hydroxyl radical footprinting in vivo: mapping macromolecular structures with synchrotron radiation. *Nucleic Acids Res* 2006, 34:e64.

11. Mortimer SA, Weeks KM: Time-Resolved RNA SHAPE Chemistry. *J Am Chem Soc* 2008.

12. Sun L, Campbell FE, Zahler NH, Harris ME: Evidence that substrate-specific effects of C5 protein lead to uniformity in binding and catalysis by RNase P. *Embo J* 2006, 25:3998-4007.

13. Fahlman RP, Dale T, Uhlenbeck OC: Uniform binding of aminoacylated transfer RNAs to the ribosomal A and P sites. *Mol Cell* 2004, 16:799-805.

14. Schaefer KP, Altman S, Soll D: Nucleotide modification in vitro of the precursor of transfer RNA of Escherichia coli. *Proc Natl Acad Sci U S A* 1973, 70:3626-3630.

15. Bajji AC, Davis DR: Synthesis of the tRNA(Lys,3) anticodon stem-loop domain containing the hypermodified ms2t6A nucleoside. *J Org Chem* 2002, 67:5352-5358.

16. Davis DR, Bajji AC: Introduction of hypermodified nucleotides in RNA. *Methods Mol Biol* 2005, 288:187-204.

17. Hsieh J, Fintushel S, Hewlett N, Walter NG, Fierke CA: Concerted Conformational Change in the B. subtilis Holoenzyme•pre-tRNA Complex Requires Contribution from Both PRNA and P Protein interaction with Pre-tRNA. *in preparation* 2008.

18. Altman S, Wesolowski D, Guerrier-Takada C, Li Y: RNase P cleaves transient structures in some riboswitches. *Proc Natl Acad Sci U S A* 2005, 102:11284-11289.

19. Gimple O, Schon A: In vitro and in vivo processing of cyanelle tmRNA by RNase P. *Biol Chem* 2001, 382:1421-1429.

20. Ko JH, Altman S: OLE RNA, an RNA motif that is highly conserved in several extremophilic bacteria, is a substrate for and can be regulated by RNase P RNA. *Proc Natl Acad Sci U S A* 2007, 104:7815-7820.

21. Hsieh J, Walker S, Fierke CA, Engelke DR: Pre-tRNA cleavage by the yeast nuclear RNase P holoenzyme is rate-limited by slow product release. . *RNA* 2008, in press.

22. Hsieh J, Niranjanakumari S, Fierke CA: Conformational change follows precursor tRNA binding to the B. subtilis RNase P holoenzyme. *in preparation* 2008.

23. Beebe JA, Kurz JC, Fierke CA: Magnesium ions are required by Bacillus subtilis ribonuclease P RNA for both binding and cleaving precursor tRNAAsp. *Biochemistry* 1996, 35:10493-10505.

24. Smith D, Pace NR: Multiple magnesium ions in the ribonuclease P reaction mechanism. *Biochemistry* 1993, 32:5273-5281.

25. Smith D, Burgin AB, Haas ES, Pace NR: Influence of metal ions on the ribonuclease P reaction. Distinguishing substrate binding from catalysis. *J Biol Chem* 1992, 267:2429-2436.

26. Brannvall M, Mikkelsen NE, Kirsebom LA: Monitoring the structure of Escherichia coli RNase P RNA in the presence of various divalent metal ions. *Nucleic Acids Res* 2001, 29:1426-1432.

27. Holzmann J, Frank P, Loffler E, Bennett KL, Gerner C, Rossmanith W: RNase P without RNA: identification and functional reconstitution of the human mitochondrial tRNA processing enzyme. *Cell* 2008, 135:462-474.

APPENDIX A

This appendix contains data from kinetic studies that were not included in Chapters III, IV, or V. The experiments are introduced and the data is shown. These data have been included in order make them easily accessible to future students and post-doctoral researchers in the laboratory. No discussion is included.

Further studies on the RNR motif

The data shown in Table 1 reports the $K_{1/2}$ of wild type, R60A, N61A, and R62A RNase P for calcium ($K_{1/2,\ Ca\ overall}$), as well as the $K_{1/2}$ for inner-sphere magnesium ions ($K_{1/2,\ Mg\ inner\text{-}sphere}$). In the calcium experiments, single turnover assays were performed to measure k_{obs} at 37°C pH 8.0, 2μM RNase P, 50 mM MES, 50 mM Tris, 150-200 mM KCl, ^{32}P 5' end labeled pre-tRNA^{Asp} possessing a 5 nucleotide long 5' leader, and various concentrations of calcium chloride. These reactions were initiated by incubating enzyme pre-equilibrated in calcium with substrate pre-equilibrated in calcium together. For the $K_{1/2,\ Mg\ inner\text{-}sphere}$ measurements, single turnover assays were performed at 37°C, pH 6.0, 2μM RNase P, 50 mM MES, 50 mM Tris, 150-200 mM KCl, 2 mM $Co(NH_3)_6^{3+}$, ^{32}P 5' end labeled pre-tRNA^{Asp} possessing a 5 nucleotide long 5' leader and various concentrations of magnesium chloride. Unlike the $K_{1/2,\ Ca\ overall}$ measurements, enzyme and substrate pre-equilibrated in 2 mM $Co(NH_3)_6^{3+}$ were incubated together for 30 minutes, and the reactions were initiated upon the addition of magnesium. For both sets of experiments, the k_{obs} values were plotted as a function of calcium to give the $K_{1/2}$

values for calcium, or inner-sphere magnesium. These studies showed that R60A and N61A mutants have a moderate 2-fold impact on the concentration of calcium required by RNase P to cleave pre-tRNA.

Table A-1 displays a summary of the effect of RNR motif mutants on the metal concentration necessary to activate RNase P catalysis.

	$K_{1/2,\ Ca\ overall}$ (mM)	$K_{1/2,\ Mg\ inner\text{-}sphere}$ (mM)
Wild Type	5 ± 1	8 ± 8
R60A	11 ± 1	10 ± 5
N61A	12 ± 2	nd
R62A	3 ± 1	5 ± 2
R65A	nd	5 ± 3

Stopped flow data were also collected in the presence of 50 mM MES, 50 mM Tris, ~180 mM KCl, 10 mM Mg^{2+}, 25°C at various pHs. These data were difficult to interpret, because two of the previously assigned kinetic phases collapsed into one. However, they were interesting because they revealed appearance of a pH dependent phase (see Figure A-1).

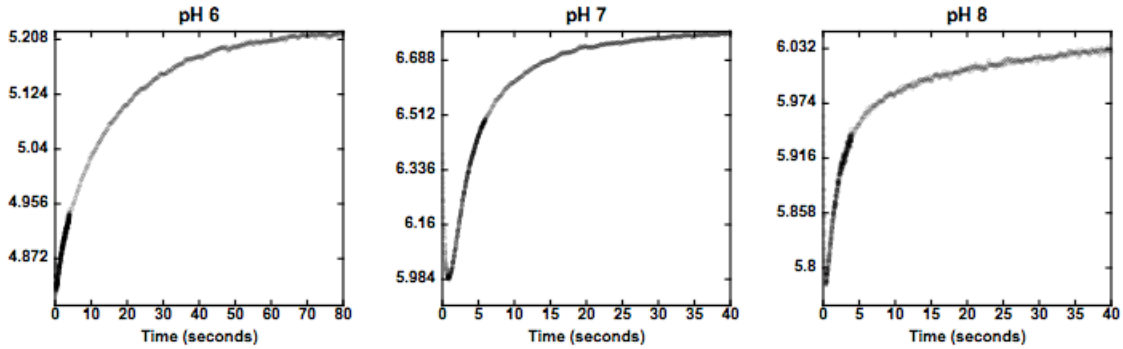

Figure A-1: Stopped flow traces of wild-type RNase P with Fl-pre-$tRNA^{5nt}$ in magnesium, showing the pH dependent appearance of a second phase.

The pH dependence of wild-type, R60A, N61A, and R62A RNase P were measured at 25°C, pH 6.0, 20mM $MgCl_2$, 50 mM MES, 50 mM Tris, 150 mM KCl. Other studies in our lab have shown that the rate-limiting step at 25°C is different than at 37°C for k_{obs}, and this explains the fact that the RNR motif mutants alter the pK_a of the enzyme at 37°C, but not at 25°C.

The $K_{D,obs}$ of wild-type, R60A, R62A, and R65A for pre-tRNA^{Asp} with 4 ($K_{D,\ obs,,\ 4nt}$) and 5 ($K_{D,\ obs,,\ 5nt}$) nucleotide long 5' leader at 25°C at pH 6.0, 50 mM MES, 50 mM Tris, 400 mM KCl, and 20 mM $CaCl_2$. These data demonstrate that while the RNR motif still moderately effects binding of pre-tRNA^{Asp} at 25°C and saturating divalent metal, the effects are much more moderate than at physiological temperatures (37°C).

Table A-2: Affinities of RNR motif mutants for pre-tRNAs at 25°C.

	$K_{D,\ obs,,\ 5nt}$ (μ M)	$K_{D,\ obs,\ 4nt}$ (μM)
Wild Type	3 ± 1	5 ± 2
R60A	8 ± 3	3 ± 1
R62A	6 ± 1	7 ± 3

Time resolved fluorescence resonance energy transfer (trFRET) studies were attempted with RNR motif mutants to see if they disrupted the conformation of P RNA. Tetramethylrhodamine-pret-RNA^{5nt} was bound to RNase P reconstituted with RNR motif mutants and circularly permuted P RNA labeled with a fluorescein in helix P4. These studies were inconclusive because the data were not physically reasonable with this construct, see Table A-4). To combat this, RNR motif double mutants (R60A/5KC, R60A/40C, R62A/K5C, and R62A/40C) have been generated and can be labeled with tetramethyl rhodamine so that distance measurements can be obtained between Fl-pret-

RNA^{5nt} and the protein, rather than between the substrate and P RNA (as has been previously successful).

Table A-3: Preliminary trFREt distance measurements. This shows that the initial construct was not reasonable for collecting distance data of the RNR motif.

	R_{avg}
WT	20.05
N61A	20.03
R62A	3.17
R68A	3.17

Further studies of mutants that alter N(-4) sequence specific recognition

Single turnover rate constants of *B. subtilis* RNase P reconstituted with wild type and F20A, Y34A, Y34F, and R60A protein mutants were measured under conditions of 2 mM $Co(NH_3)_6^{3+}$, 0.5 mM $MgCl_2$, 50 mM MES, 50 mM Tris, ~180 mM KCl, pH 7.0, 37°C. The k_{obs} measured for these studies were the same as wild type, except that of R60A. This was to be expected because these mutants impact substrate association, and the on rate (k_1 in Scheme IV-1), is not reflected in the k_{obs} term.

Table A-4: Single turnover rate constants for mutants that impact N(-4) sequence selectivity under conditions of 2 mM $Co(NH_3)_6^{3+}$, 0.5 mM $MgCl_2$, 50 mM MES, 50 mM Tris, ~180 mM KCl, pH 7.0, 37°C.

	k_{obs} (s^{-1})
WT	0.06 ± 0.003
F20A	0.1 ± 0.01
Y34A	0.07 ± 0.004
Y34F	0.1 ± 0.02
R60A	0.02 ± 0.001

Binding of pre-tRNA^{Asp} to RNase P reconsistuted with a C52G/G379C, C53G/G378C P RNA mutant

A previous graduate student, Andrew J Andrews, studied a C52G/G379C, C53G/G378C P RNA mutant and showed that they significantly decreased the catalytic efficiency of the enzyme, and inhibited metal binding. Interestingly, these are the same P RNA positions identified in Chapter V as an inner-sphere divalent metal ion binding site. To assess if they also impacted pre-tRNA binding in a metal dependent manner, I performed binding assays under various solution conditions. These assays revealed that the mutations are essential to pre-tRNA binding.

Table A-5: Affinity of wild-type and a C52G/G379C, C53G/G378C *B. subtilis* RNase P for pre-tRNA^{Asp} with a 5 nucleotide long 5' leader under various conditions. All reactions also had 50 mM MES, 50 mM Tris, 400 mM KCl, pH 6.0, 37°C.

	$K_{D,\,obs}$ (nM) 2mM $CaCl_2$, 2mM $Co(NH_3)_6^{3+}$	$K_{D,\,obs}$ (nM) 10mM $CaCl_2$, 2mM $Co(NH_3)_6^{3+}$	$K_{D,\,obs}$ (nM) 10mM $CaCl_2$
WT	20 ± 3	3 ± 1	2 ± 0.5
C52G/G379C, C53G/G378C	132 ± 90	130 ± 55	31 ± 15

APPENDIX B

This appendix includes a summary of the work completed towards obtaining an NMR structure of the *B. subtilis* P RNA catalytic domain (C-domain) in collaboration with Anette Casiano in the Al-Hashimi lab. My contributions to this project thus far have been 3 fold: 1) Optimizing the synthesis and purification of C-domain labeled for NMR; 2) folding the C-domain for NMR experiments; 3) discussion the design of NMR experiments, primarily with respect to suitable solution conditions. Below I have listed the optimized protocol for the synthesis and purification of isotopically labeled *B. subtilis* C-domain P RNA. This procedure increased the yields of this product by > 50-fold (to 150uL of 1.02mM per 5mL transcription), primarily due to the addition of PEG and pyrophosphatase to transcription conditions, and the alteration of the purification protocol. I also display preliminary spectra demonstrating that the helix P4 NMR data agree well with our initial C-domain spectra, and indicating that this is a viable approach of looking at the C-domain structure.

Synthesis and Purification of an isotopically labeled C-domain construct

The conditions for the transcription of labeled C-domain from a cut plasmid are listed below. The reactions are optimized to for a volume of 1 mL, and quenched with EDTA. The transcription products were purified directly on a large 6% PAGE (~50 mL in volume) gel run at 50W for 13 hours. Unlike typical NMR scale preparation procedures, the RNA was not concentrated before being added to the gel. After running

the gel over night, it was UV-shadowed, and the large (~1 inch) RNA band is excised with a razor blade and placed into buffer (~200 mL of 0.01% SDS, 10 mM Tris, 1 mM EDTA, 500 mM $NaCl_2$) overnight at room temperature. The elutrap electroelution method for getting RNA out of PAGE gels generally used for NMR scale preparations was not successful with this RNA, and the soaking method must be used to obtain reasonable yields. The gel is then Steri-filtered (0.2 μm cellulose filter) out of solution, and the eluate is concentrated to 2 mL in 10,000 MWCO Amicons pre-washed with TE buffer (10 mM Tris, 1 mM EDTA). The concentrated solution is subsequently washed with a total of 240 mL of TE, and re-concentrated to a total volume of 2 mL. The RNA was then ethanol precipitated out of solution at -80^{o}C overnight. The solution is then spun at 14,000 rpm at 4^{o}C for 30 minutes to pellet the RNA, and the bulk of the solution is pulled off of the pellet with a pipette. The pellet is then dried for ~15-30 minutes in a speed-vac. The pellet is then re-suspended in ~150mL H_2O, and passed through a RNase/DNase free 1.8mL volume Spin-Column (0.2μM filter) to get rid of any dust or other contaminants. The final concentration is determined by UV at λ of 260 nM with an estimated extinction coefficient of 2-2.3 x 10^6 $M^{-1}cm^{-1}$.

Table B-1: Optimized transcription conditions for synthesis of C-domain P RNA.

Reagent	Final Concentration
1M Mg	20 mM
A[a]	6 mM
U	6 mM
C[a]	6 mM
G[a]	5 mM
PEG, 8000 MW	0.08 % w/v
T7 polymerase	0.35 mg/mL
DNA	0.025 mg/mL
10X Buffer[b]	1 X
PPi	1 μL / 1 mL

[a] These nucleotides are isotopically labeled
[b] This buffer is described in Chapter V.

Preliminary spectra

Given below is an example 2D spectrum of the catalytic domain.

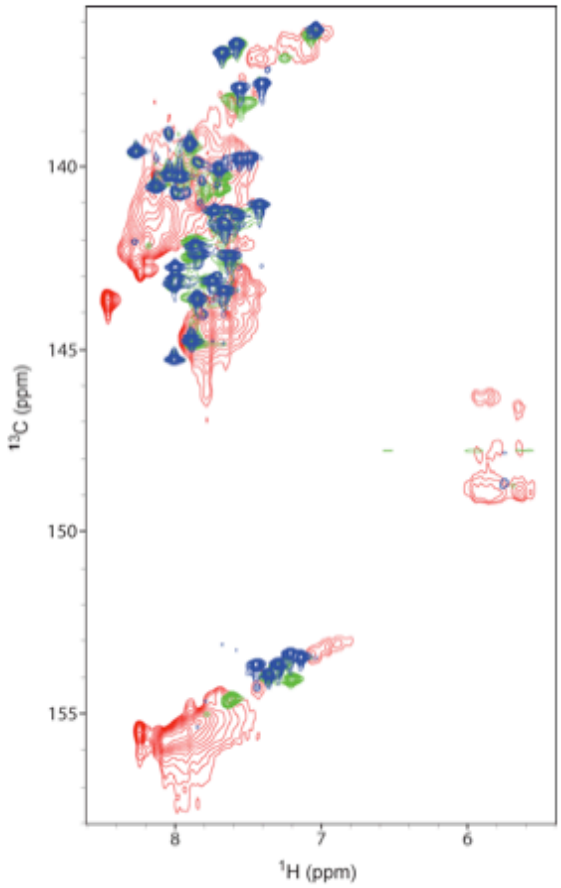

Figure B-1: C-domain overlay with P4 (blue), P4-A bulge included (green) and C-domain (red)[xii]

[xii] This figure is from Anette Negroni-Casiano. She collected the NMR data.